EVAPORATE MAPPING IN BALA REGION (ANKARA) BY REMOTE SENSING TECHNIQUES

A THESIS SUBMITTED TO
THE GRADUATE SCHOOL OF NATURAL AND APPLIED SCIENCES
OF
MIDDLE EAST TECHNICAL UNIVERSITY

BY

NİHAT SERKAN ÖZTAN

IN PARTIAL FULFILLMENT OF THE REQUIREMENTS
FOR
THE DEGREE OF MASTER OF SCIENCE
IN
GEOLOGICAL ENGINEERING

JUNE 2008

Approval of the thesis:

**EVAPORATE MAPPING IN BALA REGION (ANKARA)
BY REMOTE SENSING TECHNIQUES**

submitted by **NİHAT SERKAN ÖZTAN** in partial fulfillment of the requirements for the degree of **Master of Science in Geological Engineering Department, Middle East Technical University** by,

Prof. Dr. Canan Özgen
Dean, Graduate School of **Natural and Applied Sciences** _____

Prof. Dr. Vedat Doyuran
Head of Department, **Geological Engineering** _____

Assoc. Prof. Dr. M. Lütfi Süzen
Supervisor, **Geological Engineering Dept., METU** _____

Examining Committee Members:

Prof. Dr. Nurkan Karahanoğlu
Geological Engineering Dept., METU _____

Assoc. Prof. Dr. M. Lütfi Süzen
Geological Engineering Dept., METU _____

Assoc. Prof. Dr. Nuretdin Kaymakçı
Geological Engineering Dept., METU _____

Dr. Arda Arcasoy
Arcasoy Consultancy _____

Dr. Bora Gürçay
Remote Sensing Center, MTA _____

Date: _____

I hereby declare that all information in this document has been obtained and presented in accordance with academic rules and ethical conduct. I also declare that, as required by these rules and conduct, I have fully cited and referenced all material and results that are not original to this work.

Name, Last name : Nihat Serkan ÖZTAN

Signature :

ABSTRACT

EVAPORATE MAPPING IN BALA REGION (ANKARA) BY REMOTE SENSING TECHNIQUES

Öztan, N. Serkan
M.Sc., Department of Geological Engineering
Supervisor: Assoc. Prof. Dr. M. Lütfi Süzen

June 2008, 97 pages

Evaporate minerals were very important raw materials in very different and broad industries for years. One of the extensively used evaporate mineral gypsum has become very useful raw material in construction, agriculture, textile, dentistry and chemical industry in recent years. Since gypsum became important raw material especially in construction industry as plaster, demand to these minerals rises each following year. The aim of this thesis is to map out these industrial raw materials by using remote sensing techniques. Ankara Bala region has very rich Gypsum sites and this region is showed as one of the best gypsum potential sites of Turkey according to the studies of MTA so that this area is selected for the usage of remotely sensed data.

For the remote sensing analyses ASTER images which have high spatial and spectral resolution are used. The analyses are applied using PCI Geomatica software and ARCGIS software is used for mapping purposes. Band ratio, decorrelation stretch, principal component analysis and thermal indices are used in order to map gypsum minerals. For the base geological map, the geological maps having 1/ 100.000 scale of MTA are used. For gypsum minerals previously known

Crosta method is modified and by the selection of suitable bands and principle components, gypsum minerals are tried to map and it is seen that it has a high success. For TIR indices previously known Quartz index is modified as Sulfate index and used for gypsum mapping. The results of these methods are checked at the field and from the areas where the results show high anomalies, samples were taken for spectral and X-Ray analyses. For absolute accuracy the samples from areas with high anomalies taken from 7 different locations are verified. For relative accuracy all the results are add, percentages of the results are estimated. According to results; 288 km^2 area is mapped as gypsum with the total of four methods but it is seen that only 8 km^2 is found by every methods. According to these percentages modified Crosta method and Sulfate Index methods are showed the highest success.

Keywords: Gypsum, Mineral Mapping, ASTER, Bala

ÖZ

UZAKTAN ALGILAMA TEKNİKLERİYLE BALA (ANKARA) CİVARINDA EVAPORİT HARİTALANMASI

Öztan, N. Serkan
Yüksek lisans, Jeoloji Mühendisliği Bölümü
Tez Yöneticisi: Doç. Dr. Lütfi Süzen

Haziran 2008, 97 sayfa

Evaporit mineralleri yıllar boyunca farklı ve geniş alanlı endüstrilerde oldukça önemli hammaddeler olmuşlardır. Bunlardan en geniş kullanımı olan jipsten son yıllarda inşaat, mimarlık, tekstil, dişçilik ve kimya endüstrilerinde hammadde olarak oldukça faydalanmıştır. Özellikle inşaat endüstrisinde alçı olarak çok sık kullanıldığı için her geçen yıl artan bir talebi vardır. Bu tezin amacı bu endüstriyel hammaddenin uzaktan algılama teknikleriyle haritalanmasıdır. Ankara Bala bölgesi oldukça zengin bir jips sahası olup MTA tarafından yapılan çalışmalarda Türkiye'deki en iyi jips sahaları arasında gösterilmiştir ve bu sebeple seçilmiştir.

Uzaktan algılama analizleri için yüksek mekansal ve alansal çözünürlüğe sahip ASTER görüntüleri kullanılmıştır. Analizler PCI Geomatica yazılımı kullanılarak yapılmıştır ve haritalar ARCGIS yazılımı kullanılarak hazırlanmıştır. Band oranlama, ilişkisiz gerdirme, ana bileşenler analizi ve termal indeks methodları jips minerallerini haritalamak için uygulanmıştır. Temel jeoloji haritası MTA tarafından yapılmış 1/100.000 ölçekli haritalardan oluşturulmuştur. Jips mineralleri için önceden bilinen Crosta metodu değiştirilerek uygun kanallar ve ana bileşenler seçilerek denenmiş ve başarılı olduğu görülmüştür. Termal indekslerde kuvartz indeksi değiştirilerek sülfat indeksi olarak tanımlanmıştır. Bu metotlara ait

sonuçlar arazide kontrol edilmiş ve yüksek anomali veren yerlerden örnekler alınmıştır. Arazi kontrolünde alınan 7 örnekte yapılan X-Ray ve spektral analizlerde yüksek başarı görülmüştür. Göreli kesinlik sonuçları için bütün metotlar toplanıp yüzdeleri hesaplanmıştır. Sonuçlara göre 288 km^2 alan jips olarak haritalanmış olup sadece 8 km^2'lik alan her metot tarafından bulunmuştur. Buna göre Crosta metodu ve sülfat indeks metodu en yüksek başarıyı göstermiştir.

Anahtar Kelimeler: Jips, Mineral Haritalama, ASTER, Bala

To My Beloved Parents and My Sister Gülperi

ACKNOWLEDGMENTS

I would like to express my deepest gratitude to my supervisor Assoc. Dr. M. Lütfi Süzen for his unlimited patience, comments, motivation and valuable guidance he has provided throughout this study.

I would like to express my special thanks to B.Taner San for his valuable comments, suggestions, encouragements and also patience on me.

I am very grateful to my colleagues Dr. Engin Sümer, Dr. Bora Gürçay, Murat Koruyucu, Burcu Pekesin and Dr. Hakan Nefeslioğlu from MTA Remote Sensing Center for their continuous support and encouragements.

I would like to thank my friend Utku Ahmet Özden for his motivation and support during every stage of my thesis.

Finally I want to thank my family for their patience and encouragements during my life and my thesis.

TABLE OF CONTENTS

ABSTRACT iv
ÖZ vi
ACKNOWLEDGMENTS ix
TABLE OF CONTENTS x
LIST OF TABLES xiii
LIST OF FIGURES xiv
CHAPTER 1
1. INTRODUCTION 1
1.1. Purpose and Scope 1
1.2. Study Area 6
1.3. Organization of thesis 6
2. GEOLOGY 8
2.1. Previous Studies 8
2.2. Regional Geology 10
2.3. Geology of the Study Area 10
2.3.1. Base Units 10
2.3.1.1. Bozçaldağ Formation (Pzb) 11
2.3.1.2.Çiçekdağ Formation (Kç) 15
2.3.1.3. Karaboğazdere Gabbro Member (Kk) 15
2.3.1.4. Central Anatolia Granitoids (Kog) 15
2.3.2. Tertiary Units 16
2.3.2.1. Küreboğazı Formasyonu (Tpk) 16
2.3.2.2. Dizilitaşlar Formasyonu (Tpd) 16
2.3.2.3. Baraklı Formation (Teb) 17
2.3.2.4.Çayraz Formation (Teç) 17
2.3.2.5.İncik Formation (Toi) 18

2.3.2.6. Sekili Evaporate Member (Tois) 18
2.3.2.7. Kozaklı Limestone Member (Tmük) 19
2.3.2.8. İç Anadolu Group (Ti) 19
2.3.2.9. Insuyu Formation (Tmi) 20
2.3.2.10. Karakeçili Formation (Plka) 20
2.3.2.11. Bozdağ Volcanics (Tmbo) 20
2.3.2.12. Gölbaşı Formation (plg) 21
2.3.2.13. Old Alluvium (Qeal) 21
2.3.2.14. Alluvium (Qal) 21
3. EVAPORATE MAPPING BY USING REMOTE SENSING 22
3.1. Principles of Reflectance Spectroscopy 22
3.1.1. Causes of Absorption 22
3.1.1.1. Electronic Processes 23
3.1.1.1.1. Crystal Field Effects 23
3.1.1.1.2. Charge Transfer Absorptions 23
3.1.1.1.3. Conduction Bands 24
3.1.1.1.4. Color Centers 24
3.1.2. Vibrational Processes 22
3.1.3. Reflectance Spectra of Mixtures 25
3.2. Spectral Properties of Gypsum 27
3.3. Common Techniques of Remote Sensing For Mineral Mapping 29
3.3.1. Band Rationing 29
3.3.2. Principle Component Analysis (PCA) 31
3.3.3. Feature- Oriented Principle Component Selection 37
3.3.4. Decorrelation Stretch 38
3.3.5. Spectral Indices 40
4. DATA ANALYSIS 41
4.1. Data 41
4.1.1. ASTER image 41
4.1.2. Geological Map 43
4.2. Methodology 43

4.3. Preprocessing 46
4.3.1. Masking 47
4.3.2. Atmospheric Correction 48
4.4. Image Analyses 49
4.4.1. Band Ratio 50
4.4.2. Decorrelation Stretch Analysis 59
4.4.3. Feature- Oriented Principle Component Selection 62
4.4.4. Spectral Indices 65
5. RESULTS AND DISCUSSION 69
5.1. Absolute Accuracy Assessment 69
5.2. Relative Accuracy Assessment 77
5.3. General Aspects of the Data and the Results 81
6. CONCLUSIONS AND RECOMMENDATIONS 84
REFERENCES 85
APPENDIX A 92
APPENDIX B 94

LIST OF TABLES

Table 1.1. World Gypsum Production & Reserves 3
Table 1.2. Gypsum Potential of Turkey 5
Table 3.1. Positions of spectral features in SWIR region of common groups. 25
Table 4.1. Spectral & Spatial properties of ASTER images. 42
Table 4.2. The detailed information about the ASTER scene used. 42
Table 4.3. Minimum DN of the bands. 48
Table 4.4. Applied Band Ratios. 52
Table 4.5. Eigen Vectors of Covariance Matrix 64
Table 5.1. Hand Specimen taken from the field and their UTM coordinates. 70
Table 5.1. The values of given to the methods 77
Table 5.2. Table showing the possible values of the total map 78
Table 5.3. The four classes that are generated. 78

LIST OF FIGURES

Figure 1.1. Photos of Gypsum minerals 2
Figure 1.2. Location map of the study area. 7
Figure 2.1.a. Geological map and settlement of the study area. 12
Figure 2.1.b. Legend of the geological map 13
Figure 2.2. Generalized Columnar Section of the Study Area 14
Figure 3.1. Reflectance spectra of alunite, jarosite and mixtures of two 26
Figure 3.2. Spectral reflectance curve of Gypsum 28
Figure 3.3. Normal distribution of Band A & Band B forming ellipse shape 32
Figure 3.4. The graph showing the first principal component. 33
Figure 3.5. The graph showing the range of first principle component. 34
Figure 3.6. The graph showing second principle component. 34
Figure 4.1. The classified geological map of the study area 44
Figure 4.2. The Flowchart of the ASTER image analyses. 45
Figure 4.3. The raw ASTER image in false color (3, 2, 1) 46
Figure 4.4. Water and vegetation masking 47
Figure 4.5. Figure showing the DN before and after atmospheric correction 49
Figure 4.6. Spectral curve of Gypsum and location of ASTER bands 50
Figure 4.7. Mean value and standard deviation for band ratio 4/6 52
Figure 4.8. Band ratio 4/6 applied on the image and applied threshold. 53
Figure 4.9. Band ratio 4/9 applied on the image and applied threshold. 54
Figure 4.10. Band ratio 4+8/ 9 applied on the image and applied threshold. 55
Figure 4.11. Band ratio 8/ 9 applied on the image and applied threshold. 56
Figure 4.12. Decorrelated image 1,4,8. 60
Figure 4.13. Decorrelated image 3,2,1. 61
Figure 4.14. Decorrelated image 4,6,8. 62
Figure 4.15. The wavelength vs. reflectance curve of gypsum. 63
Figure 4.16. PCA3 image after Crosta technique 65

Figure 4.17. The spectral curve of Quartz in the interval 6 μm-11 μm..... 67
Figure 4.18. The spectral curve of Gypsum in the interval 6 μm-11 μm..... 67
Figure 4.16. The resultant image of sulfate index method..... 68
Figure 5.1. The result of sulfate index technique and areas in which photos are taken. 71
Figure 5.2. Photo from the location 1..... 72
Figure 5.3. Photo from the location 2..... 72
Figure 5.4. Photo from the location 3..... 74
Figure 5.5. Photo from the location 4..... 74
Figure 5.6. Photo from the location 5..... 75
Figure 5.7. Photo from the location 6..... 75
Figure 5.8. Photo from the location 7..... 76
Figure 5.9. Photo from the location 8..... 76
Figure 5.10. The results of the methods..... 79
Figure 5.11. Classified map having four classes……..……..80
Figure 5.12. The results showed on classified geological map …….....82

CHAPTER 1

INTRODUCTION

1.1. Purpose and Scope

The use of Remote Sensing techniques for geological purposes has been a very important tool for earth scientists to deal with many problems throughout the last four decades starting with the launch of Landsat system. Prior to the presence of many well known rule of thumb image enhancement techniques, availability of high quality images that have high spectral and spatial resolutions, has been playing an important role for the earth scientist.

The purpose of this thesis is to use remote sensing to map evaporate minerals. Main scope of this thesis is not only to apply well known Remote Sensing methods, but also searching and proposing new methodologies to discriminate and map the evaporates, while evaluating their successes. The reasons for selection of mapping evaporate minerals are; no distinct methodology is present for mapping of evaporates and among evaporates especially gypsum stands for an important industrial raw material. In this thesis all evaporate minerals in the region are called as gypsum minerals.

Gypsum is the most common sulfate mineral on the Earth and of large commercial value. It is known technically as calcium sulfate, is one of the most useful and widely used minerals of the 20^{th} century. Gypsum is consumed in large quantities worldwide, principally for use in the construction industries. Gypsum can appear as transparent crystals (selenite); fibrous, elongated crystals (stain spar); granular

and compact masses (alabaster); and in rosette-shaped aggregates called desert roses (Figure 1.1). Gypsum is used in the construction, agricultural, chemical, textile, medicine, dentistry industries. In agriculture, it is used as an amendment to neutralize sodic soils and for fertilizers. In construction, it is used in plaster, plaster of Paris, wallboard, cement, and ceramic tiles. In chemical industry it is used to obtain ammonium sulfate, sulphur, sulphur oxide and acid sulfate. The world production of gypsum by country is summarized in Table 1.1 (URL 1).

Figure 1.1. Photos of Gypsum minerals a) Selenite; b) Desert Rose, c) Stain Spar, d) Alabaster

Foreign resources are large and widely distributed; more than 90 countries produce gypsum. Iran is second to the United States in production and supplies much of the gypsum needed for construction and reconstruction in the Middle East. Spain is the largest European producer and supplies both crude gypsum and gypsum products to much of Western Europe. Increased wallboard use in Asia and new gypsum product plants in Thailand and India led to increased production in those countries. As more cultures recognize the economics and efficiency of building with wallboard, worldwide production of gypsum should increase proportionally (URL 2).

Table 1.1. World Gypsum Production & Reserves (URL 3).

	Mine production (million tons)		**Reserves (million tons)**
	2005	**2006**	
United States	21,100	21,100	700,000
Australia	4,000	4,000	
Algeria	1,460	1,460	
Austria	1,000	1,000	
Brazil	1,480	1,500	1,300,000
Canada	9,400	9,450	450,000
China	7,300	7,400	
Egypt	2,000	2,000	
France	3,500	3,500	
Germany	1,580	1,580	
India	2,400	2,500	
Iran	13,000	13,000	
Italy	1,210	1,220	
Japan	5,890	5,900	
Mexico	7,200	7,400	
Poland	1,300	1,300	
Russia	2,200	2,400	
Spain	11,500	11,500	
Thailand	6,920	7,100	
Turkey	1,000	1,100	
United Kingdom	1,500	1,500	
Uruguay	1,130	1,130	
Other countries	10,900	11,000	
World total (rounded)	**118,000**	**119,000**	Large

For Turkey an inventory of Gypsum minerals was published by DPT (State Planning Organization of Turkish Republic) in 2001. Although gypsum is widely distributed in Turkey, no sufficient and scientific studies were done before this inventory since gypsum was not involved in the Mine Law. According to the estimates on the "Sixth Five Year Progress Plan Gypsum Specialization Report", it is stated that the seen reserve is 165 million Tons and predicted seen reserve is 1.8 billion Tons.When the regions in Turkey are considered, the gypsum deposits are dense at Middle, South and East Anatolia whereas very less reserve is observed at West Anatolia. At the report of DPT (2001) potential areas are classified instead of indicating the reserve values. At the table 1.2 the potential areas having a potential of gypsum is presented. DPT (2001) classified the sites as three classes; poor, middle, fine but there is no further information about this classification at the report.

Table 1.2. Gypsum Potential of Turkey (DPT, 2001)

Region	Poor	Middle	Fine
1. Ankara-Polatlı-Sazılar			X
2. Bolu-Bakacak		X	
3. Karabük-Ovacık-Pürçükören			X
4. Çankırı			X
5. Çorum-Çukurköy			X
6. Çorum-Bayat-Emirhalil, Üçdam, Tuğlu			X
7. Amasya-Vezirköprü-Adatepe, Akören			X
8. Balıkesir-Susurluk		X	
9. Bursa-Gemlik-Adliye, Hamidiye	X		
10. Kütahya-Gediz-Akçaalan, Yayla, Gökler	X		
11. Eskişehir-Sivrihisar-Biçer			X
12. Ankara-Ayaş-Beypazarı		X	
13. Ankara-Bala-Aşıkoğlu, Bahçe Karadalak			X
14. Kırıkkale-Keskin-Halitli		X	
15. Kırıkkale-Delice-Tavaözü			X
16. Kırıkkale-Delice-Akboğaz, Kuzucak			X
17. Sivas-Ulaş-Çiftağıllar			X
18. Erzurum-Aşkale			X
19. Afyon-Emirdağ-Gülçayır	X		
20. Ankara-Şereflikoçhisar-B.Kışla, Kurutlutepe			X
21. Ankara-Bala-Sarıpınar, Çiğdemli			X
22. Aydın-Yazıkent-Karaahmetler	X		
23. Denizli-Sarayköy-Yeşilyurt			X
24. Denizli-Buldan-Derbent, Alacaoğlu	X		
25. Denizli-Güney-Aksaz	X		
26. Denizli-Honaz-Kızılyer			X
27. Siirt-Kurtalan			X
28. Niğde-Ulukışla-Emirler, Darboğaz			X
29. Mersin-Tarsus-Dadalı, Karayayla, Tepeçaylak		X	
30. Adana-Solbaş		X	
31. Hatay-Arsuz			X

1.2. Study Area

The study area is located in the Tuz Gölü Basin around Bala district. The boundary of the study area is selected according to the geography of gypsum bearing units and the ASTER AST3A1_050727084419060331 1230 image extent (Figure 1.2). The study area nearly covers the area from Bala district at west to Hirfanlı Dam Lake to the East and from Karakeçili district at North to Tuz Gölü at south. The study area is located in the UTM zone 36 and is composed of four different 1:100.000 scaled maps which are I30, I31, J30 and J31, of which detailed geological maps have been prepared by MTA.

1.3. Organization of thesis

This thesis includes five chapters and a brief description of each chapter is as follows: Chapter 1 defines the scope and purpose of the thesis and clarifies the problem at the study area of the thesis. Chapter 2 is the geology chapter of the thesis that mainly focuses on the regional and local geology of the area that is in consideration. Chapter 3 is about evaporate mapping techniques using remote sensing and their evolution. Chapter 4 is the main part of the thesis in which all the analyses are discussed and focused. Chapter 5 is the results and discussion part in which all the methods are compared with each other and also with the ground truth results. Chapter 6 is the suggestions and conclusion part in which the successes of the methods are discussed.

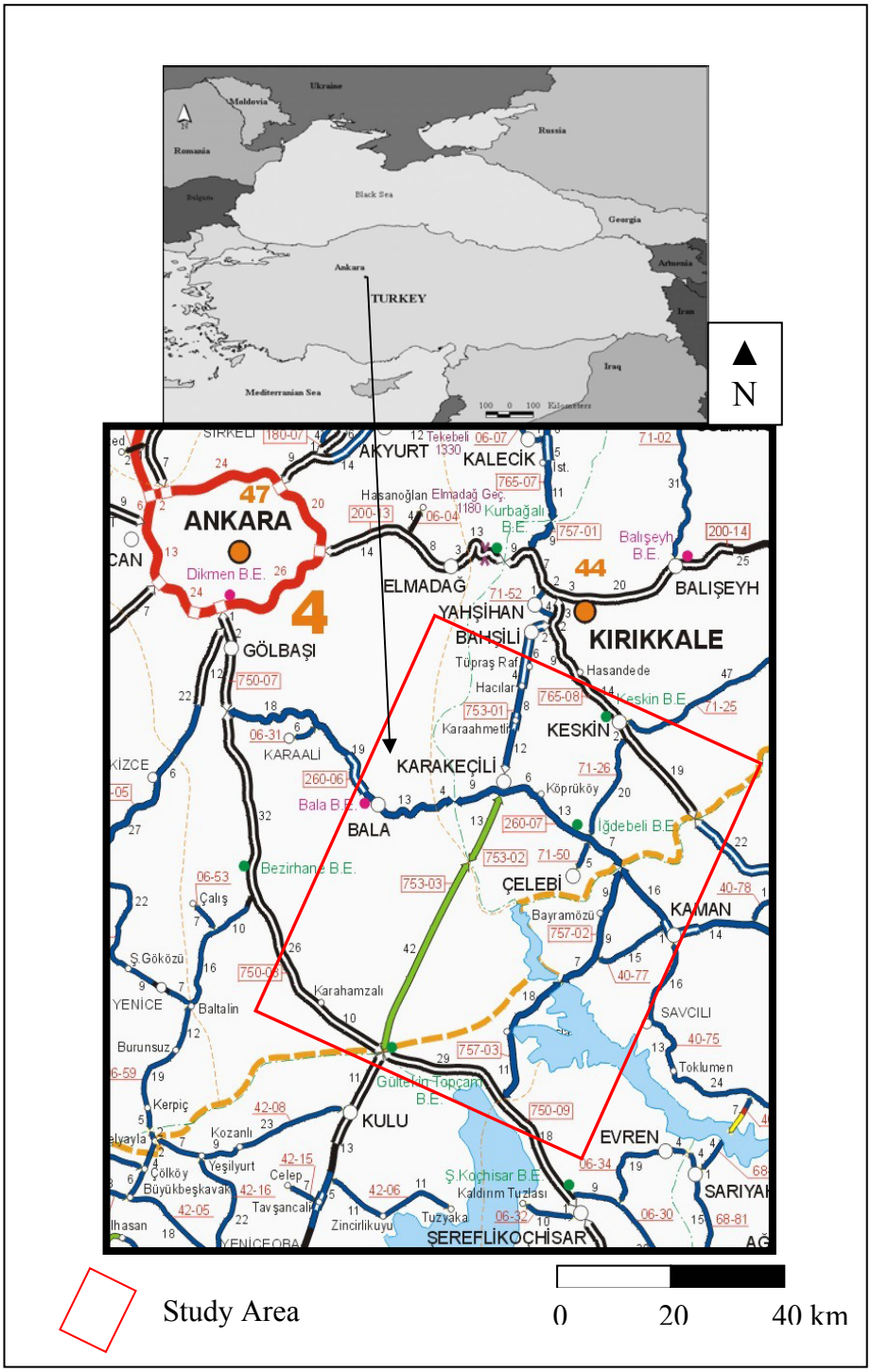

Figure 1.2. Location map of the study area

CHAPTER 2

GEOLOGY

2.1. Previous Studies

There are not many studies specifically including Bala region but the area is generally studied as a part for Tuzgölü Basin researches and some of those related to the area are summarized below:

Baykal (1943) studied at Kırıkkale-Kalecik, Keskin-Bala region and estimated that Oligocene is composed of series with gypsum.

Erol (1969) studied the geology and geomorphology of Tuzgölü Basin.

Arıkan (1975) mentioned that Tuzgölü Basin developed during Upper Senonien-Oligocene, during this period at the deepest part of the basin 10000 meter deposition occurred, a regression starting during Middle-Upper Eocene after the subsidence that occurred between upper Senonian- Lower Middle Eocene. Arıkan (1975) claimed that during Upper Senonian –Lower Middle Eocene, Tuzgölü Basin and Haymana region were one single and continuous depression area. After the deposition of Middle Eocene limestone, Tuzgölü Basin is separated from uplifted Haymana Basin. The joining of Tuzgölü Basin with Çankırı Basin developed during Paleocene and continued during Middle Eocene-Oligocene.

Arıkan (1975) mentioned development of depositional basins during Neogene because of the deformational period during Miocene and the tensional movements during Neogene-Pleistocene caused young volcanic effects. He also stated that the ophiolitic mélange which consist of serpentine, red chert, radiolites and exotic

blocks (Mesozoic and Carboniferous) is in tectonic relation with Jurassic-Lower Cretaceous aged limestone group.

Görür and Derman (1978) prepared stratigraphic and tectonic analysis of Haymana and Tuz Gölü Basins. They defined the age of the salt at the bottom as Upper Cretaceous.

Uygun (1981) studied Tuzgölü Basin and indicated that the generation of gypsum in Tuzgölü Basin is occurred during seven different periods. These are Maestrichtian, Paleocene, Lutetian, Upper Eocene- Oligocene, Upper Oligocene-Lower Miocene, Pliocene, Quaternary aged deposits. They defined the gypsum near Bala region as Mezgit Gypsum and aged as Upper Eocene-Oligocene. They give detailed information about this gypsum and economical potential of this area.

Şahbaz and Köksoy (1985) prepared 1/25.000 scaled geological map of 170 km^2 part of Aladağ region and defined tectonic lines. They defined four litho-stratigraphic units in Paleocene-Middle Eocene age which was described as one unit by previous researchers; furthermore they gave definite age to these units. These are Kurtaytepe formation (Middle Paleocene), Eğribasan Formation (Middle Paleocene), Karanlıkdere Formation (Upper Paleocene), Danatepe Formation (Lower-Middle Eocene). They mentioned about the tectonic deformation of the area, according to them; at Late Eocene, Oligo-Miocene the Pyrenian and Savian movements were dominant and at the remnant lakes of Eocene sea Gypsum was deposited, with the Rodanian movements at Late Pliocene the region took its today's tectonical view. Also they discuss because of the earthquakes seen in the region the tectonical activity is still active.

Akyürek et al. (1996) studied H29, H30, I29, I30 1/100.000 scaled maps. They correlated the units in Haymana Basin and Çankırı Basin. They estimated and mapped the presence of volcanics in Haymana or its equivalent Formation. The age of Hançılı Formation is estimated as Serrovalien-Tortonien by fossils.

Doğan et. al. (1998) discussed the origin and ore geology of the Kesikköprü iron ore near Bala region.

Uğuz et al. (1999) made 1/25.000 scaled geological mapping between the regions Kulu (Konya) –Haymana (Ankara)- Kırıkkale.

2.2. Regional Geology

Evolution of the Bala basin can be considered with the evolution of the Tuzgölü basin, a NW-SE trending continental basin. At the North of this basin Ankara orogenesis, at East Kırşehir massive, at the South Taurides and at West Sivrihisar-Bozdağ Massive take place. The basin is developed during Upper Senonian - Oligocene period. A subsidence occurred between Upper Senonian- Lower Middle Eocene and a regression developed during Middle Eocene to Oligocene (Arıkan, 1975). During upper Senonian-lower Middle Eocene, Tuzgölü basin had generated a continuous depression trending North-West with Haymana zone. After deposition of Middle Eocene aged Nummulitic Limestone, Tuzgölü basin is separated from Haymana Basin with a fault zone trending along East of Karacadağ. After the basic deformation that developed at the end of Oligocene, depositional basins generated during Neogene and at these basins continental sediments involving volcanics, lacustrine limestones, evaporates were deposited (Arıkan, 1975).

2.3. Geology of the Study Area

The geology of the area is discussed as Base units and Tertiary units, in accordance to the purpose and scope of the thesis. The geological map and legand of the study area can be seen in Figure 2.1.a and Figure 2.1b. Generalized columnar section can be seen in Figure 2.2.

2.3.1. Base Units

The Paleozoic and Mesozoic base units that are exposed in the study area are seen at the East part of the Kapulukaya Dam Lake. At the West part of the area base units are not seen, only younger units can be seen (Figure 2.1). Although base

units do not occupy a large area at the study area, they still have considerable outcrops. They are mapped as four different formations according to their rock types and ages. The oldest unit in the area is Paleozoic marble which can be observed near Ağapınar village (Figure 2.1). The gabbro seen in the area is thought to be upper Cretaceous in Karaboğazdere formation (Dönmez et al., 2005). It has a very limited outcrop in the study area at the west of Hacıyusuflu village. Upper Cretaceous granitoids are the major unit that constitutes the base units and they occupy huge areas. These granitoids can be seen near Tepeköy, Bektaşlı, Küçük Bıyık villages. They are cutting the ophiolites, hence they are younger than ophiolites (Dönmez et al., 2005). Upper Cretaceous ophiolite complex is seen near Halildede village and North of Kesikköprü village.

2.3.1.1. Bozçaldağ Formation (Pzb)

Formation is composed of marble and re-crystalline limestone forming the upper parts of Kırşehir massive, which was named by Seymen (1982). This unit is seen at the East part of the study area near Ağapınar village.

The surface outcrops of the formation is grey, fracture surfaces are light grey and white (Dönmez et al., 2005). In some places because of iron content it is observed as pinkish. The marbles generally have holocrystalline texture because of contact metamorphism (Dönmez et al., 2005). Marbles are cut by intrusives so that effects of contact metamorphism are seen very well. At the contact zones; actinolite, tourmaline, garnet, diopsite, plagioclase and pyroxene minerals are developed (Dönmez et al., 2005).

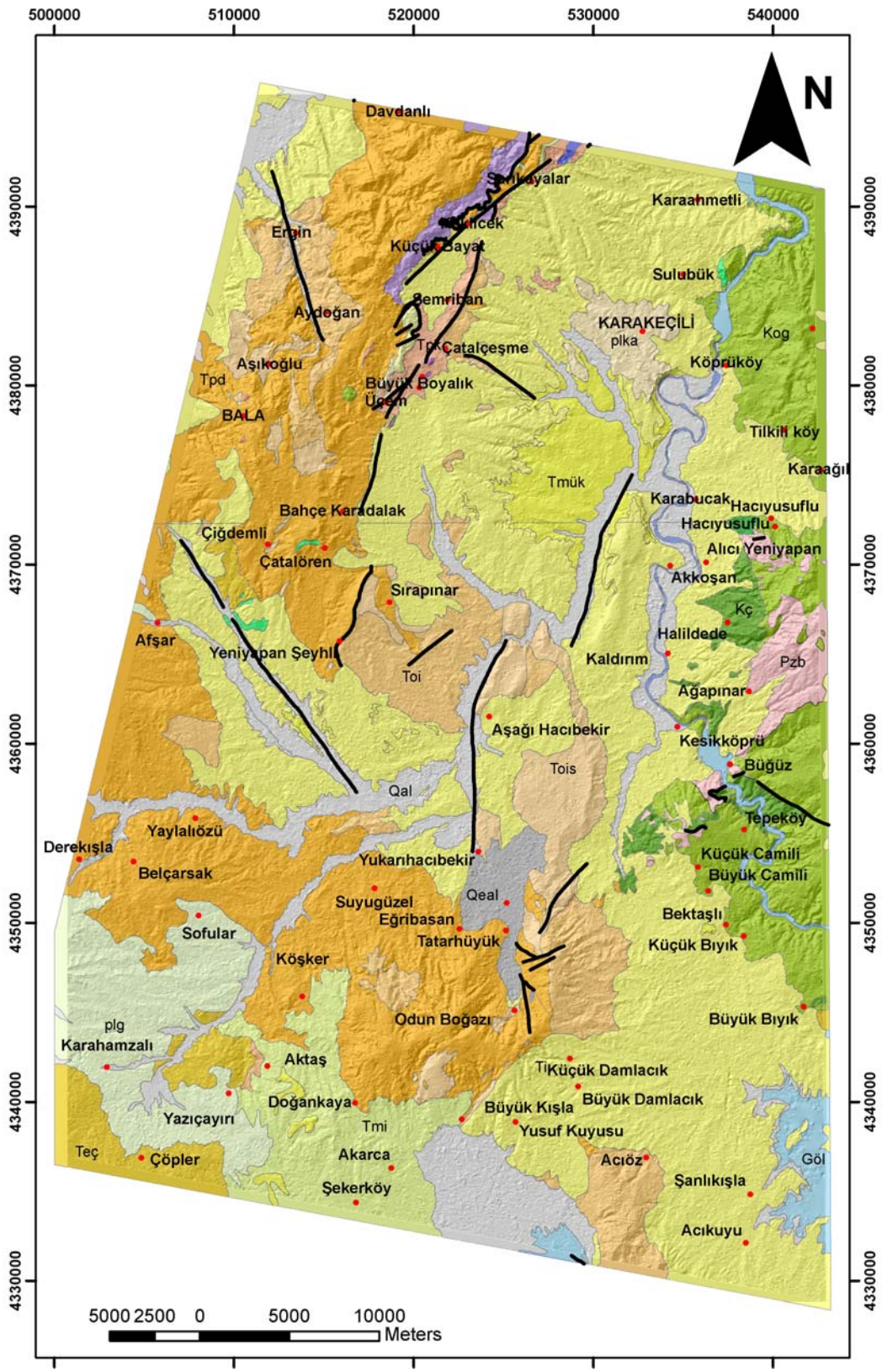

Figure 2.1.a. Geological map and settlement of the study area. (Modified from Dönmez et al. 2007 , relief shading is done with Aster DEM data)

Figure 2.1.b. Legend of the geological map (Dönmez et al.,2007)

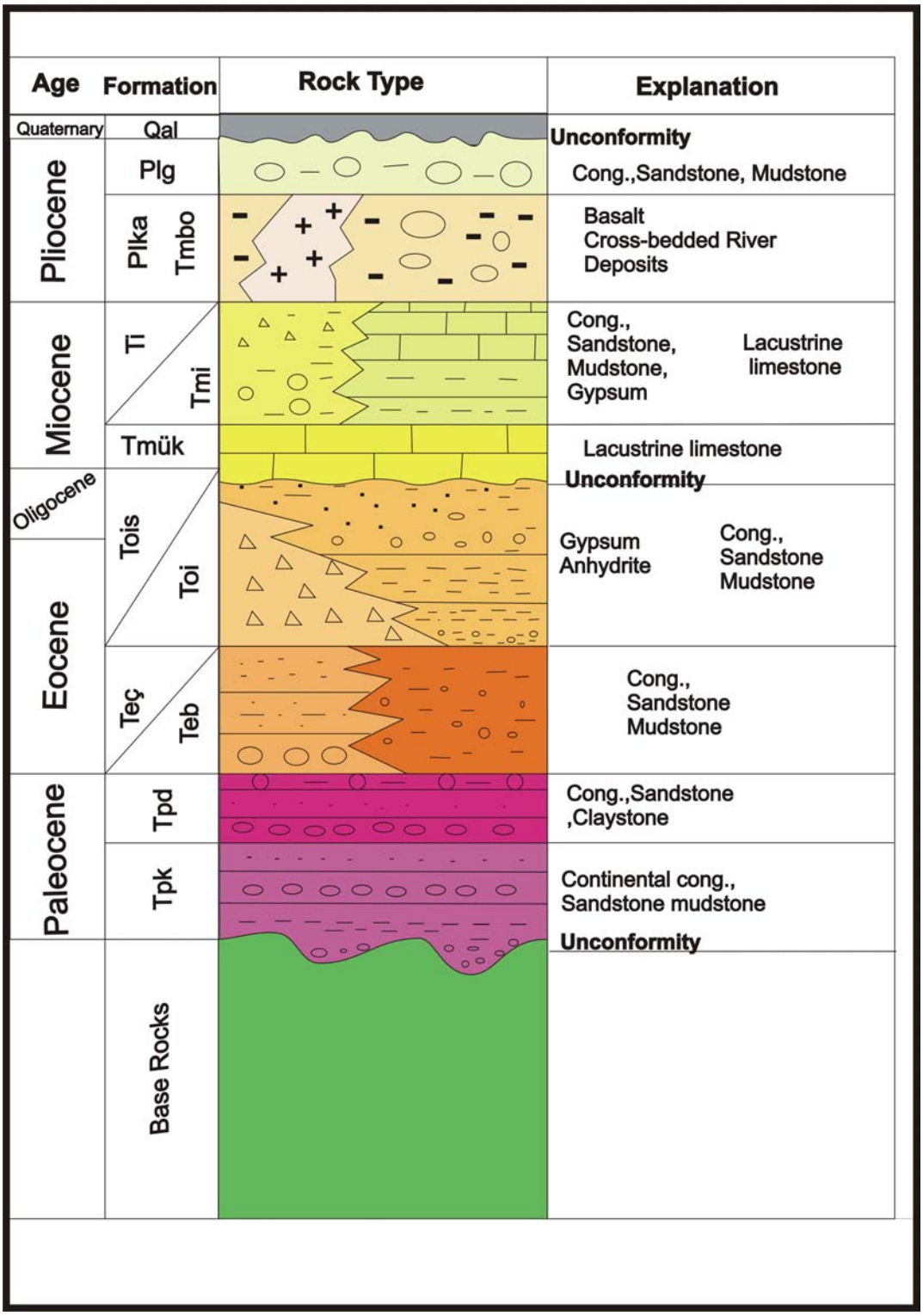

Figure 2.2. Generalized columnar section of the study area (Modified from Dönmez et al., 2005)

2.3.1.2. Çiçekdağ Formation (Kç) (Upper Cretaceous)

Çiçekdağı Formation is composed of diabase, basalt, spilitic basalt, radiolarite, chert, mudstone and pelagic limestone. The formation starts with diabase dikes, basalt, spilitic basalt, spilite and alternating pelagic limestones, mudstones, radiolarite and chert bands and ends with yellowish, brownish sandstone and siltstones with volcanic material (Dönmez et al., 2005). According to Globotruncana lapparenti (BROTZEN), Globotruncana cf. arca (CUSMAN), Globotruncana cf. tricarinata (QUEREAU), Globotruncana cf. fornicate (PLUMMER), Heterohelix sp., Hedbergella sp., Rugoglobigerina sp. and Hedbergella sp., Ticinella sp. fossils the formation is aged as Late Santonian-Campanian and since it is known that it is cut by intrusives before Maastrichtian, the aged of the unit should be Santonian. At the study area this unit is seen near Halildede village, Kesikköprü and at North of Tepeköy.

2.3.1.3. Karaboğazdere Gabbro Member (Kk) (Upper Cretaceous)

Karaboğazdere Gabbro Member that is named by Bilgin et al. (1986) is previously researched in the content of Çiçekdağı Formation by Kara and Dönmez (1990). The gabbros that are seen at the lower levels of the Çiçekdağ Formation are black and dark green color. The coarse grained minerals at bottom change to fine grained micro gabbros at upper parts (Dönmez et al., 2005). At the places which are cut by intrusives, argillic alteration can be seen. The mineral content is generally plagioclase and mafic minerals. The weathering products in plagioclase are sericite, epidote, albite and chlorite, in pyroxene actinolite-tremolite and serpentine. At the study are this unit has a very limited outcrop at West of Hacıyusuflu village.

2.3.1.4. Central Anatolia Granitoids (Kog) (Upper Cretaceous)

They are composed of granite, granodiorite, quartzdiorite, syenite and monzonite. The color, texture, structure and mineral content in granitoids depend on the rock type. Depending on differentiation, the precipitation and segregation of mafic minerals is very common and this is a distinct property. The granitoids that are covered unconformably by Lower Eocene-Quaternary aged sedimentary rocks in

the study area cut Bozçaldağ and Çiçekdağ Formation. The contact metamorphism was developed in different levels depending on the magnitude and deepness. The skarn minerals are changing as diopsite-wollastonite-garnet-epidote-tremolite-actinolite-chlorite-calcite from high degrees to low degrees. Magnetite, pyrite, chalcopyrite and specularite development are seen in the rock. In the study area these granitoids are seen at the East of Kapulukaya Dam Lake.

2.3.2. Tertiary Units

Tertiary units are treated as a group in this thesis since gypsum development is seen in the Tertiary units in the area. In the geological map 14 different Tertiary units can be seen which are discussed below.

2.3.2.1. Küreboğazı Formasyonu (Tpk)

It is composed of volcanic ash, tuffite, aglomerate and lava interbanded conglomerate, sandstone, siltstone alternations (Uğuz et al., 1999).

At the upper surface of the formation 2-3 m limestone, sandy sandstone interbanded reddish conglomerate, sandstone, siltstone is present (Uğuz et al., 1999). The lower levels of the formation are composed of agglomerate, tuffite, ash and lava flow that are generated from andesitic magmas (Uğuz et al., 1999). Aglomerate, tuffite and volcanic ash levels are generally white, yellowish white and have bedded structures. Formation is claimed to be deposited at coast-river environment at which also volcanic activity take place (Uğuz et al., 1999).

In the study area formation is seen at the North-west of the area near Çatalçeşme, Büyük Boyalık, Küçük Boyalık, Şemriban villages (Figure 2.1)

2.3.2.2. Dizilitaşlar Formasyonu (Tpd)

Formation is composed of conglomerate, sandstone, shale, clay-limestone and clastic limestone with turbiditic character (Dönmez et al., 2005). Apart from coarse pebbles, in the grains and pebbles the sorting, graduation and roundness are finely developed. The parts especially where andesite pebbles are dominant the blocks reach 3 m and these parts are carbonate supported weakly cemented. Conglomerates are yellowish, brownish, gray in color, weakly cemented and thick

bedded. The sandstones are dark-light brown, gray and yellowish colored, from place to place they are cross-bedded and the matrix is clay and carbonate. Shales are green, brownish in color, thin bedded and gradual above sandstone layers. Clayey limestones are yellowish, white, light gray in color and fine grained whereas clastic- limestones are white in color and thin-thick bedded. This unit has very dense outcrop at the Western parts of the study area.

2.3.2.3. Baraklı Formation (Teb)

Baraklı formation is composed of terrestial conglomerate, sandstone and mudstone showing alluvium fan property (Dönmez et al., 2005). It starts with reddish colored, bad sorted coarse debris material on the older rocks and passes to fluvial and lacustrine facies (Dönmez et al., 2005). At the debris facies, conglomerates with different origin are seen. Poorly bedded non sorted pebbles within the matrix are in red color. Formation passes to channel facies at the middle level. In these sections lens shaped, alternating, reddish gray colored mudstone, sandstone, conglomerate is recognized. At the center of the basin generally better sorted and bedded mudstone, sandstone and conglomerate are seen. Baraklı formation is unconformable with the older rock units and it is transitive with Çayraz formation both vertically and laterally (Dönmez et al., 2005). At the study area very limited outcrop is seen near Aktaş village.

2.3.2.4.Çayraz Formation (Teç)

Çayraz Formation is mostly composed of limestone and marl and it is very rich in Nummulites. Because of its fossil content and rock types it is thought to be deposited at shallow marine, shelf margin environment. It starts with poorly bedded, gray to reddish conglomerate and sandstone at the bottom. At the top of these light gray, gray, parallel laminated, sorted, well cemented sandstone and siltstone and very few fine-grained conglomerate are seen (Dönmez et al., 2005). The middle levels of the formation are composed of gray colored, middle-thick laminated, argillic, sandy massive limestones and upper parts are composed of turbiditic conglomerate, and sandstone interbanded mudstones. Outcrops of Çayraz Formation can be seen at the southern part of the study area.

2.3.2.5.İncik Formation (Toi)

The formation that is composed of reddish, brown, gray colored, parallel and cross tabulated, rarely sorted grained, rarely uncemented continental conglomerate, sandstone, mudstone alternation with evaporates has a regressive character (Dönmez et al., 2005). This formation is called as İncik Formation by Birgili et al. (1975) for the first time. It is equivalence of Deliceırmak Formation (Kara and Dönmez, 1990), Mezgit Formation (Rigo de Righi and Cortesini, 1959) and Mezgit Group (Uygun et al., 1981).

At the lower levels of İncik Formation, well cemented, thin-middle-thick parallel tabulated sandstone alternating gypsum, anhydrates, and mudstone exist (Dönmez et al., 2005). The middle- upper levels is composed of mudstone alternating cross bedded conglomerate and sandstone (Figure 2.2)

In the study area unit is seen, at the North of Bala, near Çatalçeşme and Şemriban Villages, the East of Yeniyapan Şeyhli village, West of Aşağı Hacıbekir village, at South of Acıöz village as huge outcrops (Figure 2.1).

2.3.2.6. Sekili Evaporate Member (Tois)

The part that is composed of reddish-brown, gray, light green, white colored, middle-thick parallel laminated evaporate, mudstone and sandstone alternated is named as Sekili Evaporate Member by Kara (1991). Generally it consists of anhydrite and gypsum, whereas at the bottom sandstone, mudstone and at upper parts mudstone and marl bands are observed. Gypsum and anhydrites are white-yellowish, middle-thick bedded, generally pure and crystalline, from place to place granular (Dönmez et al., 2005). It is observed that gypsum and anhydrites are getting thinner laterally and mudstones are getting thicker. Sandstones and mudstones are generally thin-middle layered and seen as reddish, brown, light green, green (Dönmez et al., 2005).

The formation is conformable with Çayraz Formation (Kara and Dönmez, 1990), and covered unconformably by İç Anadolu Group. The thickness at Çankırı-Çorum basin is 600-700 m (Birgili et al., 1975). The unit that is deposited at the evaporitic environment at the starting of the regression has no fossils recorded.

The age of the unit is accepted as Upper Eocene- Oligocene (Lower Miocene?) according to the stratigraphy (Dönmez et al., 2005). Unit is equivalent with Bayındır Member (Birgili et. al, 1975).

In the study area unit has a wide distribution near, Bala District and Çiğdemli, Sırapınar, Aşağıhacıbekir, Yukarıhacıbekir, Odunboğazı, Büyük kışla, Ergin villages.

2.3.2.7. Kozaklı Limestone Member (Tmük)

Inside the lacustrine deposits of İç Anadolu Group; horizontal, band or lens shaped, white-beige colored, massive, very hard, from place to place micritic, rarely clastic, with clay, limestone is seen (Dönmez et al., 2005). These are involved to Kozaklı limestone member in Ürgüp Formation by Kara and Dönmez (1990). The thickness of the unit is changing between 1 -8 m. It can be thought as it is equivalence of part of Kışladağ member by Pasquare (1968).

2.3.2.8. İç Anadolu Group (Ti)

The continental facies such as river deposits, fan, and lacustrine deposits at Central Anatolian region are called as İç Anadolu Group (Dönmez et al., 2005). The parts of the continental deposits that are represented as debris are composed of red colored, unsupported grained conglomerate, with a matrix of sand and mud (Dönmez et al., 2005). The parts that constitute channel facies are as reddish-brown, cross bedded, conglomerate, sandstone and mudstone bands and lenses (Dönmez et al., 2005). The parts that relatively constitute the upper parts of the unit and represented by mid-basin lacustrine facies are composed of loosed sandstone in some places, mudstone, gypsum and anhydrite, also in some places conglomerate, sandstone mudstone, limestone and ignimbrite levels (Dönmez et al., 2005). The deposits that belong to İç Anadolu Group cover pre- Miocene units unconformably and above the unit, Quaternary units are observed (Dönmez et al., 2005).

2.3.2.9. Insuyu Formation (Tmi)

Insuyu Formation is composed of limestone with clay, oolitic limestone, intraclastic limestone and limestone with pebbles. At bottom limestone is white to green, fine bedded and it has plant pieces. At the medium levels oolitic limestone is fine-medium textured, well sorted, thick bedded and has little Gastropod fossils. The upper limestone with intraclastic pebbles is poorly sorted, hard and thick bedded. These units indicate that at the base deep and stable lake became shallower and passed to more energetic environment and later changed to beach environment with high energy. At the study area at the South part of the area the outcrops of this formation can be seen.

2.3.2.10. Karakeçili Formation (Plka)

The formation that is basically composed of river deposits takes its name from Karakeçili town and it is at 25 km from Bala district. The outcrops of the formation are near Karakeçili town. It is composed of dirty white, ash colored, cross bedded moderately cemented conglomerate, sandstone with pebbles and sandstone (Uğuz et al., 1999). In the conglomerates it is well sorted, fine graded and the pebbles are well rounded (Uğuz et al., 1999). It has 50-70 m thickness at the outcrops near Karakeçili town. Formation is a meandering river deposit that has dominantly channel deposits.

2.3.2.11. Bozdağ Volcanics (Tmbo)

This unit which is named firstly by Akyürek et al. (1982) mainly composed of basalt and andesitic basalt. Bozdağ basalt is dark black, hard, massive and has yellowish erosional surface (Akyürek et al., 1996). It has many gas cavities and those are full of calcite. Formation is seen on top of volcanics, sedimentary rocks and volcano-sedimentary rocks. Because it is also overlying the Miocene aged rocks it is estimated that the age of this unit is Pliocene. Bozdağ Basalt is the last volcanic product that is generated depending on the active volcanics in the region (Akyürek et al., 1996). In the study area very limited outcrops can be observed.

2.3.2.12. Gölbaşı Formation (plg)

The formation is composed of gray, red, uncemented conglomerate, sandstone, mudstone that are in different size and that have different origin. The pebbles of the conglomerate are mostly quartzite, basalt, various limestone, diabase, metamorphic rock fragments, radiolarite, serpantinite and gabbro where the matrix is calcite and clay (Akyürek et al., 1996). Gölbaşı Formation overlies the older units unconformably and the upper boundary cannot be seen. Formation consists of alluvium fan and river deposits. It has pebble content depending on the rock type in front of which they developed (Akyürek et al., 1996). In the study area the units belonging to this formation are seen at the South-Western part of the area near Sofular, Karahamzalı, Yazıçayırı villages.

2.3.2.13. Old Alluvium (Qeal)

In the study area old alluvium has seen at the North of Tatarhüyük village and composed of uncemented sand and pebbles (Figure 2.1).

2.3.2.14. Alluvium (Qal)

Alluvium is outcropped along the rivers and springs and is the youngest formation seen. It is composed of uncemented reddish mud, silt, clay mixture. In the study area it has widespread extend (Figure 2.1).

.

CHAPTER 3

EVAPORATE MAPPING BY USING REMOTE SENSING

3.1. Principles of Reflectance Spectroscopy

Reflectance Spectroscopy is the study of light as a function of wavelength that has been emitted, reflected or scattered from a solid, liquid, or gas. When photons enter minerals three possibilities occur; they are reflected from surface, pass through the grain or absorbed. The reflected photons from grain surfaces or refracted photons through a particle are said to be scattered. Because of the scattering process photons may be detected and measured. Photons are absorbed in minerals by several processes and variety of absorption processes and their wavelength dependence allows us to derive information about the chemistry of a mineral from its reflected light. Clark (1999) explains that the human eye is a reflectance spectrometer, our eyes and brain is processing for the visible light photons and distinguishing what we are observing. However a spectrometer can measure very small details in a broad wavelength interval with a greater precision.

3.1.1. Causes of Absorption

There are two general processes that causes absorption are electronic and vibrational processes.

3.1.1.1. Electronic Processes

Absorption of photons of a specific wavelength causes a change from one energy state to a higher one. Emission of a photon occurs as a result of a change in an energy state to a lower one. When a photon is absorbed it is usually not emitted at the same wavelength.

3.1.1.1.1. Crystal Field Effects

The most common electronic process revealed in the spectral reflectance curves of minerals is due to unfilled electron shells of transition metal ions such as Fe, Ni, Cr, Co, etc. For all transition elements, d orbitals have identical energies in an isolated ion, but the energy levels split when the atom is located in a crystal field. This splitting of the orbital energy states enables an electron to be moved from a lower level into a higher one by absorption of a photon having energy, matching the energy difference between the states. This effect is called as the crystal field effect which varies with crystal structure from mineral to mineral, thus the amount of splitting varies and the same ion (eg. Fe^{+2}) produces obviously different absorptions, making specific mineral identification possible from spectroscopy.

3.1.1.1.2. Charge Transfer Absorptions

Absorption bands can also be caused by charge transfers, or inter-element transitions where the absorption of a photon causes an electron to move between ions. The transition can also occur between the same metal in different valence states, such as between Fe^{2+} and Fe^{3+}. Clark (1999) describes that absorption bands caused by charge transfers are diagnostic of mineralogy and their strengths are typically hundreds to thousands of times stronger than crystal field transitions. The band centers usually occur in the ultraviolet with the wings of the absorption extending into the visible. For example; charge transfer absorptions are the main cause of the red color of iron oxides and hydroxides.

3.1.1.1.3. Conduction Bands

In some minerals, there are two energy levels in which electrons may reside: a higher level called the "conduction band," where electrons move freely throughout the lattice, and a lower energy region called the "valence band," where electrons are attached to individual atoms. The difference between the energy levels is called the band gap. The band gap is typically small or non-existent in metals, and very large in dielectrics. According to Clark (1999); in semiconductors, the band gap corresponds to the energy of visible to near-infrared wavelength photons and the spectrum in these cases is approximately a step function. For example; the yellow color of sulfur is caused by such a band gap.

3.1.1.1.4. Color Centers

A color center is caused by irradiation (eg. by solar UV radiation) of an imperfect crystal (Clark, 1999). Very few minerals show their color according to “color center” absorption. The periodicities of the crystals in nature are disturbed by impurities. These defects can produce discrete energy levels and electrons can become bound to them. The movement of an electron into the defect requires photon energy. As examples; the yellow, purple and blue colors of fluorite are caused by color centers.

3.1.2. Vibrational Processes

According to Clark (1999); the bonds in a molecule or crystal lattice behave like springs with weights attached that cause the system to vibrate. This means that the frequency of vibration depends on the strength of each spring and their masses. The vibrational motions between atoms or molecules within a crystal lattice are called normal modes and fundamentals. For a molecule with N atoms, there are 3N-6 normal modes of vibrations called fundamentals. Additional vibrations are called overtones when involving multiples of single fundamental, and combinations when involving different types of vibrations.

When we think this property, the absorption features observed in the Short Wave Infrared Region (SWIR), are the result of combinations and overtones of fundamental lattice vibrations which occur at longer wavelengths (Clark, 1999). The bonds giving rise to absorption features in the SWIR are found in molecules such as hydroxyl, water, carbonate and ammonia and between Al-OH, Mg-OH, and Fe-OH. Table 3.1 summarizes the common groups and the positions of their major spectral features in the SWIR region.

Table 3.1. Positions of major spectral features in SWIR region of common groups of minerals (from Hauff, 2002).

POSITION	MECHANISM	MINERAL GROUP
~1.4 μm	OH and WATER	CLAYS, SULFATES HYDROXODES, ZEOLITES
~1.56 μm	NH_4	NH_4 SPECIES
~1.,8 μm	OH	SULFATES
~1,9 μm	MOLECULAR WATER	SMECTITE
2.02, 2.12 μm	NH_4	NH_4 SPECIES
~2,2 μm	AL-OH	CLAYS, AMPHIBOLES SULFATES, MICAS
~2,35 μm	CO_3^{-2}	CARBONATES

3.1.3. Reflectance Spectra of Mixtures

The real world (and for that matter, the universe) is a complex mixture of materials, at just about any scale we view it. In general, there are 4 types of mixtures (Clark, 1999):

1) *Linear Mixture*: The materials in the field of view are optically separated so there is no multiple scattering between components. The combined signal is simply the sum of the fractional area times the spectrum of each component. This is also called areal mixture.

2) *Intimate Mixture*: An intimate mixture occurs when different materials are in intimate contact in a scattering surface, such as the mineral grains in a soil or rock. Depending on the optical properties of each component, the resulting signal is a highly non-linear combination of the end-member spectra.

3) *Coatings*: Coatings occur when one material coats another. Each coating is a scattering/transmitting layer whose optical thickness varies with material properties and wavelength.

4) *Molecular Mixtures*: Molecular mixtures occur on a molecular level, such as two liquids, or a liquid and a solid mixed together. Examples: water adsorbed onto a mineral; gasoline spilled onto a soil. The close contact of the mixture components can cause band shifts in the adsorbate, such as the interlayer water in montmorillonite, or the water in plants.

An example mixture comparison is shown in Figure 3.1 for alunite and jarosite. Note in the intimate mixture how the jarosite dominates and the 0.4 to 1.3-µm region.

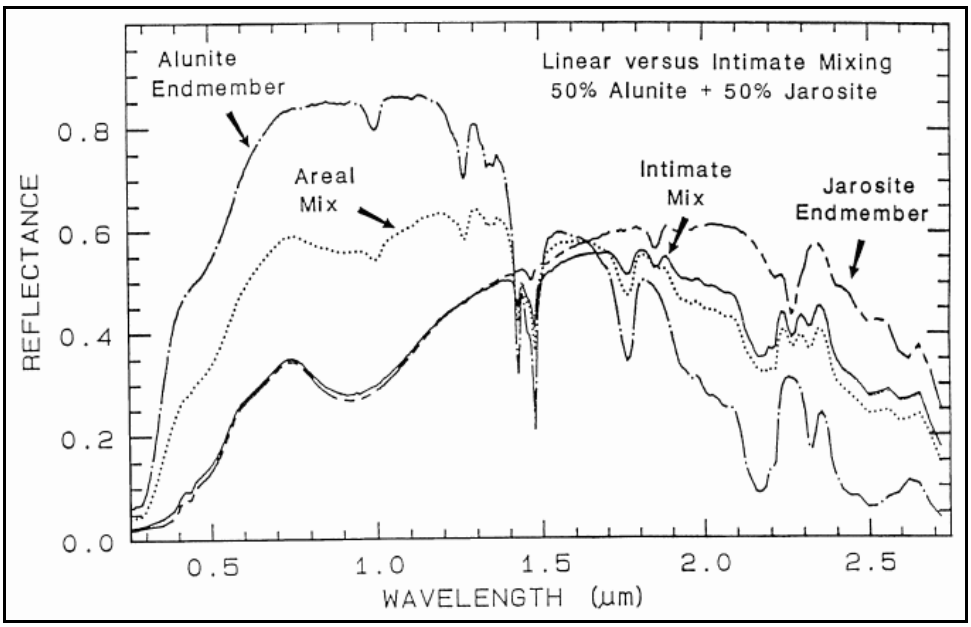

Figure 3.1. Reflectance spectra of alunite, jarosite and mixtures of two (Clark, 1999).

The reason why in the intimate mixture jarosite dominates is because in an intimate mixture, the darker material dominates because photons are absorbed when they encounter a dark grain. In the areal mixture, the brighter material dominates (Clark, 1999).

3.2. Spectral Properties of Gypsum

Many minerals show diagnostic absorption features in the visible to short-wave infrared range due to either electronic or vibrational processes (Hunt et al., 1971). The vibrational processes are more important in evaporate minerals (Crowley, 1991). They are typically caused by excitation of bonds between anion groups.

A sample of USGS Library spectrum of gypsum is shown in Figure 3.2. The spectrum of gypsum shows major absorption features in VNIR and SWIR regions due to overtones and combination tones of molecular water (Hunt et al., 1971). The intensity of the absorption features will decrease and their shapes will change when gypsum is mixed with other salts and substrate minerals (Lindberg and Smith, 1973). The absorption minimum around 1.2 μm is due to a combination of the H-O-H bending fundamental and the first overtones of the O-H stretch (Figure 3.2). The absorption features between 1.4 and 1.6 μm are due to the first overtone of the O-H stretching fundamental. The absorption near 1.74 μm is due to combinations involving the fundamental H-O-H bend, the fundamental O-H stretch, and low frequency vibration modes of the structural water molecules. The strong absorption features near 1.9 μm is due to a combination of the OH stretching and the H-O-H bending fundamentals. The absorption around 2.2 μm is attributed to a combination of the fundamental O-H stretch and the first overtone of the water. All the absorption intervals and the causes of the absorption can be seen in Figure 3.2.

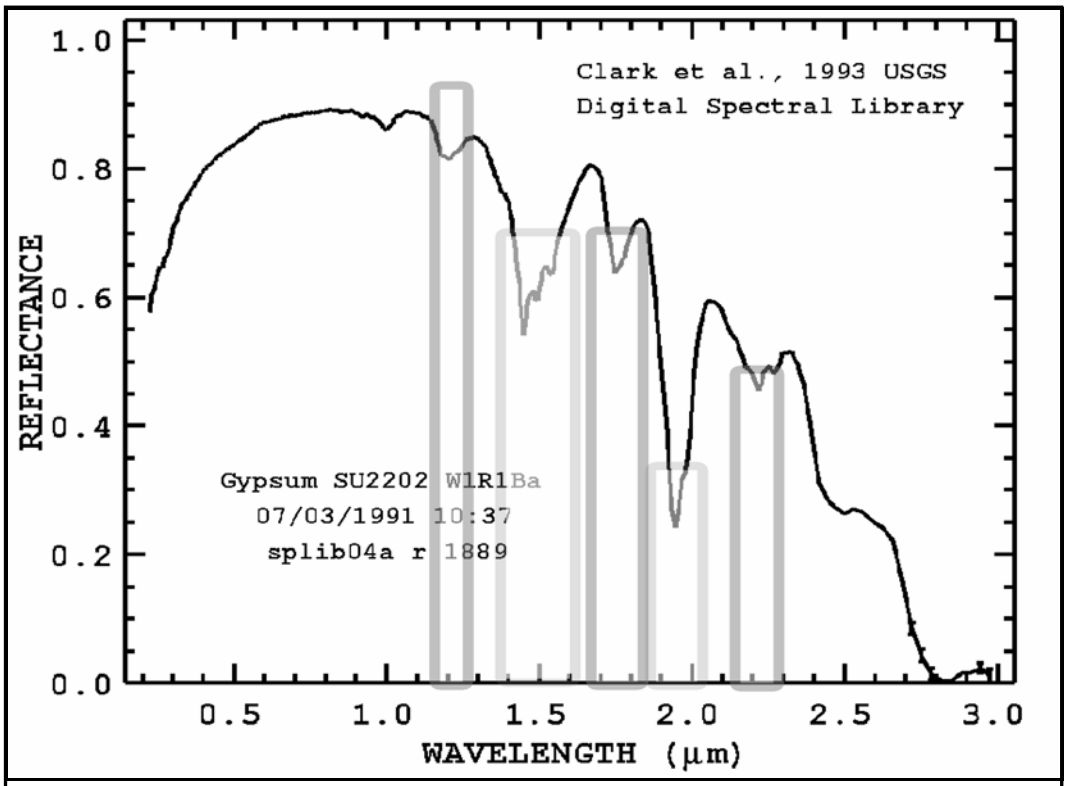

Interval	Reason
1.2 µm	H-O-H bending fundamental and the first overtones of the O-H stretch
1.4 - 1.6 µm	first overtone of the O-H stretching fundamental
1.74 µm	the fundamental H-O-H bend, fundamental O-H stretch, low frequency vibration modes of water.
1.9 µm	OH stretching, the H-O-H bending fundamentals
2.2 µm	fundamental O-H stretch, the first overtone of the water

Figure 3.2. Spectral reflectance curve of Gypsum (USGS Digital Spectral Library) and the absorption intervals of the gypsum mineral (µm) and the causes of the absorption in these intervals.

3.3. Common Techniques of Remote Sensing For Mineral Mapping

There are various methods for mineral mapping by remote sensing. The most common ones are; Band rationing (BR), principal component analysis (PCA), decorrelation stretch (DS) and spectral indices (SI) methods.

3.3.1. Band Rationing

Band rationing is simply dividing numerical values in one band by those in another for each pixel to produce ratio images and it is widely used technique for discriminating lithologies and other surface cover in a scene. By ratioing the data from two different spectral bands, the resultant image enhances variations in the slopes of the spectral reflectance curves between the two different spectral ranges that may otherwise be masked by the pixel brightness variations in each of the bands. The method produces images in which geological materials are enhanced by eliminating the proportionally constant radiance variations from band to band such as terrain illumination or albedo, in addition the result is intensity blind.

Band selection for image ratios depends first on the spectral properties of the surface material and its abundance relative to other surface cover types (Sabine, 1999). The second, selection depends on optimum index factor, OIF; a statistical approach used to determine the highest ranking of combinations of three channels out of the spectral bands (Chaves et al., 1980) and is based on the selection of the greatest variance bands with the least correlation (Jensen, 1996). Generally, the numerator band is chosen in which the material is highly reflective and for the denominator, absorptional property of the material is considered and selection is done according to this feature.

Correlation analysis of Landsat Thematic Mapper (TM) data by Crippen (1989) showed that for arid areas, a combination that includes one ratio from the short-wavelength bands (TM 1-4), one from the long- wavelength bands (TM 5-7) and one ratio with bands from each group produces the best discrimination of

geological materials. Numerous investigators have shown that TM 3/1 best discriminates ferric oxides and TM 5/7 discriminate materials containing hydroxyl-bearing minerals and carbonates with absorption features in the region 2.2 to 2.3 μm (Brickey, 1986; Huntsinpillar, 1988; Kowalczyk and Logan, 1989; Re Kühl, 1992; Bennett, 1993; Sabins and Miller, 1994). TM 4/3 accentuates the red edge in vegetation and TM 5/4 ratio is also used for ferric oxides in areas where vegetation is a problem. Davis et al. (1989) used a color composite of TM ratios 1/4, 3/4, 4/7 to discriminate phosphorite beds in Saudia Arabia. In SPOT and Landsat MSS imaginary, 2/1 ratio is used to enhance ferric oxides. Fadda (2003) used a band ratio composite of 5/7, 3/1, 5/4 on Landsat TM image to distinguish several basaltic flows, regional structure and dykes in Jordan.

Band ratio became an important method for studying earth materials with ASTER imagery also. Similar to Landsat TM and ETM, ASTER band-ratio combinations are effective in emphasizing spectral characteristics of certain rocks and minerals and hence are more effective in lithological mapping compared to the RGB band combination images (Abdeen et al., 2001; Bedell, 2001; Hewson et al., 2001; Rowan and Mars, 2003; Rowan et al., 2003; Velosky et al., 2003).

Gad and Kusky (2006) introduced an ASTER band ratio image; 4/7, 4/6, 4/10 that has a high optimum index factor (OIF) and indicative spectral features within these bands. As ASTER band-ratio combination include SWIR bands (band 4,6,7) together with TIR bands (band 10) that have different spectral resolution (90 m) the TIR pixel size is resized to that of SWIR bands (30 m). They compared the band combination with other combinations such as 4/7-3/4-2/1 and 7/6-6/5-6/4 which were used by Abdeen et al (2001) and Wolters et al. (2005) respectively. They emphasize that the ASTER band-ratio image 4/7-4/6-4/10 is powerful in distinguishing the subtle differences between the various rock units including migmatites, meta-pelites, meta-psammites, meta-acidic volcanics, gabbro and granitic rocks in the study area. San et al. (2004) compared band ratio and spectral index methods for mapping alunite and kaolinite minerals. They used ASTER 4/5

and 7/6 band ratios to discriminate alunite and kaolinite respectively. Tommasso and Rubinstein (2006), used band combinations 4/5, 4/6, 4/7 and 4/6, 4/7, 3/1 successfully for alteration mapping using ASTER images in Argentina. Gürçay (2008) applied band ratio method to extract gypsum and alunite by using ASTER images at Kayseri region in Turkey.

3.3.2. Principle Component Analysis (PCA)

Principal Component Analysis (PCA) is a multivariate analysis technique that was first introduced by Pearson in 1901. The principal-components transformation, originally known as the Karhunen-Loeve transformation is used to compress multispectral data sets by calculating a new coordinate system (Sabins, 1987). It is commonly used to reduce the dimensionality of a data set with a large number of interdependent variables. This reduction is achieved by finding a set of N_t orthogonal vectors in the input space of dimensions N_c, with $N_t < N_c$ which accounts for much of the data variance.

Most of the variation of radiant spectral flux measured by a sensor depends on slope aspect relative to solar illumination and albedo effects at the surface. Very little of this variation arises from spectral reflectance features of surface materials. According to Sabine (1999) the principal component analysis (PCA) is a powerful means of suppressing irradiance effects that dominate all bands so that geologically interesting spectral reflectance features of surface materials can be examined. PCA is also useful in reducing the dimensionality of multispectral data and the high degree of band-to-band correlation that is inherent in such data sets.
A principle component (PC) transformation requires data rotation and translation into a new set of statistically independent orthogonal axes which are the principal components (eigenvalues of the covariance matrix) of the data set. The origin of the new coordinate system is the mean of the original data set. The number of the PCs is the same as the number of spectral bands used in the transformation. For each PC, new numerical values are assigned to each pixel according to its new coordinates and may have no relationship to values in the original data.

PC1 is usually dominated by illumination effects arising from differences in slope aspect relative to the sun and provides a good noise-free representation of topography. Spectral reflectance features of surface materials and noise appear in higher-numbered PCs (Sabine, 1999). Because PCA is a statistical procedure, the information in each PC is scene dependent.

The process is easily explained graphically with an example of data in two bands. Figure 3.3 is an example of a two-band scatter plot, which shows the relationships of data file values in two bands. The values of one band are plotted against those of the other. If both bands have normal distributions, an ellipse shape results (Figure 3.3).

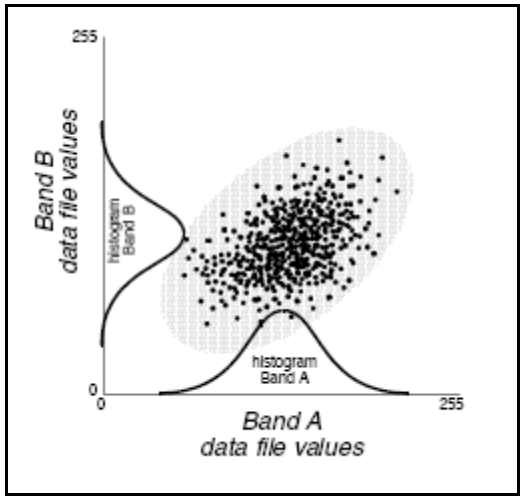

Figure 3.3. Normal distribution of Band A & Band B forming ellipse shape

To perform PCA, the axes of the spectral space are rotated, changing the coordinates of each pixel in spectral space, as well as the data file values. The new axes are parallel to the axes of the ellipse.

The length and direction of the widest transect of the ellipse are calculated using matrix algebra in a process explained below. The transect, which corresponds to the major (longest) axis of the ellipse, is called the first principal component of the

data. The direction of the first principal component is the first eigenvector, and its length is the first eigen value (Taylor, 1977).

A new axis of the spectral space is defined by this first principal component. The points in the scatterplot are now given new coordinates, which correspond to this new axis. Since, in spectral space, the coordinates of the points are the data file values, new data file values are derived from this process. These values are stored in the first principal component band of a new data file.

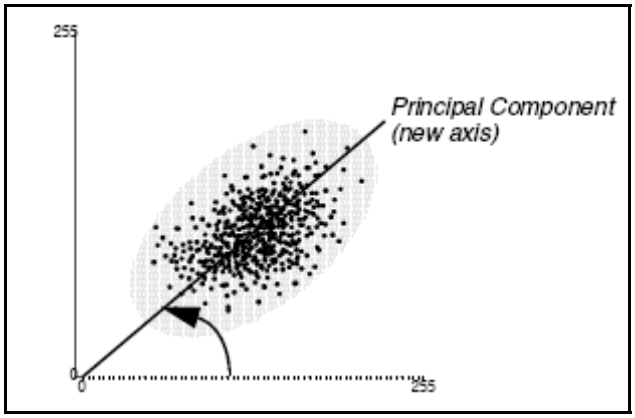

Figure 3.4. The graph showing the first principal component.

The first principal component shows the direction and length of the widest transect of the ellipse (Figure 3.4). Therefore, as an axis in spectral space, it measures the highest variation within the data. In Figure 3.5 it is easy to see that the first eigenvalue is always greater than the ranges of the input bands, just as the hypotenuse of a right triangle must always be longer than the legs.

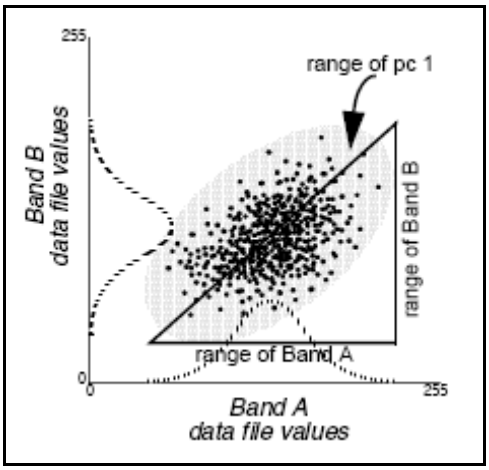

Figure 3.5. The graph showing the range of first principle component.

The second principal component is the widest transect of the ellipse that is orthogonal (perpendicular) to the first principal component. As such, the second principal component describes the largest amount of variance in the data that is not already described by the first principal component (Taylor, 1977). In a two-dimensional analysis, the second principal component corresponds to the minor axis of the ellipse (Figure 3.6).

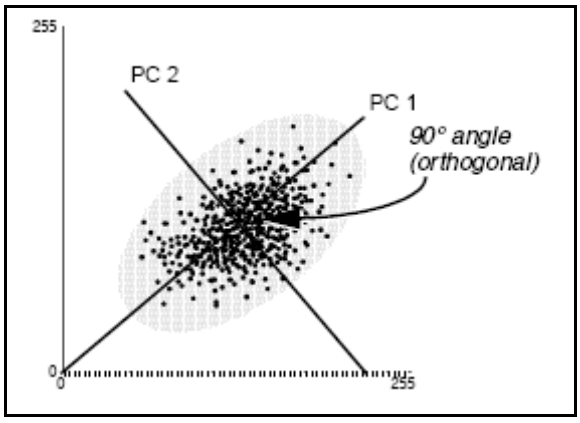

Figure 3.6. The graph showing second principle component.

In *n* dimensions, there are *n* principal components. Each successive principal component:

• is the widest transect of the ellipse that is orthogonal to the previous components in the *n*-dimensional space of the scatterplot (Faust, 1989), and

• accounts for a decreasing amount of the variation in the data which is not already accounted for by previous principal components (Taylor, 1977).

To compute a principal components transformation, a linear transformation is performed on the data, meaning that the coordinates of each pixel in spectral space (the original data file values) are recomputed using a linear equation. The result of the transformation is that the axes in *n*-dimensional spectral space are shifted and rotated to be relative to the axes of the ellipse.

To perform the linear transformation, the eigenvectors and eigenvalues of the *n* principal components must be mathematically derived from the covariance matrix, as shown in the following equation:

$$V = \begin{bmatrix} v_1 & 0 & 0 & \dots & 0 \\ 0 & v_2 & 0 & \dots & 0 \\ & & \dots & & \\ 0 & 0 & 0 & \dots & v_n \end{bmatrix} \qquad \mathrm{E}\, Cov\, \mathrm{E}^{\mathrm{T}} = \mathrm{V}$$

Where:

Cov = the covariance matrix
E = the matrix of eigenvectors
T = the transposition function
V = a diagonal matrix of eigenvalues, in which all nondiagonal elements are zeros

V is computed so that its nonzero elements are ordered from greatest to least, so that;

v1 > *v2* > *v3*... > *vn* (Faust, 1989)

The matrix *V* is the covariance matrix of the output principal component file. The zeros represent the covariance between bands (there is none), and the eigenvalues are the variance values for each band. Because the eigenvalues are ordered from *v*1 to *vn*, the first eigenvalue is the largest and represents the most variance in the data.

Each column of the resulting eigenvector matrix, *E*, describes a unit-length vector in spectral space, which shows the direction of the principal component (the ellipse axis). The numbers are used as coefficients in the following equation, to transform the original data file values into the principal component values.

$$P_e = \sum_{k=1}^{n} d_k E_{ke}$$

Where:

e = the number of the principal component (first, second)

P_e = the output principal component value for principal component band *e*

k = a particular input band

n = the total number of bands

d_k = an input data file value in band *k*

E = the eigenvector matrix, such that E_{ke} = the element of that matrix at row *k,* column *e* (Gonzalez and Wintz, 1977)

In summary, the principal-components transformation is very useful technique for geological remote sensing analysis and has various advantages such as: (1) most of the variance in a multispectral data set is compressed into one or two PC images; (2) noise may be sent to the less- correlated PC images; (3) spectral differences between materials may be more apparent in PC images than in individual bands.

3.3.3. Feature- Oriented Principle Component Selection (FPCS)

Crosta and Moore (1989) developed a technique based on PCA for mapping iron oxide/hydroxides related to sulphide ore bodies in granite–greenstone belt terrains using Landsat TM. The technique, called 'feature-orientated principal component selection' (FPCS), relied on establishing the relationship between the spectral responses of target materials (ferric-oxide-rich soils) and numeric values extracted from the eigenvector matrix used to calculate the principal component (PC) images. Using this relationship, they were able to determine which PCs contained the spectral information due to iron minerals and whether the digital numbers (DNs) of pixels containing the target materials had high (bright) or low (dark) values.

Loughlin (1991) modified the FPCS technique by selecting specific Landsat TM band sets and applying PCA separately to them, to ensure that certain materials (e.g. vegetation) would not be mapped and that spectral information due to target materials (alteration minerals) would be mapped into a single PC. The procedure proposed by Loughlin used Landsat TM band sets comprising bands 1, 3, 4 and 5 for deriving spectral information related to ferric oxides/hydroxides, which would be uniquely mapped into either PC3 or PC4. Another band set, comprising bands 1, 4, 5 and 7, was similarly used to derive information related to hydroxyl-bearing minerals and carbonates, also uniquely mapped into either PC3 or PC4.

This procedure, modified by Loughlin (1991) the 'Crosta technique', has been successfully used for mineral exploration purposes due to its ease of use and power (Bastianelli et al. 1993, Davidson et al. 1993, Ruiz-Armenta and Prol-Ledesma 1998, Souza Filho and Drury 1998, Tangestani and Moore 2001, 2002, Carranza and Hale 2002). In regions subject to mineral exploration and with favorable conditions (sparse or no vegetation, exposed bedrock, etc.), such as in the South American Cordillera, this technique has become a standard operational tool for alteration mapping using Landsat TM.

The idea of applying PCA to derive mineral abundance maps using high spectral resolution data was proposed by Crosta et al. (1996), He used 24-band Geoscan data, covering the VNIR, SWIR and thermal infrared (TIR) portions of the electromagnetic spectrum (a similar spectral coverage to that provided by ASTER), to produce abundance images of hematite, goethite, calcite– chlorite, muscovite–sericite–kaolinite and silica concentrations, related to gold mineralization in hydrothermally altered greenstone belt rocks.

Crosta (2003) applied PCA to subsets of four ASTER bands, using an adaptation of the Crosta technique proposed by Loughlin (1991). After applying PCA, the eigen matrix used to calculate PCA for each subset was examined, to identify which PC contained the target (mineral) information. The criterion for the identification is the same proposed by Loughlin (1991): the PC that contains the target spectral information shows the highest eigenvector loadings from the ASTER bands, coinciding with the target's most diagnostic features but with opposite signs (+ or -). With the use of this method he distinguished Kaolinite, Illite and Alunite and checked the results using field spectroscopy. Results were in agreement with the minerals identified by the PCA method at each side and provide qualitative evidence support the validity of the method.

3.3.4. Decorrelation Stretch

"Decorrelation stretching" was introduced by Soha and Schwartz (1978), improving earlier work by Taylor (1973). The technique is based on a principle component (PC) transformation of the acquired data. Often such transformed images themselves are contrast-stretched and arbitrarily assigned primary colors for display as a color composite picture. "Decorrelation stretching" differs in that after contrast enhancement the statistically independent (decorrelated) PC images are retransformed to the original coordinates for display, so that in general there is little distortion of the perceived hues due to the enhancement (Gillespie et al., 1986)

The principal component transformation provides a straightforward method of removing the correlation from multispectral image data, and has the added benefit of providing a method of reducing the dimensionality of multispectral images. Its primary drawback arises from the fact that its color assignments are not readily associated to any physical quantity, and may be dramatically scene and processing dependent.

Taylor (1973) pointed out that once the multispectral data have been decorrelated by a coordinate system rotation, and the variances equalized in this new coordinate space, any additional rotation of the new coordinate space would not re-introduce correlation. He went on to compare several alternative additional rotations for a return to a more interpretable coordinate system.

Soha and Schwartz (1978) proposed that for most remote sensing applications, the simple inverse rotation to the original color space was the rotation most suitable for image interpretation. It is this technique that has been given the name "decorrelation stretch", despite the fact that all of the above techniques involve contrast stretching and yield uncorrelated outputs.

Decorrelation stretching is accomplished in four steps. In the first step, the covariance matrix is determined for the image and the eigenvectors are calculated. In the second step, the image is actually transformed from the radiance domain to the PC space. It is just a special linear transformation of the radiance space, but the transformed data have the unique property that they are statistically independent or “decorrelated”. In the third step, the PC images are separately contrast-stretched, generally to equalize the variances of the three or more images with the highest signal-to-noise ratios. In the fourth step, the inverse transformation is calculated that would rotate the unstretched PC images back to the original radiance space, and this transformation is applied to the stretched data. Even though the data are retransformed to the radiance space, the covariance of the enhanced images is reduced (Gillespie, 1992).

3.3.5. Spectral Indices

The concept of the spectral index was initiated by Kauth and Tomas (1976), who proposed four indices called Brightness, Greenness, Yellowness and Nonsuch using the four Landsat MSS bands. This method has been widely accepted as the Tasselled Cap transformation for assessing vegetation (Crist and Cicone 1984). Richardson and Wiegand (1977) developed a two-dimensional Perpendicular Vegetation Index (PVI) using two bands of the Landsat MSS. Jackson (1983) showed that these indices were special cases of a class of spectral indices, formed by linear combinations of n spectral bands, in n-dimensional space.

A spectral index is similar to PCA in the sense that both are orthogonal transformations of multispectral data. A fundamental difference between these two methods is that the spectral indices define the transform axes to represent specific spectral patterns of interest, while PCA determines the transform axes mathematically to maximize variance of multispectral data. PCA can also be used to reduce dimensionality of multispectral data without significant information loss. Visual interpretation for discrimination and mapping of surface materials may be enhanced by a color composite image of major principal components (Yamaguchi and Naito, 2003).

In contrast, as spectral indices uses pre-determined transform coefficients, it is possible to know physical meanings of a transformed result to some degree (Crist and Cicone 1984). This means that it is easy to interpret resultant spectral index images from a geological point of view, if we use spectral indices for discrimination and mapping of surface rock types (Yamaguchi and Naito, 2003).

For ASTER images both for SWIR and TIR bands some indices are calculated by different researchers. Yamaguchi and Takeda (2003) defined alunite, kaolinite, calcite, brightness indices in SWIR region. Ninomiya (2002) defined quartz, carbonate and silica indices in TIR region of ASTER and discussed the possibility of mapping quartz, carbonate minerals and silicate rocks with them.

CHAPTER 4

DATA ANALYSIS

4.1. Data

Data used for the analysis of remote sensing techniques in this thesis include ASTER data and geological map of the area.

4.1.1. ASTER image

As previously discussed for the analysis in this thesis to map evaporate minerals, ASTER image is used. The Advanced Spaceborne Thermal Emission and Reflection Radiometer (ASTER) is an advanced multispectral imager that was launched on board NASA's Terra spacecraft in December, 1999. ASTER covers a wide spectral region with 14 bands from the visible to the thermal infrared with high spatial, spectral and radiometric resolution. An additional backward-looking near-infrared band provides stereo coverage. The spatial resolution varies with wavelength: 15 m in the visible and near-infrared (VNIR), 30 m in the short wave infrared (SWIR), and 90 m in the thermal infrared (TIR) (Table 4.1). Each ASTER scene covers an area of 60 x 60 km. The Terra spacecraft is flying in a circular, near-polar orbit at an altitude of 705 km. The orbit is sun-synchronous with equatorial crossing at local time of 10:30 a.m., returning to the same orbit every 16 days (ASTER User Handbook, Version 2).

Table 4.1. Spectral and spatial properties of ASTER images in different wavelength intervals.

Subsystem	Band No.	Spectral Range (μm)	Spatial Resolution, m	Quantization Levels
VNIR	1	0.52-0.60	15	8 bits
	2	0.63-0.69		
	3N	0.78-0.86		
	3B	0.78-0.86		
SWIR	4	1.60-1.70	30	8 bits
	5	2.145-2.185		
	6	2.185-2.225		
	7	2.235-2.285		
	8	2.295-2.365		
	9	2.360-2.430		
TIR	10	8.125-8.475	90	12 bits
	11	8.475-8.825		
	12	8.925-9.275		
	13	10.25-10.95		
	14	10.95-11.65		

Throughout the thesis the image with AST3A1 050727084419060331 1230 granule ID is used. The details about the scene can be seen at the Table 4.2. All the VNIR, SWIR and TIR bands of the image are used for the analysis.

Table 4.2. The detailed information about the ASTER scene used.

Granule ID	AST3A1 050727084419060331 1230
Processing Level	3
Acquisition Date	2005-07-27
Source data Product	ASTL1A 050727084419050801 0463
Scene Center	39.401273, 33.394811
Scene Upper Left	39.729527, 32.954812
Scene Upper Right	39.726497, 33.840073
Scene Lower Right	39.070573, 33.832242
Scene Upper Left	39.073534, 32.955234
Solar Direction	139.059897, 65.064964
Map Projection Name	Universal Transverse Mercator
Ellipsoid and Datum	WGS 84, WGS 84
UTM Zone Code	36

4.1.2. Geological Map

Geological map used as base map in this thesis is modified from Dönmez et al. (2007) which is done by MTA. This map is a collection of previous studies which are performed by different researchers for years. They used common names for formations in order to end the conflict about the names also they defined new members and formation names. For detecting the areas including gypsum all the geological maps in MTA archives are searched and final gypsum bearing unit map is formed. The geological map is classified as base rocks, the Tertiary formations that don't include gypsum and the Tertiary formations that include gypsum (Figure 4.1). According to this map our results should be located in the parts shown by 0.

4.2. Methodology

The ASTER image analyses in the thesis starts with the selection of proper scene since it is very important to have the best cloud free image for analyses. From MTA Remote Sensing Center Library the scene with AST3A1 05072708441906033112230 granule ID is selected. After obtaining the raw data, preprocessing, methods for mineral mapping, comparison of methods with geological map, ground truth and selection of the best result steps were done during the study (Figure 4.2).

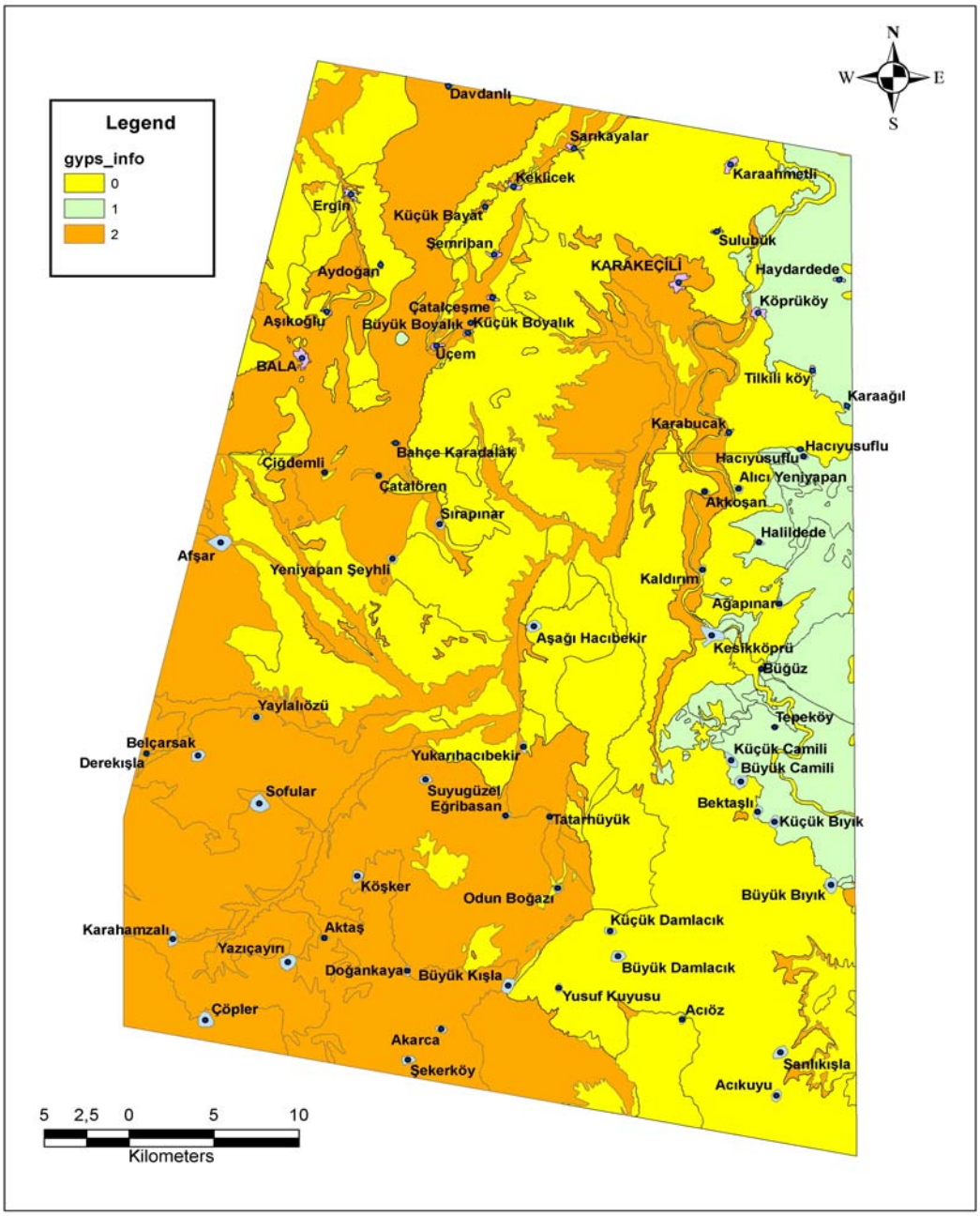

Figure 4.1. The classified geological map of the study area; 0 stands for formations including gypsum, 1 stands for base rocks, 2 stands for Tertiary formations do not include gypsum (Modified from Dönmez et al. 2007)

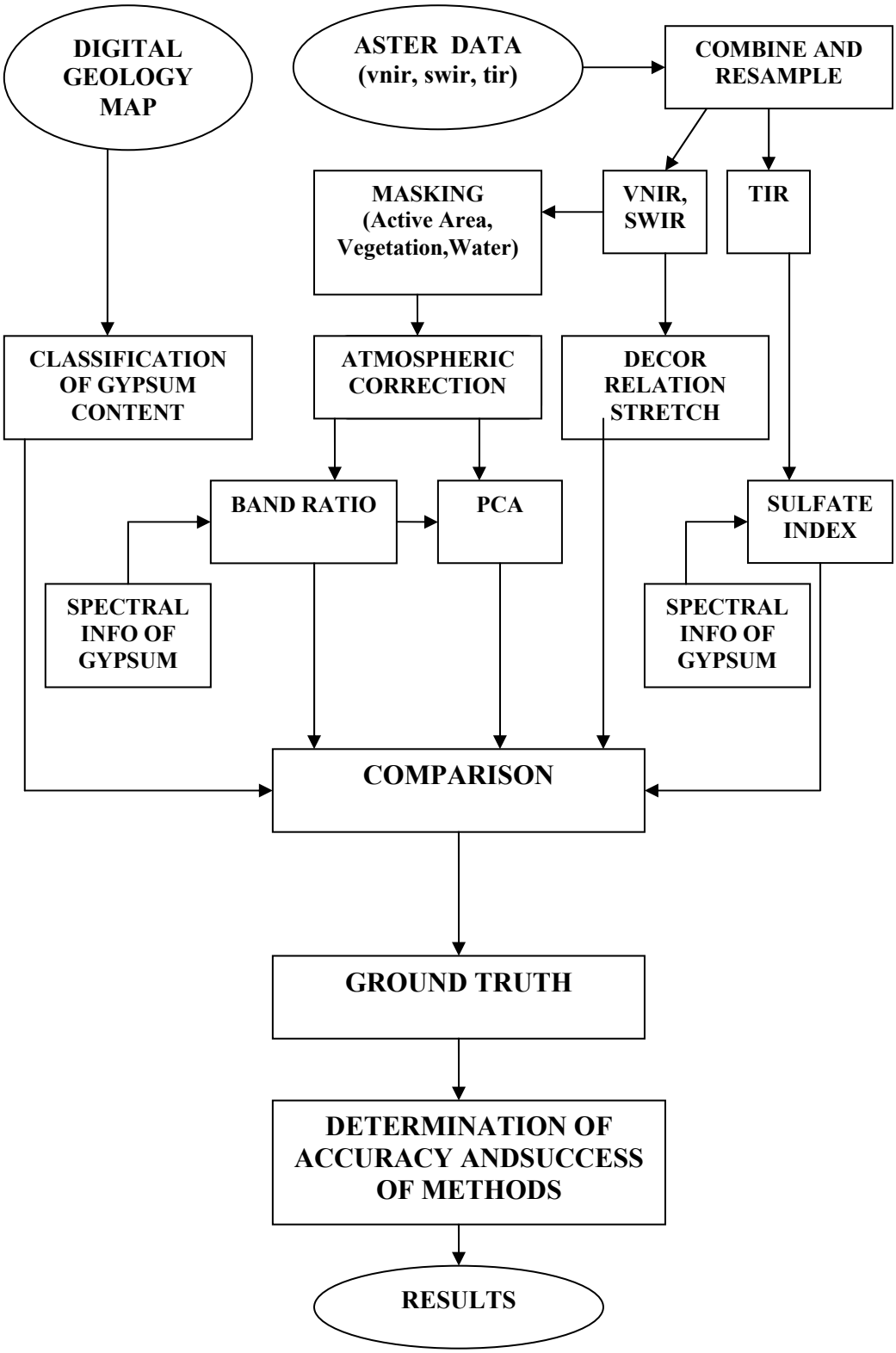

Figure 4.2. The Flowchart of the ASTER image analyses.

4.3. Preprocessing

Preprocessing of ASTER image includes registering, masking and atmospheric correction. First the data have been registered to UTM Zone 36 WGS 84 using PCI Geomatica Software. The VNIR, SWIR and TIR bands of the ASTER image are imported separately using PCI Geomatica software and then they are combined under a single file. The coordinated image can be seen in Figure 4.3.

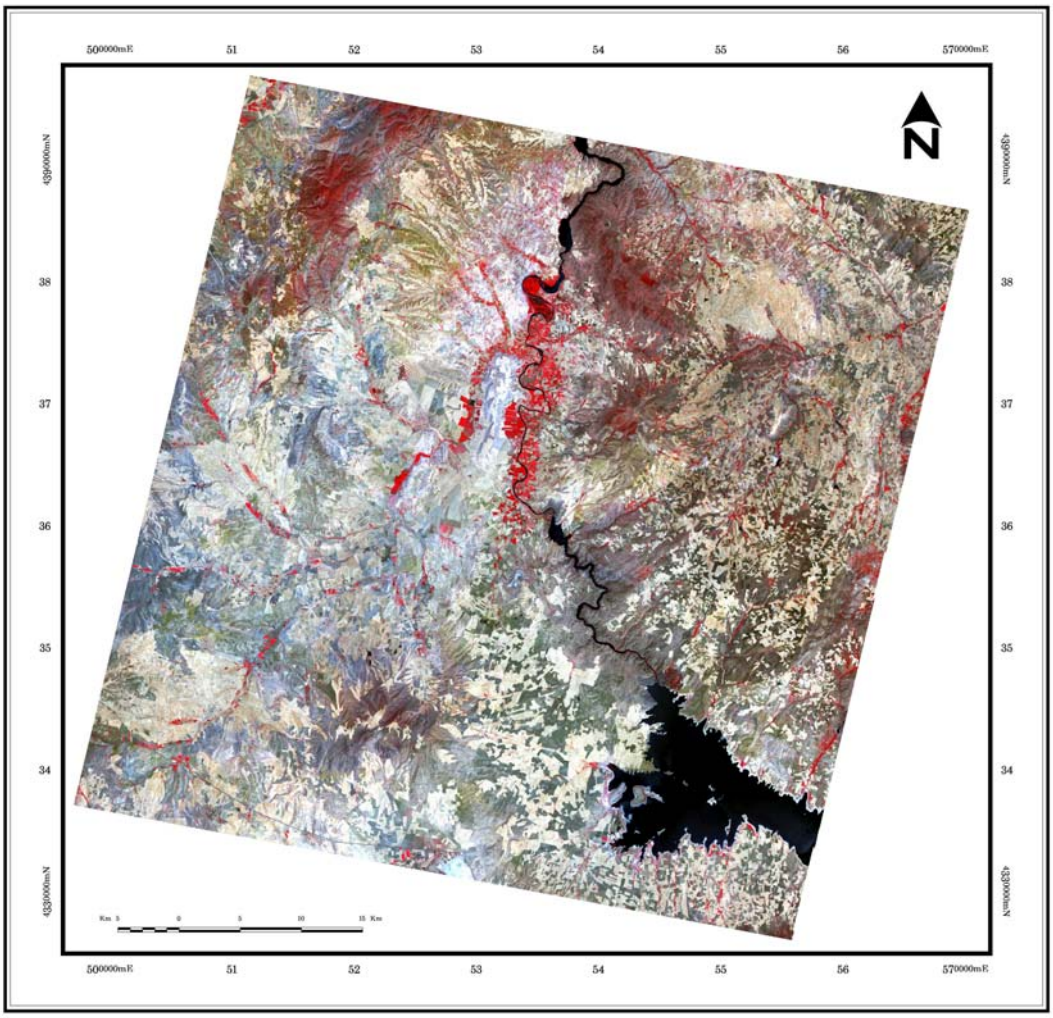

Figure 4.3. The coordinated ASTER image in false color (3, 2, 1)

4.3.1. Masking

Before starting analysis of satellite data, it is important to reduce as possible as or remove non-related data values from original image data. Thus the data to be removed should not be related to our interest. In this thesis we deal with rock units and minerals so that vegetation and water bodies should be removed or reduced.

First active area masking, then water body mask is applied to the image and finally vegetation is masked for the image and in order to mask vegetation NDVI (Normalized Difference Vegetation Index) is used (Figure 4.4).

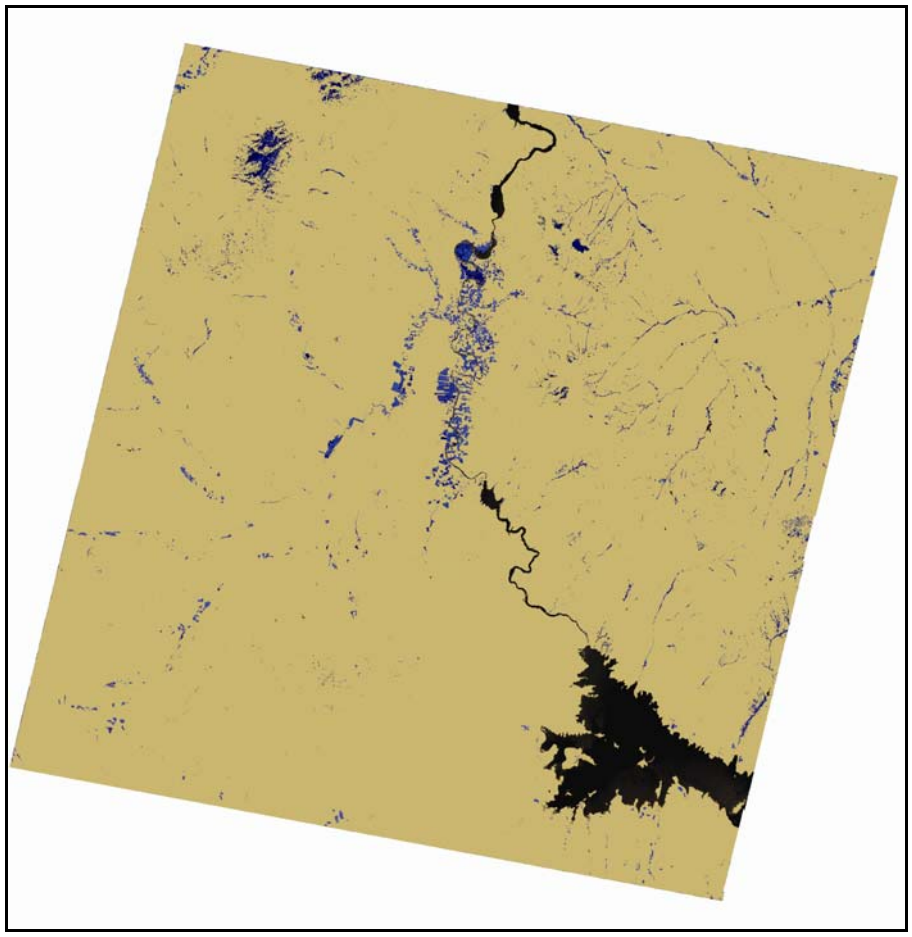

Figure 4.4. Water and vegetation masking, black color show water areas, blue color shows vegetation, beige areas show the data that will be used in our analysis.

4.3.2. Atmospheric Correction

Path radiance is the result the light scattering back to the satellite sensor by haze in the earth's atmosphere. Since the amount of scattering varies with wavelength, the path radiance effect is greatest for the shortest wavelengths, falling off rapidly with increasing wavelength.

In this thesis, dark object subtraction method is used for atmospheric correction. The main advantages of this method are that it is strictly an image-based procedure, does not require in-situ field measurements and it is simple.

In order to use this method the minimum DN number of each band should be found (Table 4.3.). After determination of these values subtraction is applied for all VNIR- SWIR bands and an example can be seen in Figure 4.5. In this example atmospheric correction is applied to band 3. The minimum DN is subtracted from raw DN.

Table 4.3. Minimum DN of the bands.

BAND	MINIMUM
1	57
2	31
3	20
4	12
5	15
6	13
7	16
8	14
9	17

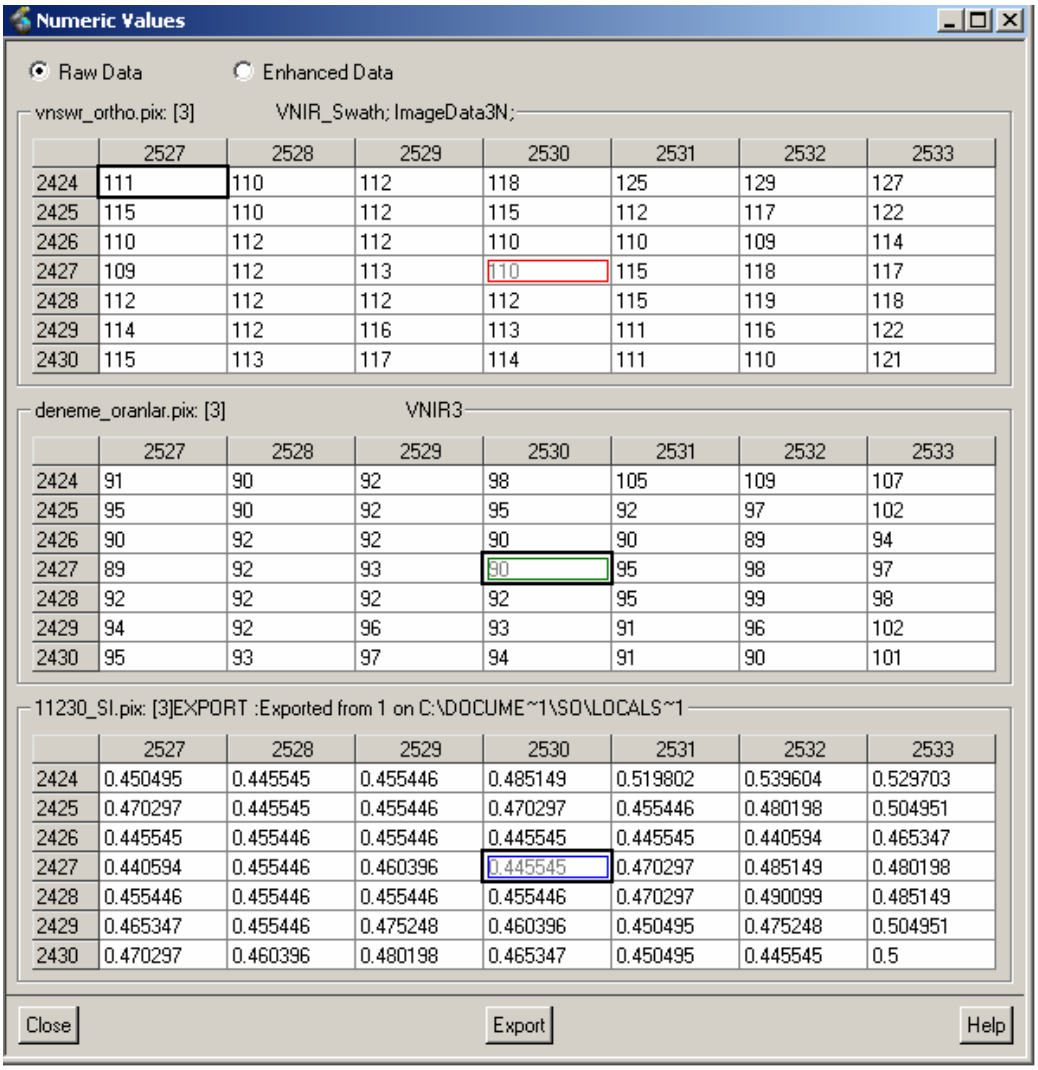

	2527	2528	2529	2530	2531	2532	2533
2424	111	110	112	118	125	129	127
2425	115	110	112	115	112	117	122
2426	110	112	112	110	110	109	114
2427	109	112	113	110	115	118	117
2428	112	112	112	112	115	119	118
2429	114	112	116	113	111	116	122
2430	115	113	117	114	111	110	121

	2527	2528	2529	2530	2531	2532	2533
2424	91	90	92	98	105	109	107
2425	95	90	92	95	92	97	102
2426	90	92	92	90	90	89	94
2427	89	92	93	90	95	98	97
2428	92	92	92	92	95	99	98
2429	94	92	96	93	91	96	102
2430	95	93	97	94	91	90	101

	2527	2528	2529	2530	2531	2532	2533
2424	0.450495	0.445545	0.455446	0.485149	0.519802	0.539604	0.529703
2425	0.470297	0.445545	0.455446	0.470297	0.455446	0.480198	0.504951
2426	0.445545	0.455446	0.455446	0.445545	0.445545	0.440594	0.465347
2427	0.440594	0.455446	0.460396	0.445545	0.470297	0.485149	0.480198
2428	0.455446	0.455446	0.455446	0.455446	0.470297	0.490099	0.485149
2429	0.465347	0.455446	0.475248	0.460396	0.450495	0.475248	0.504951
2430	0.470297	0.460396	0.480198	0.465347	0.450495	0.445545	0.5

Figure 4.5. Figure showing the DN before and after atmospheric correction. Red box shows the raw DN value, green box shows the atmospherically corrected DN.

4.4. Image Analyses

Image analyses constitute the most commonly used analyses that are used for mineral mapping. In this thesis for mapping gypsum minerals Band Ratio, Decorrelation Stretch, Feature Oriented Principle Component (Crosta) Technique and Spectral Indices methods are used.

4.4.1. Band Ratio

As discussed in Chapter 3 band ratio is widely used technique for discriminating lithology and is simply dividing numerical values in one band to the values of the other band. Selection of the bands for band ratio depends on the spectral reflectance properties of the materials you want to distinguish.

When the spectral reflectance curve of the gypsum is considered according to the band intervals of ASTER image band 4 and band 8 gives high reflectance whereas band 6 and band 9 gives low reflectance (Figure 4.6). Although the minimum reflectance is near 1.9-2.0 micrometer, there is no ASTER band covering that interval.

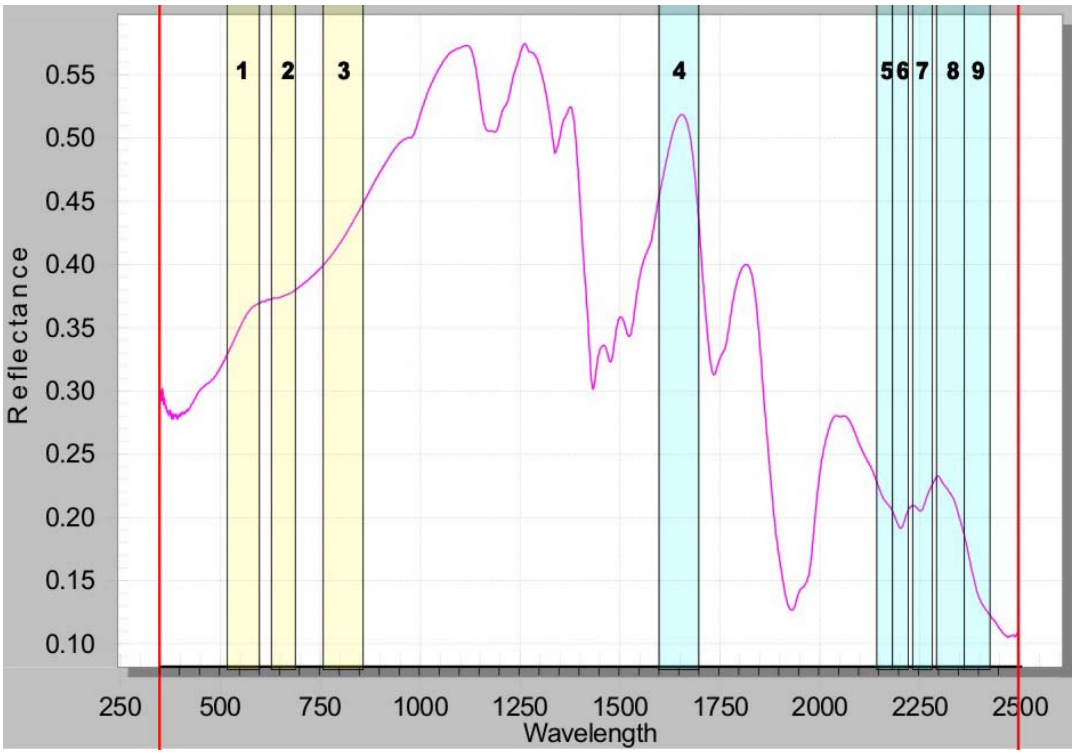

Figure 4.6. Spectral curve of Gypsum and location of ASTER bands.

According to the spectral reflectance curve of gypsum mineral the high reflectance and low reflectance areas are considered so that 4/6, 4/9, 8/9, 8/6 band ratios are

tried. Since ASTER bands 4 and 8 give high reflectance and bands 6 and 9 give low reflectance first dividing high reflectance bands to low ones are considered. Also using combination of the high reflectance bands 4+8 / 6 and 4+8 / 9 ratios are tried. Some thresholds should be set in order to assess the success of the band ratios with respect to field observations and the gypsum bearing rock units map. After the band ratio operation the mean value and the standard deviation under total mask can be read from PCI Geomatica software (Figure 4.7). For deciding the thresholds that will be applied to this image, the best known places that we are sure to have gypsum are used as anchor points. Within these areas the minimum values are selected for the thresholds. All the mean values, standard deviations and threshold applied to the ratios are listed in the Table 4.3. The results of the different used band ratios after thresholding are occurred as bitmaps. These results are put above band 3 to get better visualization that can be seen in Figure 4.8, 4.9, 4.10, 4.11, 4.12, 4.13.

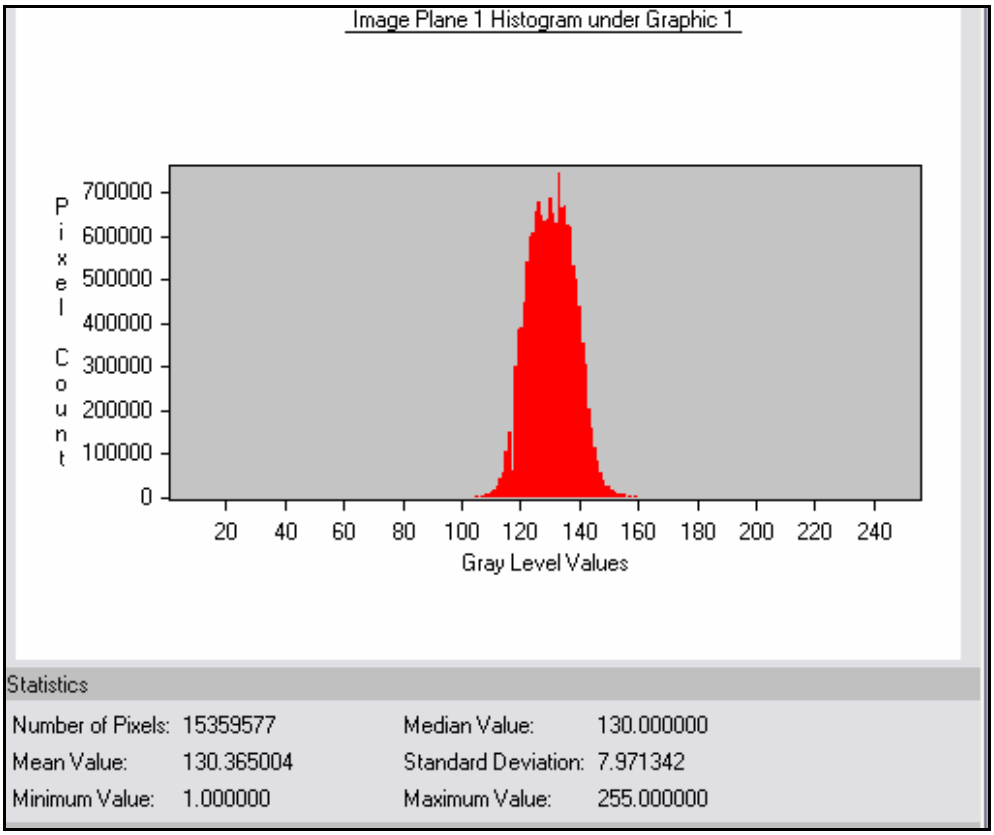

Figure 4.7. Mean value and standard deviation calculated by PCI Geomatica for band ratio 4/6.

Table 4.4. Applied Band Ratios and their mean, standard deviation, threshold values.

Band Ratio	Mean	Standard Dev.	Threshold
4 / 6	130,36500	7,97100	146
4 / 9	79,02650	10,87270	105
8 / 9	54,99403	4,54397	64
(4 + 8) / 6	79,37715	4,63732	89
(4 + 8) / 9	93,82737	6,49189	108
8 / 6	46,99058	4,63783	55

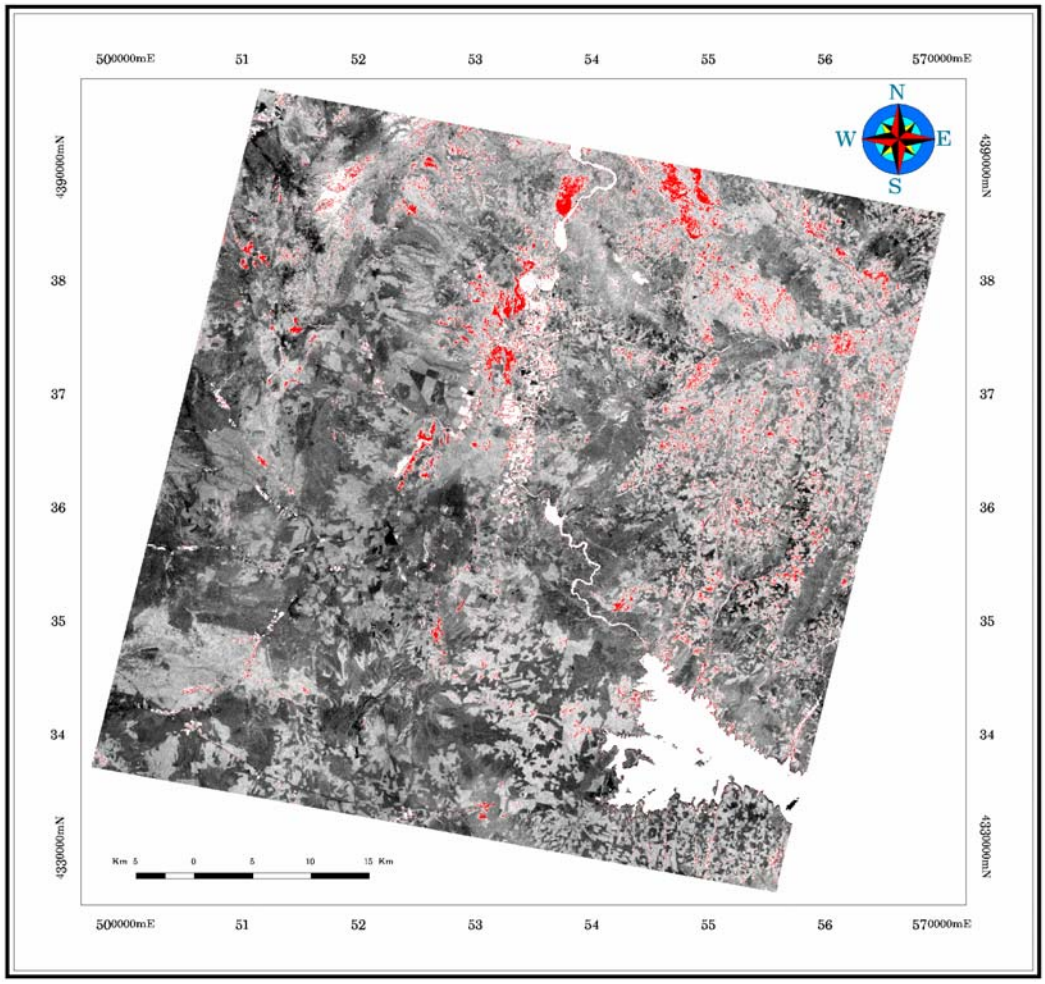

Figure 4.8. Band ratio 4/6 applied on the image and applied threshold. The red parts showing the resultant areas the below image is band 3.

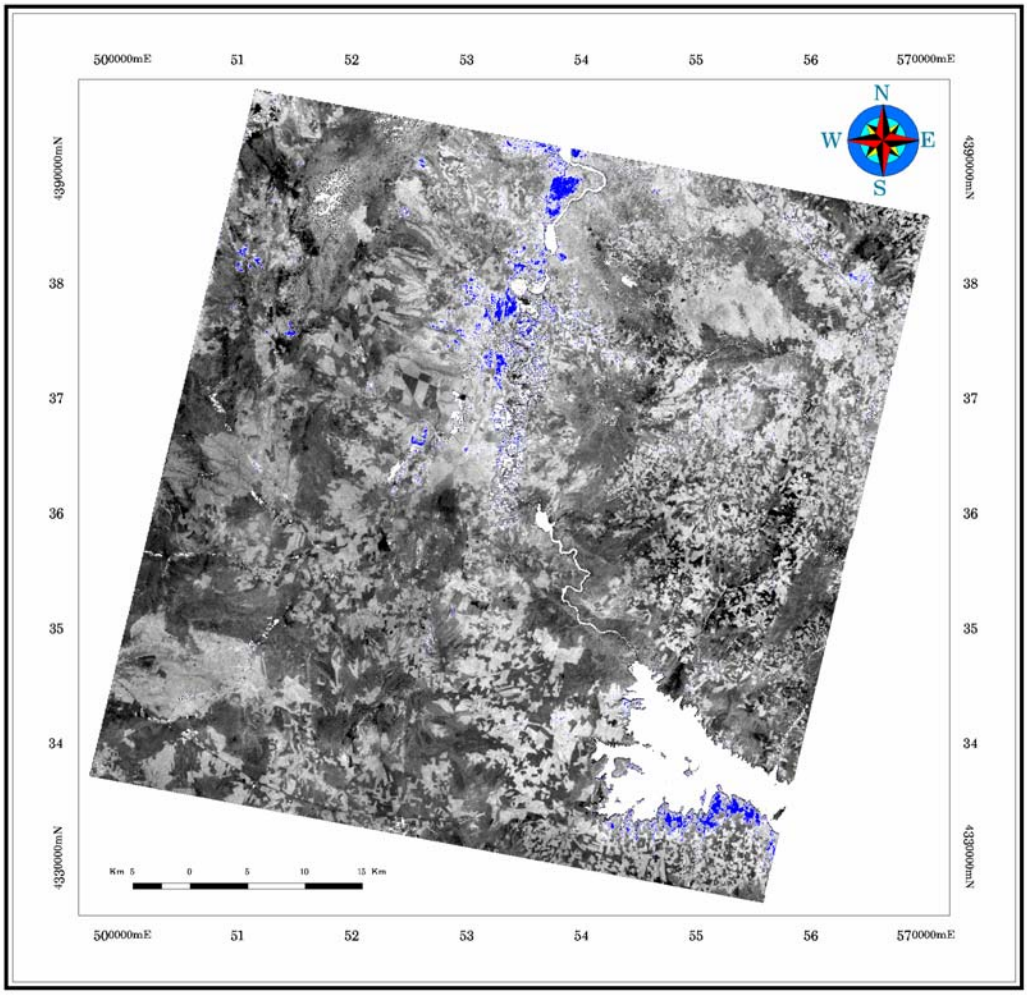

Figure 4.9. Band ratio 4/9 applied on the image and applied threshold. The blue areas show the results and below image is band 3.

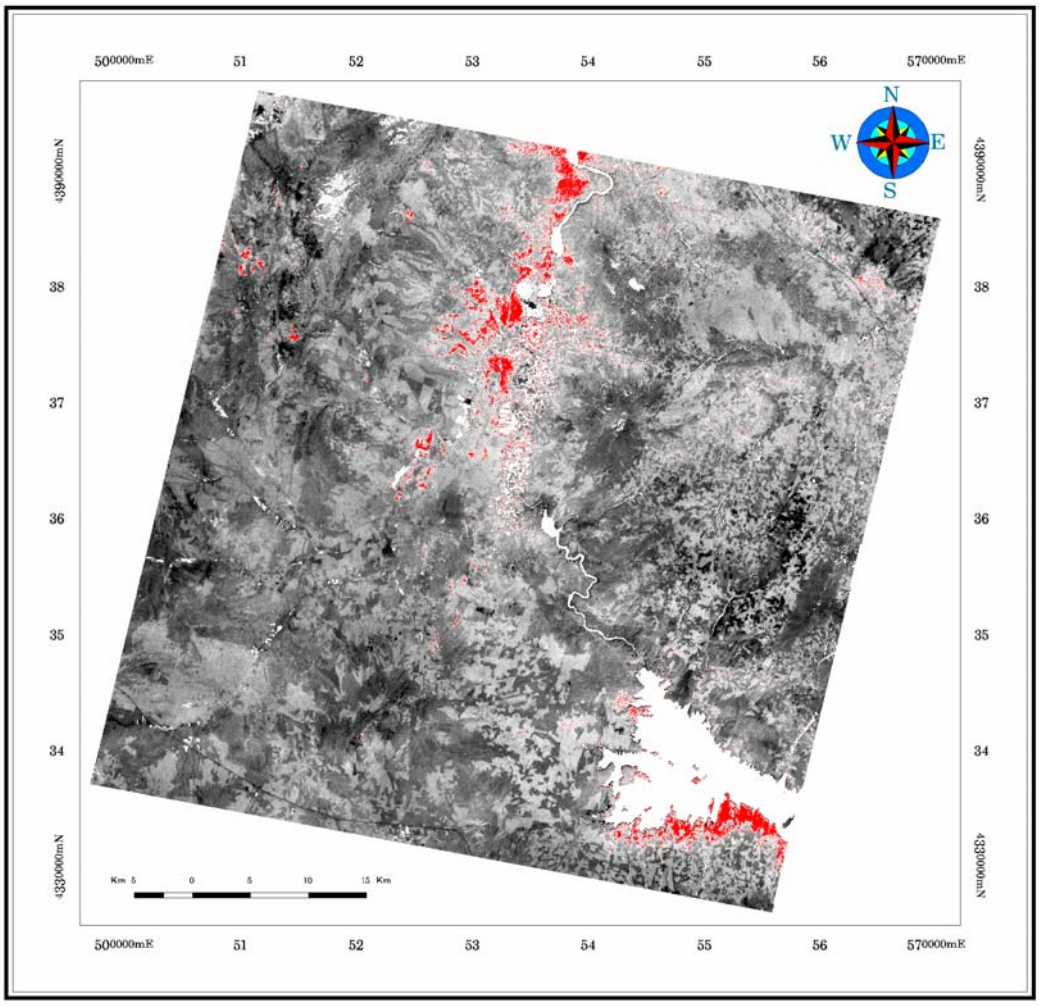

Figure 4.10. Band ratio 4+8/ 9 applied on the image and applied threshold. The red parts showing the resultant areas the below image is band 3.

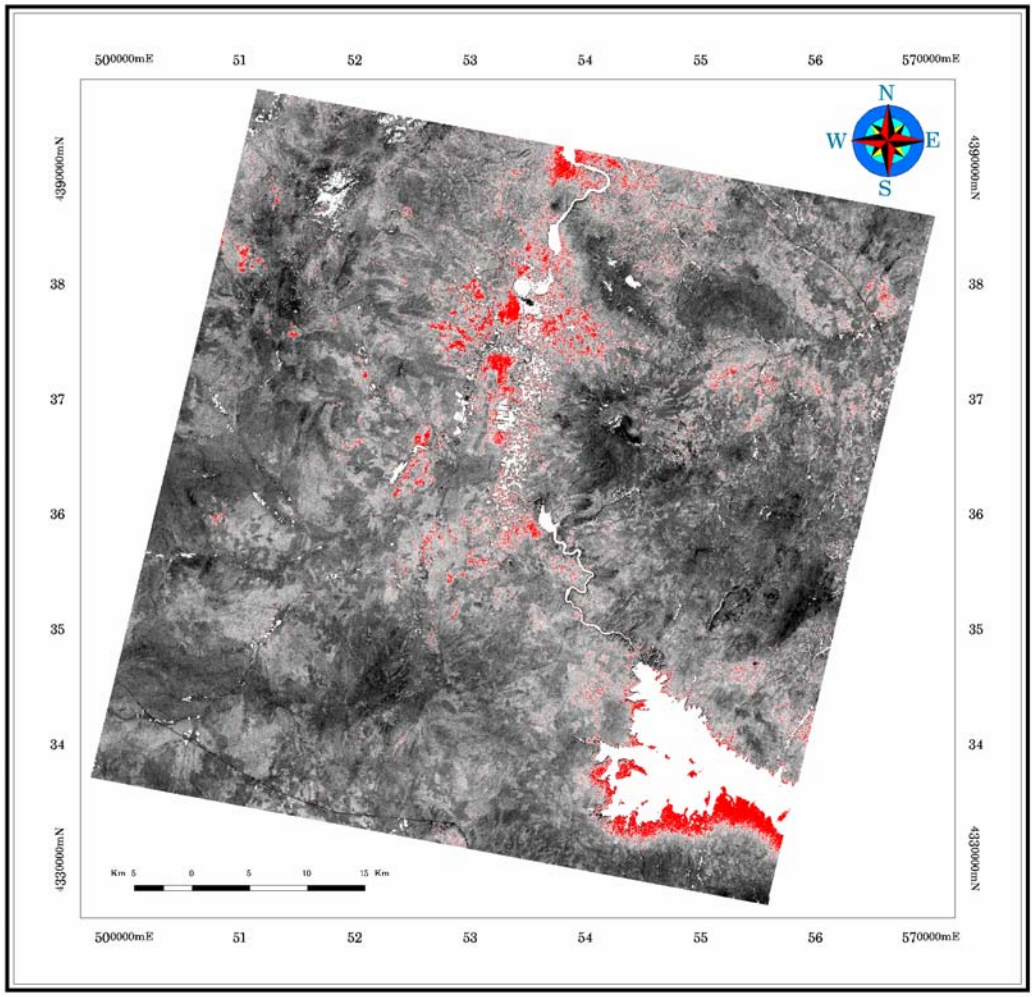

Figure 4.11. Band ratio 8/ 9 applied on the image and applied threshold, the red parts showing the resultant areas the below image is band 3.

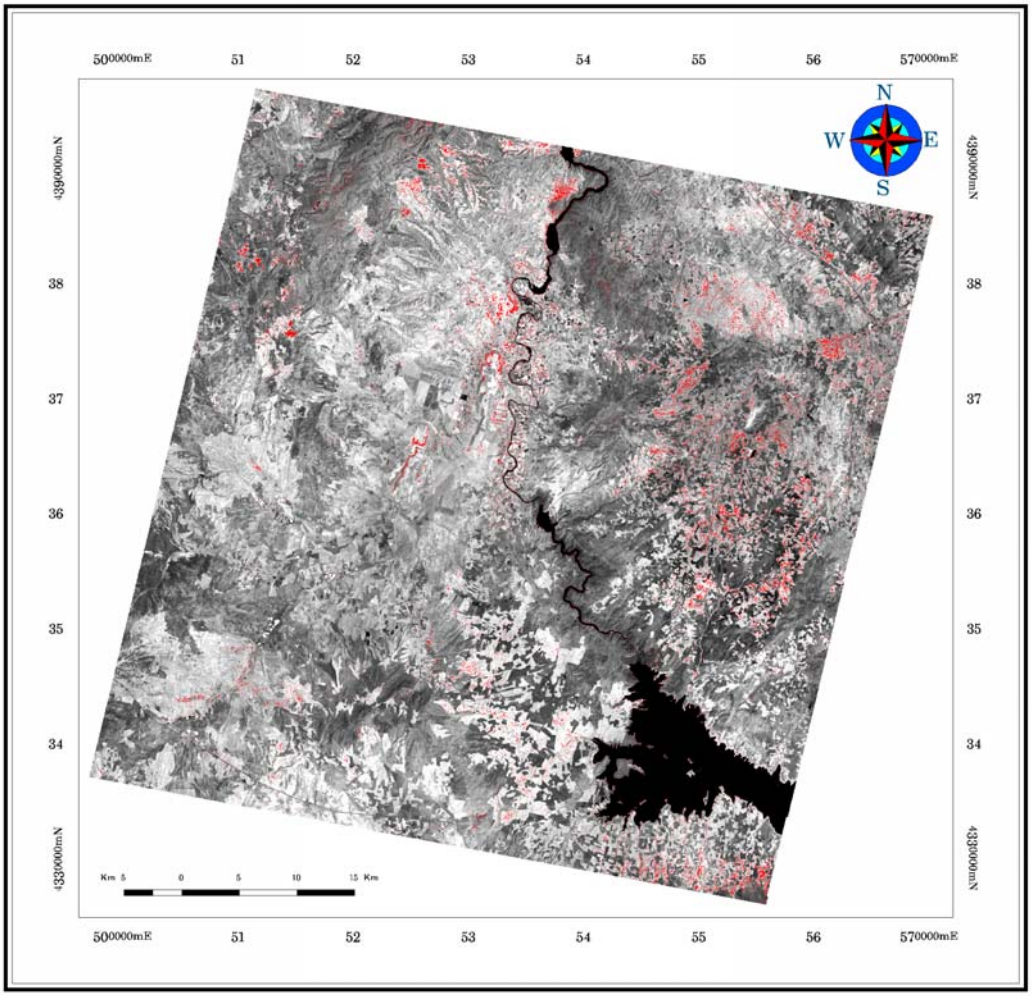

Figure 4.12. Band ratio 4+8/ 6 applied on the image and applied threshold, the red parts showing the resultant areas the below image is band 3.

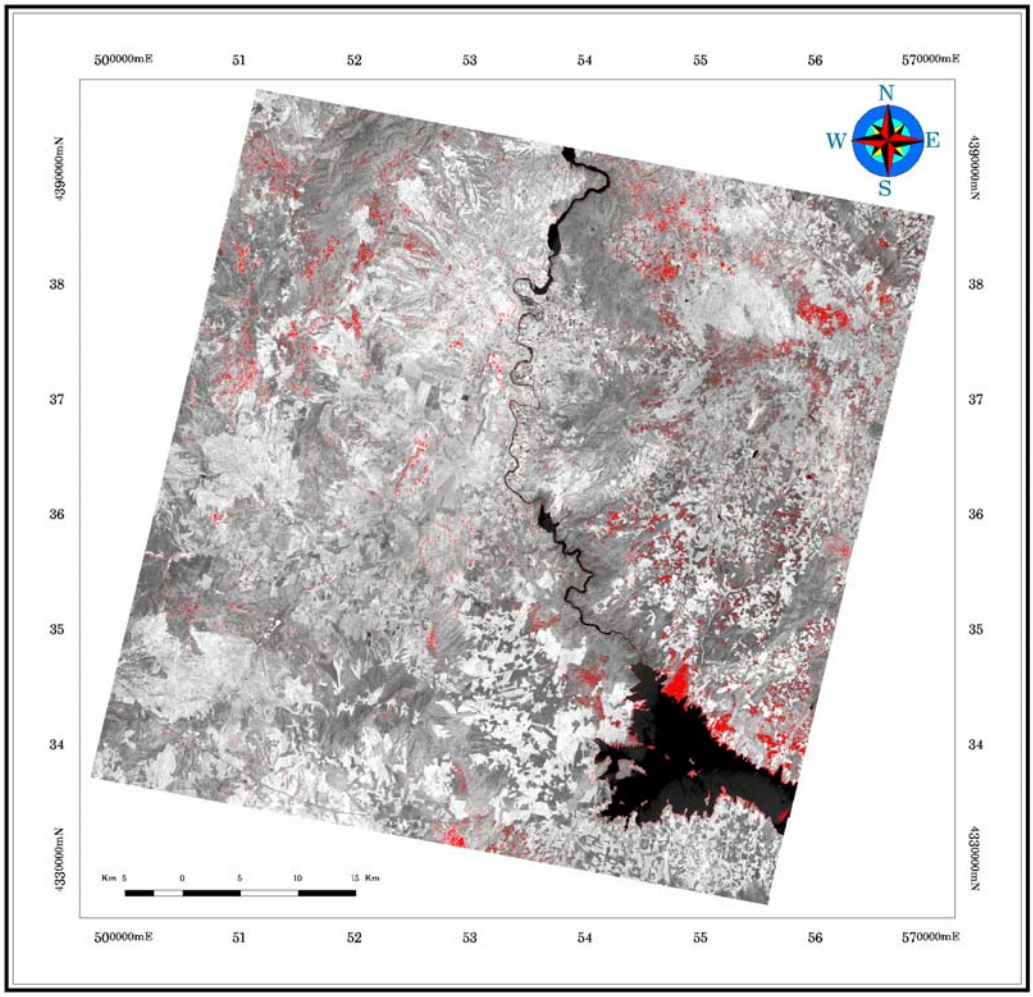

Figure 4.13. Band ratio 8/ 6 applied on the image and applied threshold, the red parts showing the resultant areas the below image is band 3.

4.4.2. Decorrelation Stretch Analysis

For decorrelation stretch analysis as discussed in chapter 3, after contrast enhancement the statistically independent (decorrelated) PC images are retransformed to the original coordinates for display, so that in general there is little distortion of the perceived hues due to the enhancement.

Decorrelation stretched method is applied by DECORR module of PCI Geomatica software. Decorrelation stretch is applied to all bands of ASTER image. First it is applied to VNIR and SWIR bands (9 bands totally) and is applied to TIR bands (5 bands) separately. For this application raw data of ASTER is used for each band and total mask (water mask and vegetation mask) is applied.

The results of the decorrelation stretch methods are put into RGB display and examined. According to the known places of gypsum in the geological map the combinations of the bands are tried.

For the RGB band combination of decorrelated image band 1, 4, 8 combination can be seen in Figure 4.14. In this combination the brightest parts most probably show gypsum rich parts since 1, 4, 8 bands gives the highest reflectance in the spectrum.

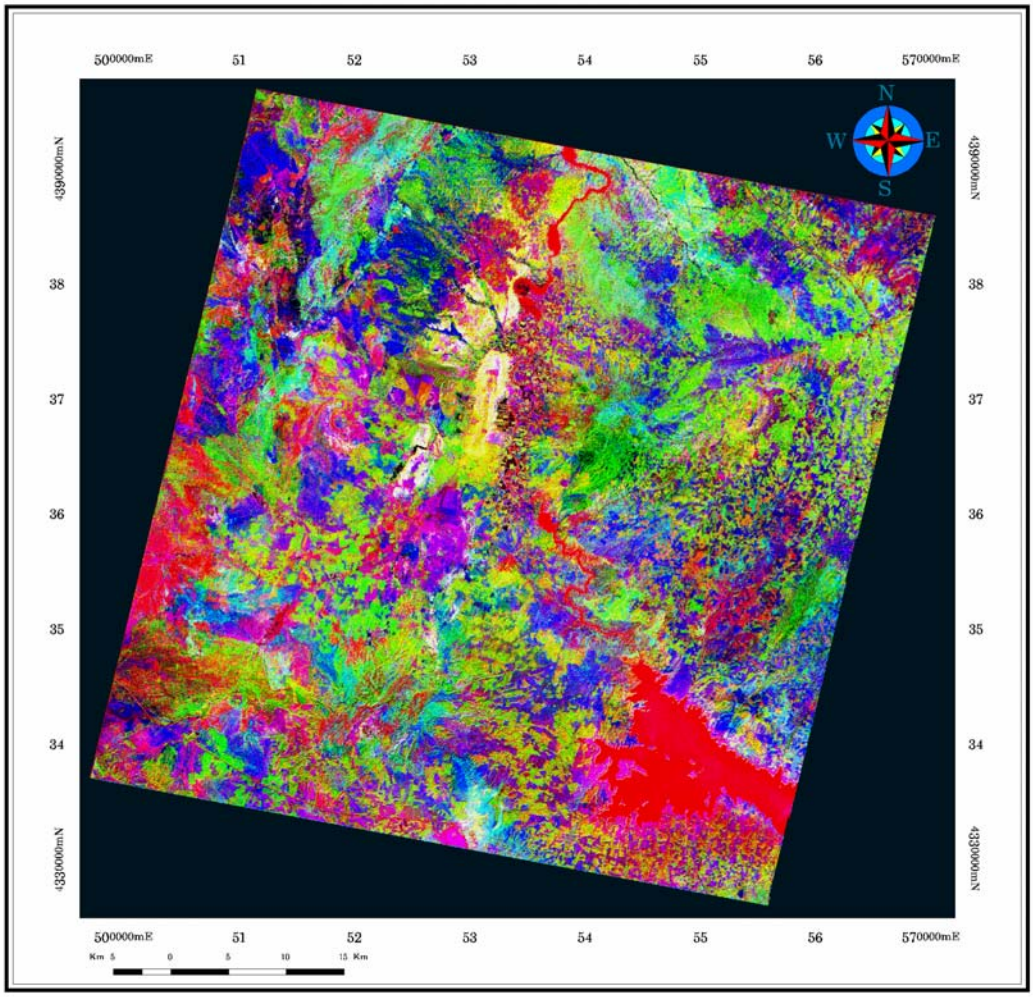

Figure 4.14. Decorrelated image 1,4,8.

Another combination is RGB 3,2,1 bands that can be seen in Figure 4.15 in which some different type of rocks can be separated. But it seems that it is not so much useful for mapping of gypsum.

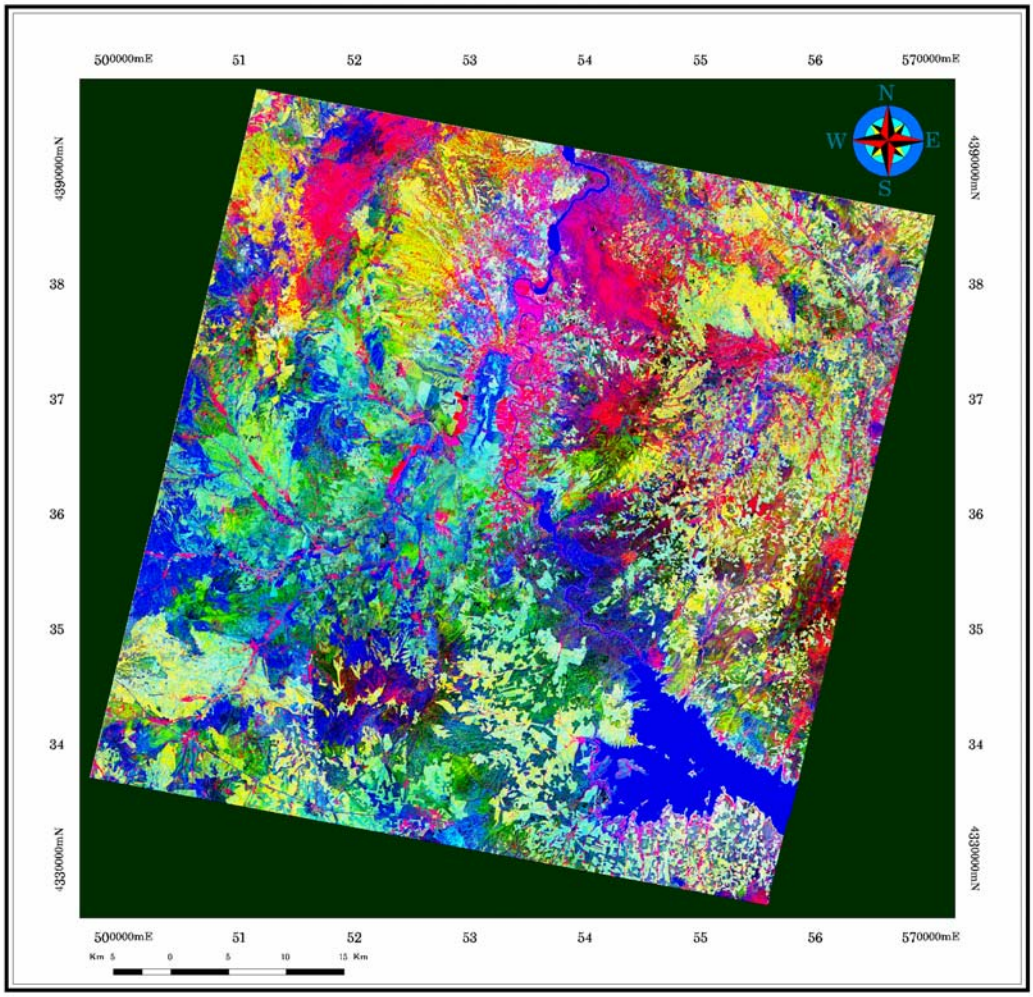

Figure 4.15. Decorrelated image 3,2,1.

Decorrelated bands 4, 6, 8 in RGB combination gives a result that is seen in Figure 4.16. In this combination it is seen that neither of this result is very successful for discriminating gypsum from other lithologies.

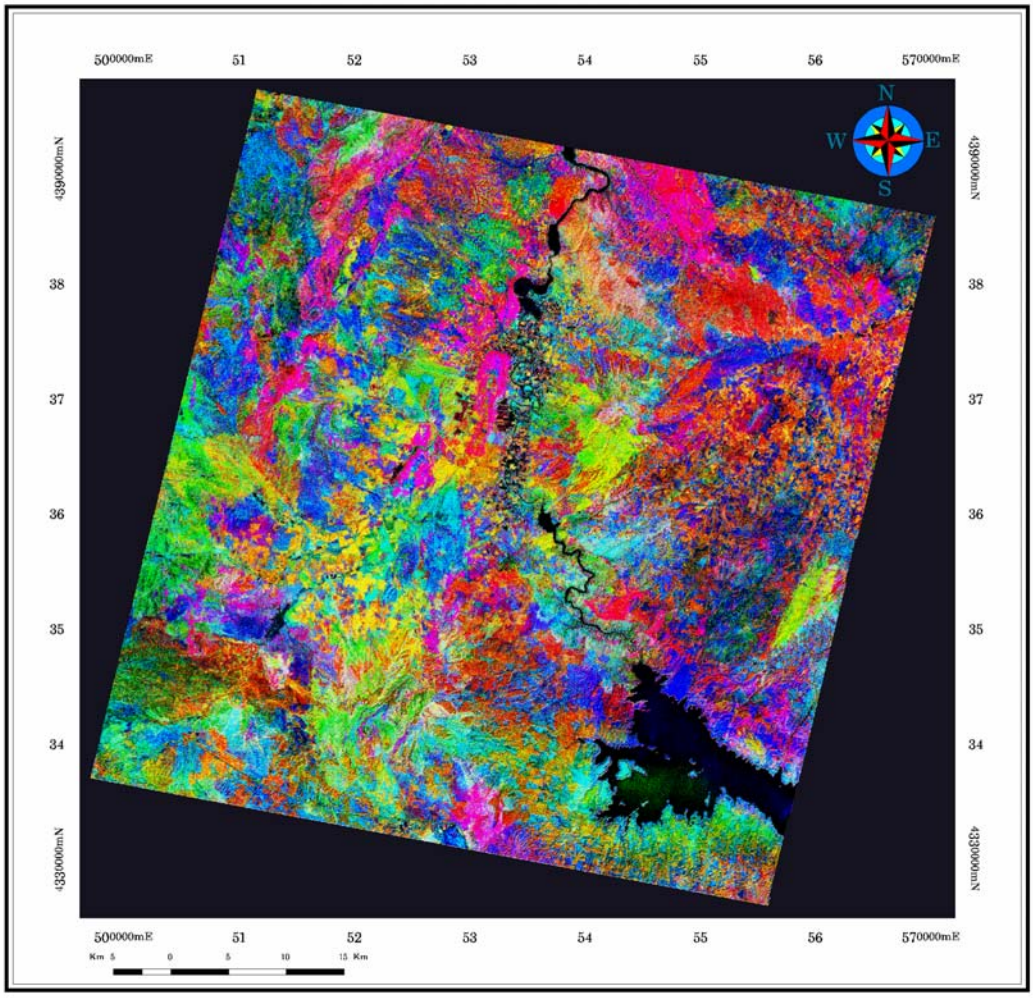

Figure 4.16. Decorrelated image 4,6,8.

4.4.3. Feature- Oriented Principle Component Selection

A special feature-oriented principle component technique named as Crosta method as discussed in Chapter 3 of the thesis, is generally used for detecting alteration minerals especially for kaolinite, illite and alunite. Since it has considerably successful results this method is commonly used by different researchers to map alteration minerals. When PCA applied to the selective bands certain materials such as vegetation, would not be mapped and that spectral information due to target material (in our case gypsum) would be mapped into a single PC. In the previous studies the selective PC is either PC3 or PC4 according to the highest

eigen vector loadings. According to Crosta (2003), he selected the high reflected and low reflected band intervals of the target minerals and checked the eigen vector loadings after the PCA analyses to decide which one has the needed information.

According to these studies it is thought that also gypsum minerals can be mapped using this method in a similar way. In order to select the suitable bands on which to apply PCA, the spectral reflectance curve of the gypsum mineral is examined. According to this phenomena band 4, band 6, band 8, band 9 are selected due to their high, low, high, low reflectances respectively and PCA is applied just these four bands (Figure 4.17).

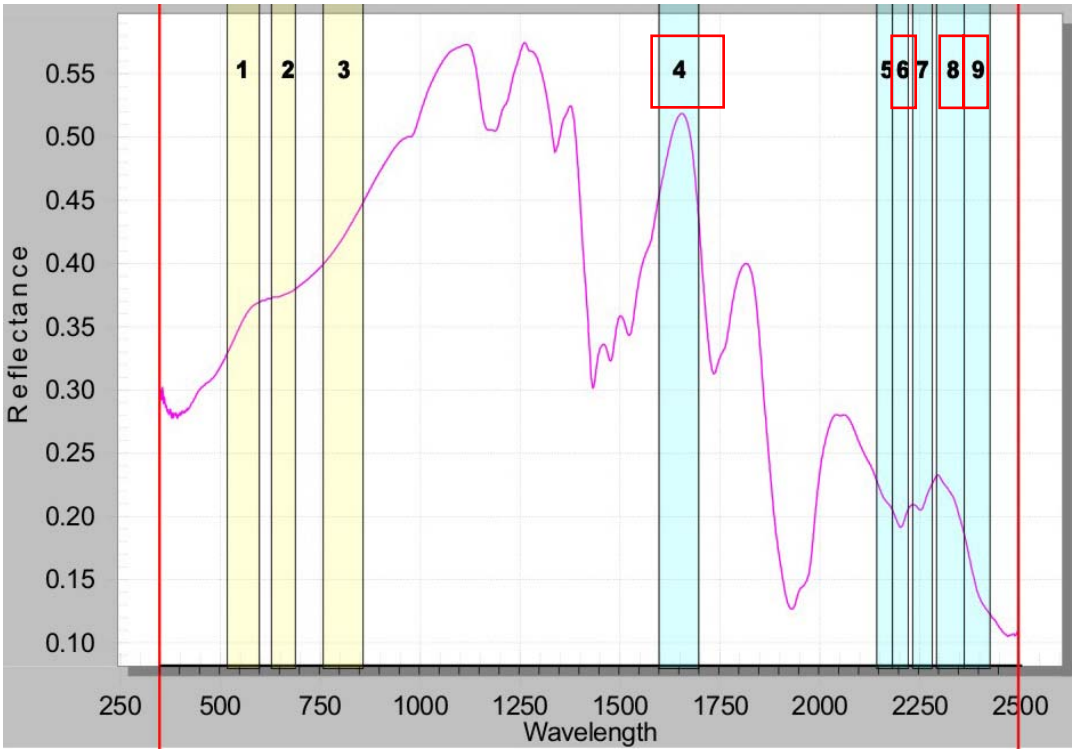

Figure 4.17. The wavelength vs. reflectance curve of gypsum and the bands selected for the crosta method are in red box.

To apply this method the area located at the east of Kapılıkuyu Dam Lake are extracted and a spatial subset is taken out from the image. This is done because at the eastern part of the image we know that geologically older base rocks are located in which no gypsum minerals can be seen. A vector file is constituted to prepare a subset image from the whole image and to this new subset PCA analysis is applied according to the selected bands. After applying this analysis the eigen vector statistics are saved and examined.

Table 4.5. Eigen Vectors of Covariance Matrix

	Band 4	**Band 6**	**Band 8**	**Band 9**
PCA1	0.59580	0.59580	0.45847	0.38188
PCA2	-0.75727	0.13189	0.52457	0.36603
PCA3	0.22735	-0.63614	0.68261	-0.27871
PCA4	-0.14100	0.53753	0.22061	-0.80157

After applying PCA the results of eigenvector statistics are saved and examined (Table 4.5). According to this results PCA3 is selected to map the target mineral (gypsum) because very high values are seen at both band 6 and 8 and having correct signs. Band 6 has low reflectance value and has a negative sign whereas band 8 has a high reflectance value and has a positive sign. It is taught that PCA3 should give us the target mineral. The resultant image can be seen in Figure 4.18.

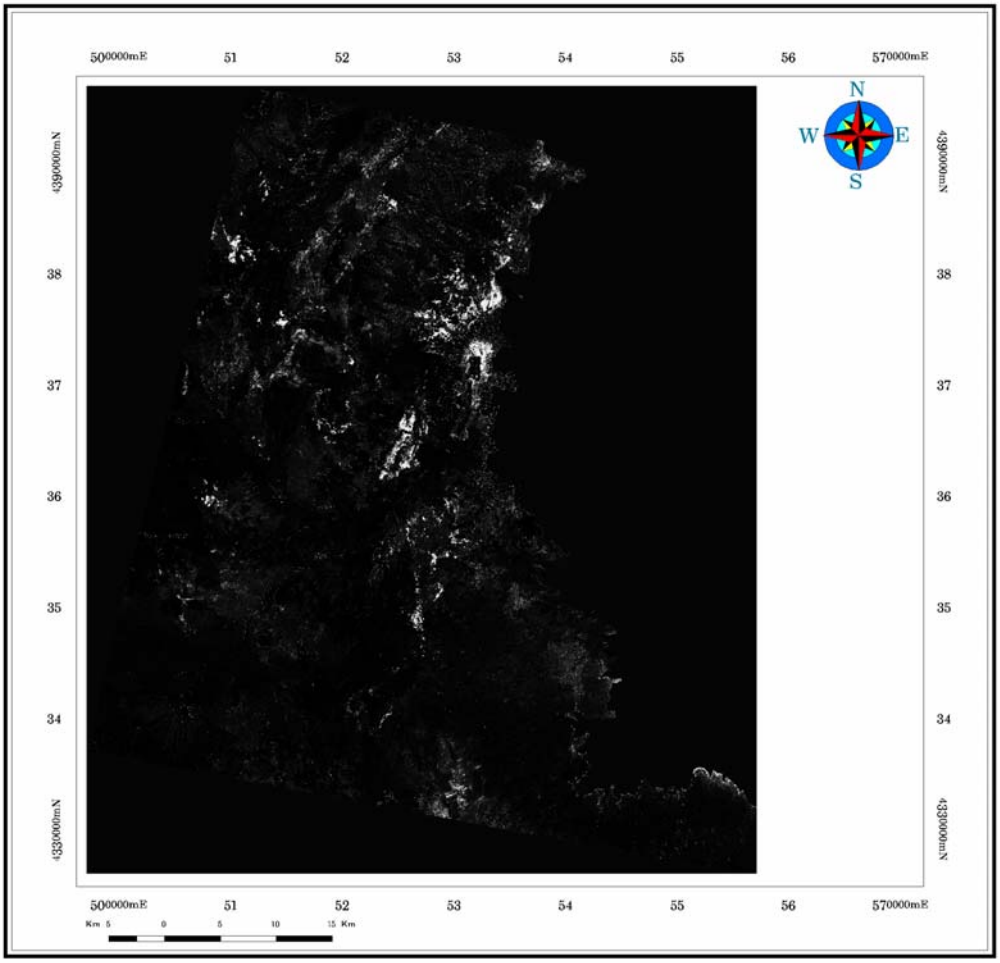

Figure 4.18. PCA3 image after applied FPCS technique.

4.4.4. Spectral Indices

Spectral indices method is very useful method to get information about certain minerals from satellite imagery. As explained in Chapter 3, a spectral index is similar to PCA in the sense that both are orthogonal transformations of multispectral data. From geological point of view for discriminating and mapping surface rock types, spectral indices are easy to interpret. As discussed in Chapter 3, there are indices used both in SWIR and TIR wavelengths.

Hardly any example of spectral indices is found in literature to be used as a gypsum mapping tool. The known indices in SWIR region are not useful for mapping gypsum mineral.

In TIR indices Quartz index is defined before by Ninomiya (2002) which uses band 10, band 11 and band 12 for ASTER images (Figure 4.19). The formula of the quartz index is defined as:

$$QI = \frac{\text{Band 11} * \text{Band 11}}{\text{Band 10} * \text{Band 12}}$$

This index is defined due to the fact that the silica minerals have relatively higher emissivity at 8.65 micron region corresponding to the ASTER band 11 than at 8.3 micron region corresponding to ASTER band 10 and at 9.1 micron region corresponding to ASTER band 12 (Figure 4.17) (Ninomiya, 2002).

As the spectral emissivity curve of gypsum mineral is considered in thermal wavelength region it is observed that the critical intervals correspond to ASTER bands of 10, 11 and 12 (Figure 4.20). The important thing is that in this interval sulfate group minerals behaves differently and gives a curve opposite of quartz minerals. By using this property it is claimed that the sulfate minerals (gypsum in our case) should give a negative anomaly when quartz index is applied to the image. This means that when quartz index is applied to the image, darker parts in the resultant image should give the places where gypsum mineral is exposed. So the equation is modified as sulfate index which is:

$$\text{Sulfate Index} = \frac{\text{Band 10} * \text{Band 12}}{\text{Band 11} * \text{Band 11}}$$

The resultant image can be seen in Figure 4.21 in which the brighter parts show the gypsum minerals. It is seen that the result is very compatible with the result of Crosta method and with the geological map.

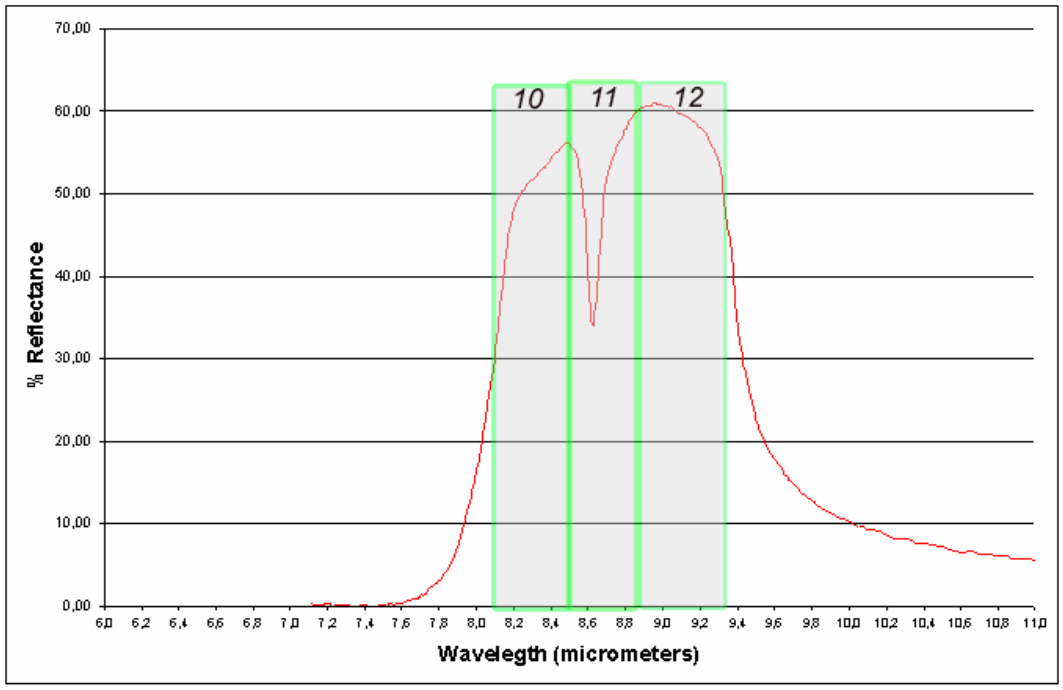

Figure 4.19. The spectral curve of Quartz in the interval 6 µm-11 µm and corresponding ASTER bands (Modified from ASTER spectral library).

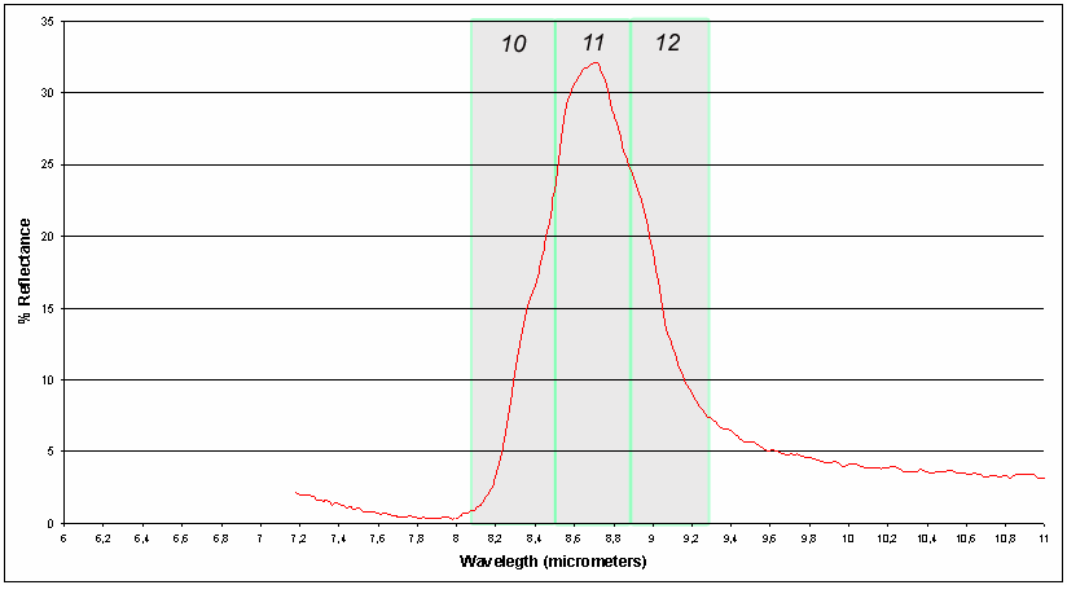

Figure 4.20. The spectral curve of Gypsum in the interval 6 µm-11 µm and corresponding ASTER bands (Modified from ASTER spectral library).

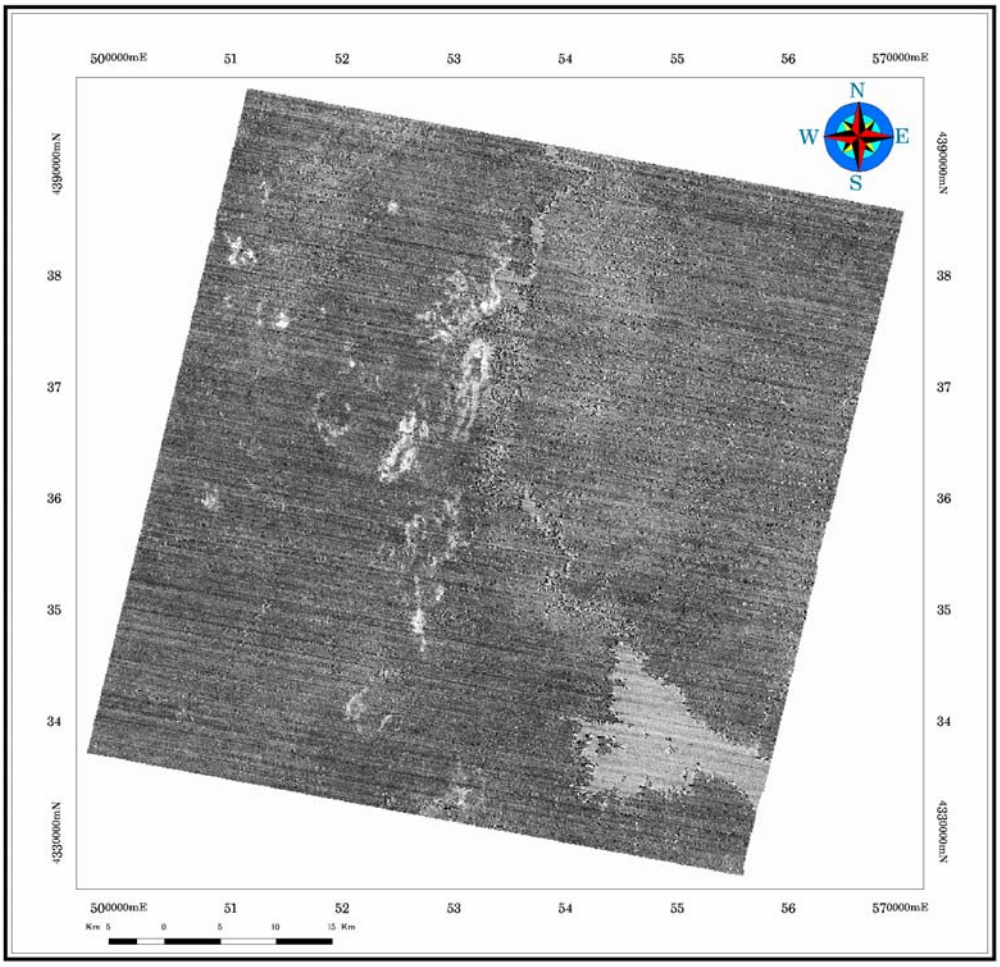

Figure 4.21. The resultant image of Sulfate index method.

CHAPTER 5

RESULTS & DISCUSSION

In this chapter all the procedure used for mapping gypsum minerals will be discussed and the compatibility among themselves & success of all the methods are tested. The methods of Band Ratio, Decorrelation Stretch, Crosta technique and Quartz index are checked at the field and also they are correlated with each other. For the band ratios, best one is selected according to the geological map and it is seen that 4\9 band ratio shows the best results among other band ratios. Also for decorrelation stretch method among all RGB combinations it is seen that 1,4,8 combination best fits with the geological map. For the Crosta technique PC3 is selected and suitable threshold is given concerning the geological map. Quartz index method gives us a single result and suitable threshold is selected again according to the geological map.

5.1. Absolute Accuracy Assessment

In order to check the accuracy and success of the methods used for mapping gypsum minerals field verification is done after getting the results. Target areas are selected according to the anomalies given by the results (Figure 5.1). At the field, the areas with high anomalies are visited and some samples are taken in order to have spectral information about the minerals. Photos are taken from the field where the anomalies are dominant. Also samples are taken from 7 different location and they are selected to characterize the area. The list of the samples can be seen in table 5.1. The spectral curves of the specimen are gathered using Field Spectrometer; photos and spectral curves of the specimen can be seen in the

Appendix-1. Also X-Ray Analyses are done to these samples to check the mineralogy of the samples. The results of these analyses can be seen in Appendix-2.

Table 5.1. Hand Specimen number and coordinates of ground truth locations.

Specimen	X	Y
1	515350	4377200
2	524500	4386500
3	518100	4377150
4	527050	4352.125
5	528000	4386550
6	533500	4334140
7	511520	4382150

The graphs of the spectral curves are prepared using FieldSpec Pro and Specmin Pro software. The graphs are reflectance versus wavelength. According to the results of the spectral curves of the specimen they are correlated with the spectral libraries of the software.

For the location 1, all the methods give us anomalies. This area is found by all the methods and it is well-known area called Aşıkoğlu mine area. The photo from this area can be seen in Figure 5.2. The results of Quartz index and Band Ratio 4/9 are very similar in this location 1. Crosta method gives very high accuracy in the area and Decorrelation Stretch result found the minimum area of gypsum in this location. According to the X-ray result the specimen 7 from this location gives gypsum (Appendix-2).

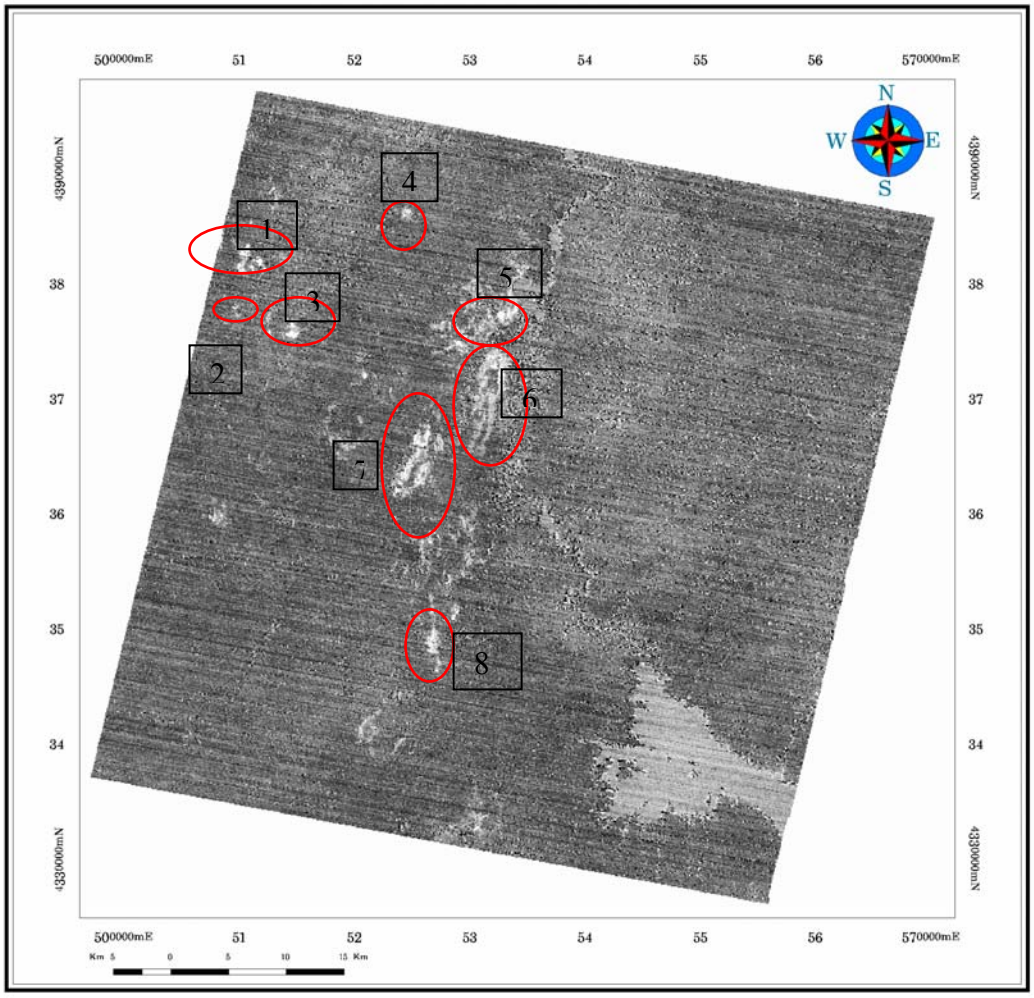

Figure 5.1. The result of sulfate index technique and areas in which photos are taken. (Red circles show the areas and black rectangles show ground truth location numbers)

For location 2, rather small area is seen as gypsum but they are detected with the methods. Quartz index method and Crosta methods gives very coherent and successful results for this location 2. The photo of this location can be seen in Figure 5.3. Band ratio and decorrelation stretch methods also give very small anomalies in this location so that all the methods can find this area also.

Figure 5.2. Photo from the location 1.

Figure 5.3. Photo from the location 2.

Location 3 is also very good area to see gypsum outcrops since it was mined before. The photo can be seen in figure 5.4. The location is situated 5 km to Bala district. This area is mapped as Sekili Evaporate Member (Tois) in the geological map. In this location all the methods found the gypsum rocks however Crosta method gives us the best fit boundary comparing with the geological map.

In location 4, all the methods give us anomalies. In the geological map this area is mapped as Tois again concerning that this area is gypsum site. Sample is taken very near to this location from the valley seen in Figure 5.5.

In the location 5, no outcrops of the gypsum minerals can be seen however the soil is composed of gypsum. It gives anomaly in the results of all the methods. This result shows us that the methods also find the gypsum rich soils. According to the results band ratio method gives us the maximum area and quartz method give us the least. The photo of this area can be seen in Figure 5.6.

Location 6 and consists of a hill that is composed of alternating lacustrine beds with important amount of gypsum layers. Also this can be detected by all the methods. The photo of this location can be seen in Figure 5.7. Also locations 7 and 8 are visited and hand specimen from these locations also gives gypsum result. All the methods give anomalies in these regions. The photos of location 7 and 8 can be seen in Figures 5.8 and 5.9.

Figure 5.4. Photo from the location 3.

Figure 5.5. Photo from the location 4.

Figure 5.6. Photo from the location 5.

Figure 5.7. Photo from the location 6.

Figure 5.8. Photo from the location 7.

Figure 5.9. Photo from the location 8.

In all the locations all the methods give considerable results. The ground truth is done for 8 locations in which the anomalies are very highly distributed. It is seen that the methods give very accurate results after checking the area. It is not practical to make this ground truth in every km^2 of the study area but the methods give anomalies also at different places so that a relative accuracy assessment is needed which is discussed below.

5.2. Relative Accuracy Assessment

For the relative accuracy assessment all the methods are correlated with each other. In order to compare the results of the analyses all the results are put into one map. For comparison, the common extents are used; hence spatial subsets are taken, for all of the resultant maps. The results are converted to binary images this means either they have 1 or 0 values. For band ratio result, the best ratio is selected as 4/9 and the pixels giving the possible gypsum areas are defined as 1 whereas the other parts are defined as 0. For Decorrelation stretch method the pixels giving the possible gypsum areas are defined as value 10. For crosta method value 100 is assigned for the possible areas and for quartz index method 1000 is defined for the possible gypsum areas. The values can be seen in Table 5.2.

Table 5.1. The values of given to the methods

Method	**Values**
Band Ratio	0 – 1
Decorrelation Stretch	0- 10
Crosta Technique	0- 100
Quartz Index	0-1000
Total	0-1111

After giving the thresholds all the results have values as seen in Table5.1. When we add all of these methods at the end we have results as seen in Table 5.2. In this table it is seen that band ratio method results in very large area. However the other 3 methods seem more compatible with each other. These results are put into one

map to visualize the areas, four synthetic classes are generated (Table 5.3). Class 1 corresponds to the areas where only one method found, Class 2 corresponds the areas of any two methods found at the same time, Class 3 corresponds the areas of any 3 methods found and Class 4 corresponds to the areas that all of the methods found.

Table 5.2. Table showing the possible values of the total map, BR is Band Ratio Method, DS is Decorrelation Stretch method, C is Crosta method, QI is Quartz index method.

VALUE	METHODS	Number of pixels	Percentage (%)
1	BR	139031	43
10	DS	38947	12
11	BR+DS	5731	1,8
100	C	50685	15,8
101	C+BR	10030	3,1
110	C+DS	10510	3,2
111	C+DS+BR	7440	2,3
1000	QI	24135	7,5
1001	QI+BR	3763	1,2
1010	QI+DS	3335	1
1011	QI+DS+BR	1324	0,4
1100	QI+C	5835	1,8
1101	QI+C+BR	6343	2,2
1110	QI+C+DS	4456	1,5
1111	QI+DS+C+BR	8876	3

Table 5.3. The four classes that are generated and the number of pixels they have.

Class	Number of Pixels	Percentage(%)
1	252798	79
2	39204	12
3	19563	6
4	8876	3
Total	320441	100

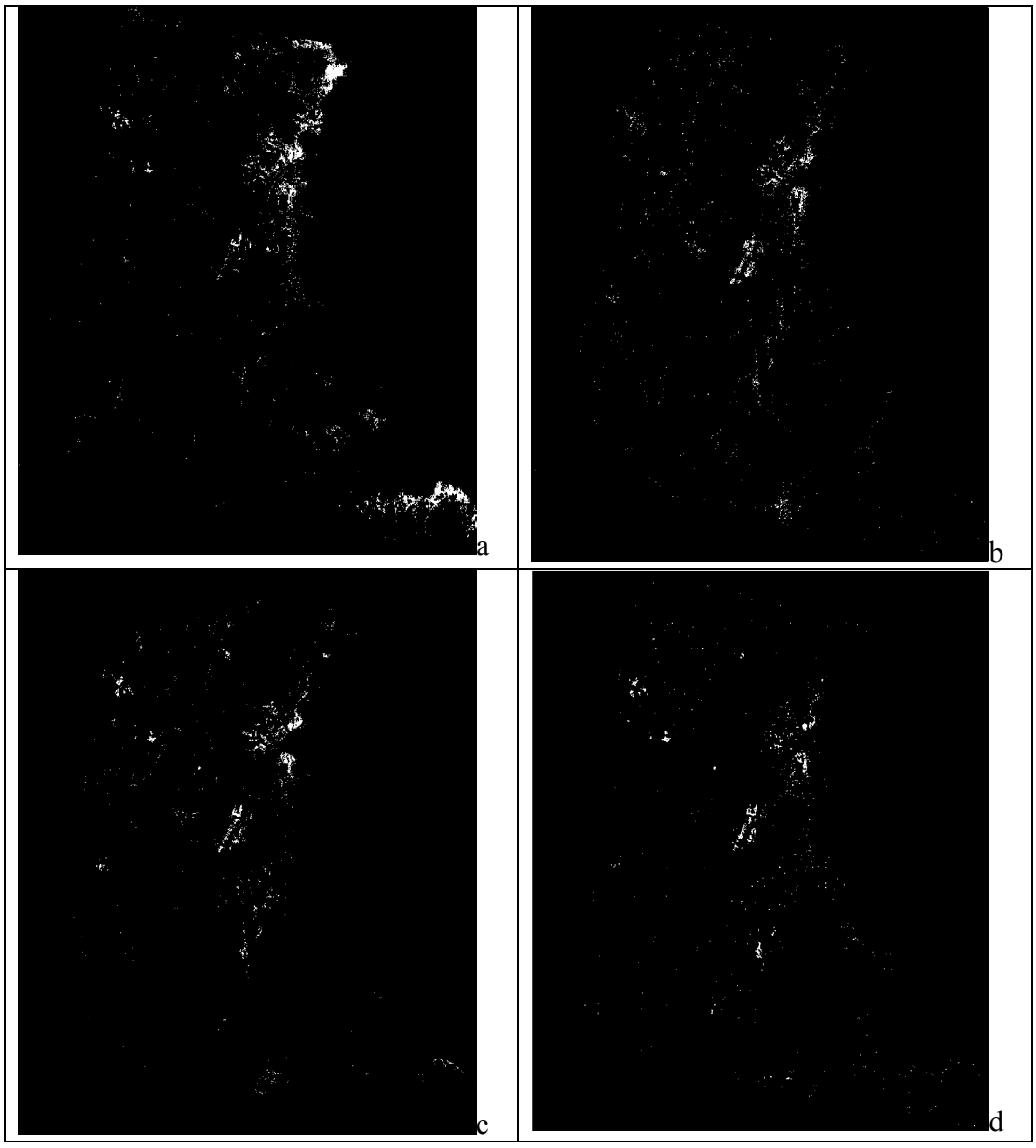

Figure 5.10. The results of the methods a) Band Ratio b) Decorrelation Stretch c) Crosta d) Sulfate Index

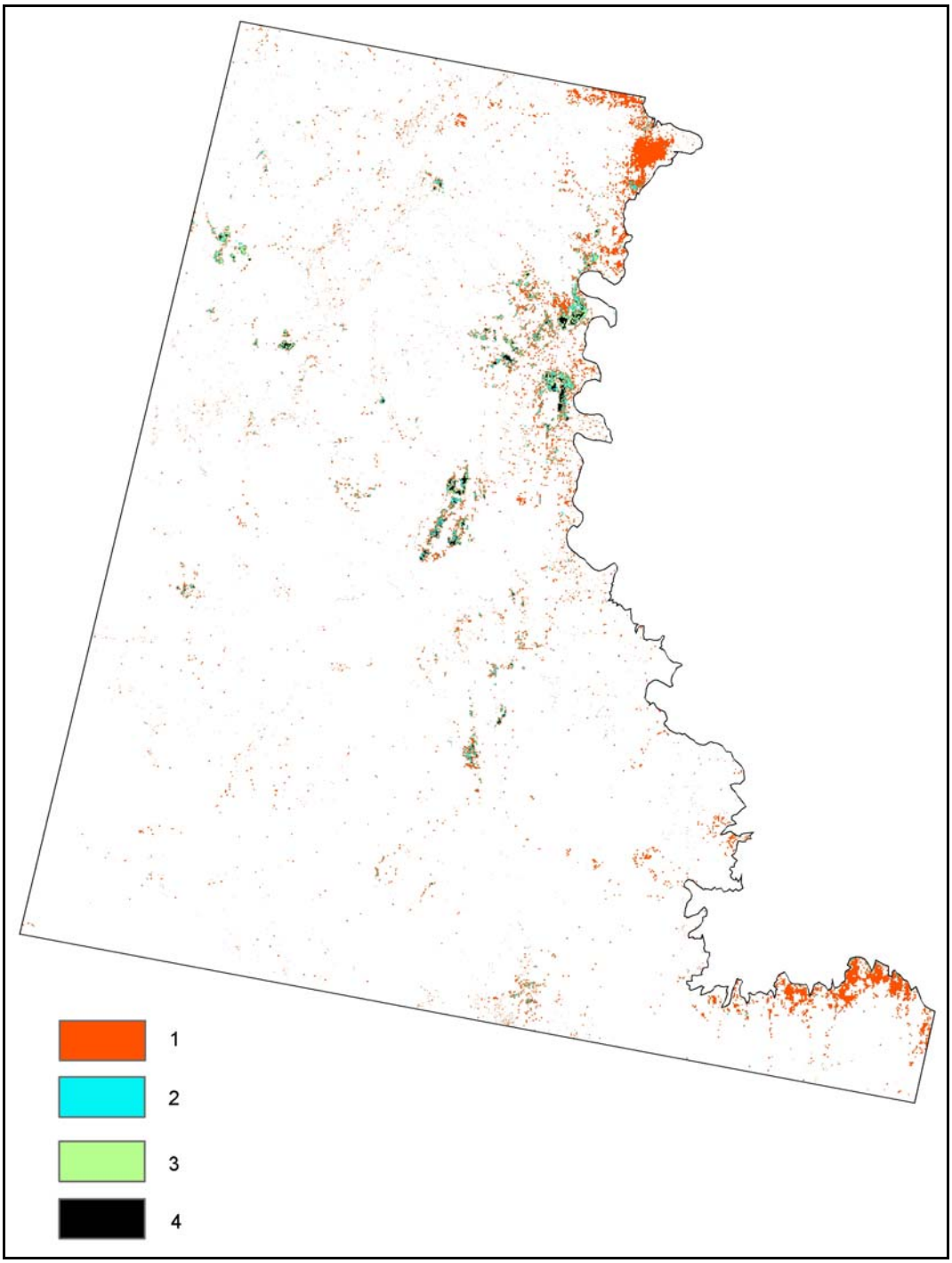

Figure 5.11. Classified map having four classes; 1 means only one method give the result, 2 means two methods give the result, 3 means three of the methods give the result, 4 means four of the methods give the result.

According to these classes except Band Ratio method the methods show a high correlation (Figure 5.10 and 5.11). This is because the band ratio used in thesis is 4/9 which corresponds to very wide interval of spectrum and not enough to determine only one mineral. However among all other band ratios it is selected as the best one. The other methods find the target areas and since they are checked at the field it is seen that they are very useful for mapping gypsum mineral. The percentage of the areas where all the methods found is very low because Band Ratio itself gives very large areas so that the percentage of class 1 is very high. If we omit band ratio result from the total results, it is seen that the percentage of common areas increases rapidly.

5.3. General Aspects of the Data and the Results

The geological map used in this thesis is modified from Dönmez et al. (2007) 1/100.000 scaled map which will be published from MTA this year. It is a collection of the previous studies done by MTA staff. However to avoid the conflicts for the formation names they generated common names for the formations. The difference of this map from the previous one is that they defined a new member of the evaporate rocks. This is more useful for our study because there is no map just showing gypsum minerals. It was better to have only gypsum map in this area to correlate the results directly but still at least we know in which area there is possibility to have gypsum and in which area no gypsum should be seen. For the preparation of the geological map the I30 and J30 maps are used. If we want to have more information we should have bigger scaled map for the region. The results on the classified geological map can be seen in Figure 5.12.

ASTER image is selected for mapping gypsum mineral by remote sensing techniques. The reason for selection of ASTER data is that it has medium spatial resolution and higher spectral resolution than similar image data. For example if we compare ASTER images with Landsat TM images, ASTER has finer ground resolution and also it has more bands in SWIR & TIR regions where the minerals have characteristic information.

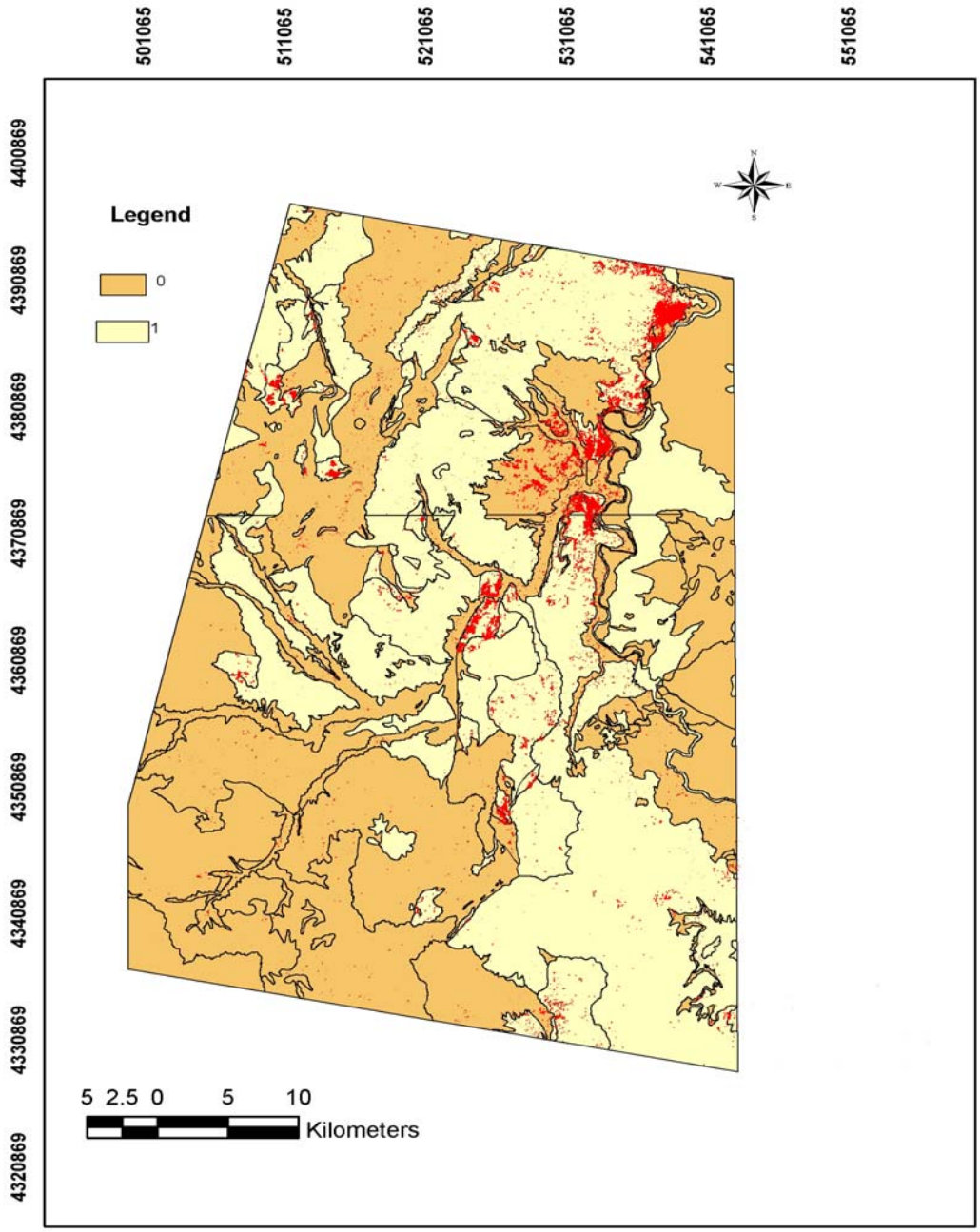

Figure 5.12 The results showed on classified geological map (Geological map is modified from Dönmez et al. 2007, 0 shows formations without gypsum, 1 shows formations containing gypsum, red areas show the results of the methods that find gypsum.

The ground resolution of ASTER image is 15 m for VNIR but there are images having better spatial resolutions such as Quickbird (0.6m) or Ikonos (1m). Although it seems that they would better for discriminating minerals because of their high resolution ASTER is more successful because of its bands in SWIR and TIR region since the other images have bands in only VNIR interval. So the most suitable ASTER image without clouds having an acquisition date in summer period should be taken for the analysis.

Common known methods are tried to map out the target mineral in this thesis. Band ratio, Decorrelation Stretch and Crosta techniques are applied to VNIR and SWIR bands of ASTER image whereas Sulfate index method is applied to TIR of the image. So for the results since SWIR is resampled to 15 m for the analysis the results for the first methods are all 15m in resolution. For the Sulfate Index method TIR is used so that the image is 90 m for that region and the analysis results are in 90 m resolution. This means that the result for Sulfate Index method is yielding in more regional results where the other methods are more sensitive to local spectra. It can be thought that Sulfate index method is much easier because one should apply the formula and the brighter parts show the gypsum minerals. For band ratio and decorrelation stretch methods, one should decide which combination would be better for discrimination.

CHAPTER 6

CONCLUSIONS AND RECOMMENDATIONS

As conclusions for this study first it is seen that ASTER images are suitable for mapping evaporate minerals with their balanced spatial and spectral resolutions. It is observed that ASTER images are successful to map gypsum minerals both in SWIR and TIR intervals. According to results; 288 km^2 area is mapped as gypsum with the total of four methods but it is seen that only 8 km^2 is found by all the methods. The most successful methods are Crosta and Sulfate Index methods. Crosta method which is used mainly for alteration minerals is modified for Gypsum minerals by selection of bands 4,6,8,9. Sulfate index is modified from Quartz index for TIR region and it is successful for gypsum minerals. The areas that have gypsum rich soils also can be mapped by using band ratio, decorrelation stretch, Crosta and sulfade index methods.

For recommendations; these methods should be applied to different areas where there are gypsum minerals to check the accuracy and success. Chemical analysis could be applied to the specimen to understand the chemical composition of the minerals so that the purity of the mineral can be estimated.

REFERENCES

Abdeen, M.M., Allison, T.K., Abdelsalam, M.G., Stern, R.J., 2001. Application of ASTER band-ratio images for geological mapping in arid regions; the Neoproterozoic Allaqi Suture, Egypt. Abstract with Program Geological Society of America, vol. 3(3), p. 289.

Akyürek, B,, Bilginer, E,, Akbaş B., Hepfen, N,, Pehlivan, Ş., Sunu, O., Zafer, Z,, Çatal, B., Şözeri B, Yıldırım H, ve Hakyemez;Y., 1982, Ankara-Elmadağ-Kalecik dolayının jeolojisi: MTA Raporu. 7298

Akyürek, B., Duru, M., Sütçü, Y.F., Papak, Saroglu, F., Pehlivan, N., Gönenç, O., Granit, S., Yasar, T., 1996, Ankara ilinin çevre jeolojisi ve doğal kaynaklar projesi, M.T.A. Report No:9961.

Arıkan, Y., 1975. Tuz Gölü Havazası 'nın jeolojisi ve petrol imkanları. MTA Enstitüsü Derg. 85, 17-37.

ASTER Users Handbook, Abrams, M., Hook, S., Version 2, Jet Propulsion Laboratory California Institute of Technology

Bastianelli, L., Bela, G. D., and Tarsi, L., 1993, Alteration mapping: a case study in mid-south Bolivia. Proceedings of the 9th Thematic Conference on Geologic Remote Sensing, Pasadena, CA (Ann Arbor, MI: Environmental Research Institute of Michigan), pp. 1133–1144.

Baykal, F., 1943, Kırıkkale-Kalecik ve Keskin-Bala mıntıkalarındaki jeolojik etütler. *M.T.A. Rep.,* no. 1448, Ankara.

Bedell, R.L., 2001. Geological mapping with ASTER satellite: new global satellite data that is a significant leap in remote sensing geologic and alteration mapping. Special Publication, vol. 33. Geo. Soc. of Nevada, pp. 329–334.

Bennett, S.A., 1993. "Use of Thematic Mapper Imagery to Identify Mineralization in the Santa Teresa District, Sonora, Mexico" Int. Geol. Rev. 35, 1009–1029.

Bilgin, Z.R.; Akarsu, B.; Erbaş, A.; Elibal, E.; Yaşar, T.; Esentürk, K.; Güner, E. ve Kara, H., 1986, Kırıkkale - Kesikköprü - Çiçekdağı alanının jeolojisi: MTA Rap., 7876, (yayımlanmamış), Ankara.

Birgili, S., Yoldaş, R. and Ünalan, G., 1975. Cankırı-Corum havzasının jeolojisi ve Petrol olanakları. MTA Rapor No: 5621, pp: 78.

Brickey, D. W., 1986. The use of thematic mapper imagery for mineral exploration in the sedimentary terrain of the Spring Mountains, Nevada, in Proceedings of the 5th Thematic Conference on Geological Remote Sensing, Environmental Research Institude of Michigan, Ann Arbor, Mich., pp 607-613.

Carranza, E. J. M., and Hale, M., 2002, Mineral imaging with Landsat Thematic Mapper data for hydrothermal alteration mapping in heavily vegetated terrain. International Journal of Remote Sensing, 23, 4827–4852.

Chavez, P.S., Berlin, G.L., Sowers, L.B., 1980. Statistical methods for selecting of Landsat MSS ratios. Journal of Applied Photographic Engineering 8, 30–32.

Clark, R. N., 1999, Chapter 1: Spectroscopy of Rocks and Minerals, and Principles of Spectroscopy, in *Manual of Remote Sensing, Volume 3, Remote Sensing for the Earth Sciences*, (A.N. Rencz, ed.) John Wiley and Sons, New York, p 3- 58.

Crippen, R. E., 1989. Selection of Landsat TM band and band ratiocombinations to maximize lithologic information in color composite displays, in Proceedings of the 7th Thematic Conference on Remote Sensing for Exploration Geology, Vol. II, Environmental Research Institute of Michigan, Ann Arbor, Mich., pp. 917-921.

Crist, E. P., and Cicone, R. C., 1984, A physically-based transformation of Thematic Mapper data – the TM tasseled cap. IEEE Transactions on Geoscience and Remote Sensing, 22, 256–263.

Crosta, A. P., and Moore, J. McM., 1989, Enhancement of Landsat Thematic Mapper imagery for residual soil mapping in SW Minas Gerais State Brazil: a prospecting case history in greenstone belt terrain. Proceedings of the 9th Thematic Conference on Remote Sensing for Exploration Geology, pp.1173-1187.

Crosta, A. P., Prado, I. D. M., and Obara, M., 1996, The use of Geoscan AMSS Mk-II data for gold exploration in the Rio Itapicuru greenstone belt, Bahia, Brazil. Proceedings of the 11th Thematic Conference on Remote Sensing for Exploration Geology, Las Vegas, NV (Ann Arbor, MI: Environmental Research Institute of Michigan), pp. 205–214.

Crosta, A. P., De Souza Filho, C. R., Azevedo, F., and Brodie, C., 2003, Targetting key alteration minerals in epithermal deposits in Patagonia, Argentina, using

ASTER imagery and principle component analysis, International Journal of Remote Sensing, v.24, n.21, pp.4233-4240.

Crowley, J.K., 1991. Visible and near-infrared (0.4-2.5 mm) reflectance spectra of playa evaporate minerals, Journal of Geophysical Research, Vol.96, pp. 16231 -16240

Davidson, D., Bruce, B., and Jones, D., 1993, Operational remote sensing mineral exploration in a semi-arid environment: the Troodos Massif, Cyprus. Proceedings of the 9th Thematic Conference on Remote Sensing for Exploration Geology, Pasadena, CA (Ann Arbor, MI: Environmental Research Institute of Michigan), pp. 845–859.

Davis, P.A., K.F. Mullins, G.L.Berlin, A.M. Al-Farasani, and S.M. Dini, 1989. Phosphorite exploration in the Thaniyat and Sanam districts, Kingdom of Saudi Arabia, using Landsat thematic mapper data, in Proceedings of the 7th Thematic Conference on Remote Sensing for Exploration Geology, Vol. II, Environmental Research Institude of Michigan, Ann Arbor, Mich., pp. 105-1221.1989

Doğan, B., Ünlü, T., Saylı, I.S., 1998, Kesikköprü (Bala- Ankara) demir yatağının kökenine bir yaklaşım, M.T.A. Dergisi s.120, pp: 1-33.

Dönmez M., Bilgin Z.R., Akçay, A.E., Kara, H., Yergök, A.F., Esentürk, K., 2005, Türkiye Jeoloji Haritaları No:46 Kırşehir- İ31 Paftası, M.T.A. publishment.

Dönmez M., Bilgin Z.R., Akçay, A.E., Kara, H., Yergök, A.F., Esentürk, K., 2007, Türkiye Jeoloji Haritaları No:46 Kırşehir- İ30 Paftası, M.T.A (unpublished).

DPT Madencilik Özel İhtisas Komisyonu Raporu, Endüstriyel Hammaddeler Alt Komisyonu Yapı Malzemeleri (Alçı-Kireç-Kum-Çakıl-Mıcır-Boya Toprakları- Tuğla Kiremit) Çalışma Grubu Raporu, Ankara, 2001.

Erol, O., (1969). Tuz gölü Havzasının jeolojisi ve jeomorpholojisi, T.B.T.A.K. Raporu, 116 s, Ankara.

Fadda, E.H.R., 2003. Using remote sensing to produce the geological map of Wadi Al Awsaji area, Jordan, Geoinformation for European-wide Integration, Benes, Rotterdam.

Faust, N., L., 1989, “Image Enhancement.” Volume 20, Supplement 5 of Encyclopedia of Computer Science and Technology, edited by Allen Kent and James G. Williams. New York: Marcel Dekker, Inc.

Gad S. and Kusky T., 2006, ASTER spectral ratioing for lithological mapping in the Arabian–Nubian shield, the Neoproterozoic Wadi Kid area, Sinai, Egypt,

International Association for Gondwana Research. Published by Elsevier B.V.

Gillespie A.R., A.B. Kahle, and R.E. Walker, 1986.Color enhancement of highly correlated images:I.Decorrelation and HIS contrast stretches, Remote Sensing Environment, 20, 209-235.

Gillespie, A.R., 1992. Enhancements of multispectral thermal infrared images: decorrelation contrast stretching, Remote Sensing Environment, 42, 147-156.

Gonzalez, R.C., and Wintz, P., 1977, *Digital Image Processing*. Reading, Massachusetts: Addison-Wesley Publishing Company.

Görür and Derman, 1978, Tuzgolu-Haymana Havzasi'nin stratigrafik ve tektonik analizi. TPAO Report No: 1514 (in Turkish) unpublished.

Görür, N., 1981, Tuzgölü-Haymana havzasının stratigrafik analizi, İç Anadolu'nun jeolojisi simpozyumu, TJK publishment, pp. 60-65.

Gürçay (2008), Jips ve Alunit Minerallerinin ASTER Uydu Verileri ile Belirlenmesi, 61. Türkiye Jeoloji Kurultayı bildiri özleri kitabı, pp. 353.

Hauff, P. L., 2002, Applied Reflectance Spectroscopy, Spectral International Inc.

Hewson, R.D., Cudahy, T.J., Huntington, J.F., 2001. Geologic and alteration mapping at Mt Fitton, South Australia, using ASTER satellite-borne data. International Geosciences and Remote Sensing Symposium 2, 724–726.

Hunt, G.R., Salisbury, J.W., and Lenhoff, C., 1971. Visible and near- infrared spectra of minerals and rocks:IV. Sulphides and Sulphates, Modern Geology, Vol.3, pp.1-14.

Hutsinpillar A. 1988. Distribution of Hydrothermal Alteration Mineral Assemblages at Virginia City, Nevada, Using the Airborne Imaging Spectrometer. Remote Sensing of Environment 24, 53-66.

Jackson, R.D., 1983, Spectral indices in n-space. Remote Sensing of Environment, 13, 409–421.

Jensen, 1996. Introductory digital image processing: a remote sensing prospective, 2nd edition. Prentice-Hall, Englewood Cliffs, NJ. 316 pp.

Kara, H., 1991, 1/100.000 ölçekli açınsama nitelikli Türkiye Jeoloji haritaları serisi, Kırşehir- G18 paftası, No:34, M.T.A, Ankara

Kara, H., Dönmez, M., 1990, 1/100.000 ölçekli açınsama nitelikli Türkiye Jeoloji haritaları serisi, Kırşehir- G17 paftası, No:34, M.T.A, Ankara.

Kauth, R. J., and Thomas, G. S., 1976, The tasseled cap – a graphic description of the spectral-temporal development of agricultural crops as seen by Landsat. Proceedings of the Symposium on Machine Processing of Remotely Sensed Data, Purdue University, 29 June–1 July 1976, West Lafayette, Indiana (West Lafayette, Indiana: Laboratory for Applications of Remote Sensing), pp. 41–51.

Kowalczyk, P., and Logan, K., 1989. TM processing for routine use in mineral exploration, in Proceedings of the 7th Thematic Conference on Remote Sensing for Exploration Geology, Vol. I, Environmental Research Institude of Michigan, Ann Arbor, Mich.,pp. 323-329

Lindberg, J.D., and Smith, M.S., 1973. Reflectance spectra of gypsum sand from the White Sands National Monument and basalt from nearby lava flow, The American Mineralogist, Vol. 58, pp. 1062-1064.

Loughlin, W., 1991, Principal component analysis for alteration mapping. Photogrammetric Engineering and Remote Sensing, 57, 1163-1169.

Ninomiya, Y., 2002, Mapping quartz, carbonate minerals and mafic-ultramafic rocks using remotely sensed multispectral thermal infrared ASTER data, proceedings of SPIE, vol. 4170 , pp. 191-202.

Pasquare, G., 1968, Geology of Cenozoic volcanic area of Central Anatolia, atti Della academia Nazionella Des Lincei Memorie serie VII Volume IX Roma.

Pearson, K. (1901). "On Lines and Planes of Closest Fit to Systems of Points in Space". *Philosophical Magazine* **2** (6): 559–572.

Re Kühl, G.E.,1992. Landsat thematic mapper band ratio discrimination of altered and unaltered volcanic rocks in the Andes of Argentina, Bolivia and Chile; [M.S. thesis], 169 p.

Richardson, A. J., and Wiegand, C. L., 1977, Distinguishing vegetation from soil background information. Photogrammetric Engineering and Remote Sensing, 43, 1541–1552.

Rigo de Righi, M. and Cortesini, A., 1959, Regional Studies Central Anatolia basin, progress report 1 Turkish Gulf Oil Comp. Petrol İşleri General Directorate, Ankara.

Rowan, L., Hook, S.J., Abrams, M.J., Mars, J.C., 2003. Mapping hydrothermally altered rocks at Cuprite, Nevada, using the Advanced Spaceborne thermal emission and reflection radiometer (ASTER), a new satellite-imaging

system. Economic Geology and the Bulletin of the Society of Economic Geologists 98 (5), 1019–1027.

Rowan, L.C., Mars, J.C., 2003. Lithologic mapping in the Mountain Pass, California area using Advanced Spaceborne Thermal Emission and Reflection Radiometer (ASTER) data. Remote Sensing of Environment 84, 350–366.

Ruiz-Armenta, J. R., and Prol-Ledesma, R. M., 1998, Techniques for enhancing the spectral response of hydrothermal alteration minerals in Thematic Mapper images of Central Mexico. International Journal of Remote Sensing, 19, 1981–2000.

Sabine, C. ,1999, Strategies for Mineral Exploration, Ch. 8 in *Manual of Remote Sensing*, 3rd Edition, Vol. 3, A. Rencz, Ed. John Wiley in cooperation with ASPRS.

Sabins, F. F., 1987, Remote Sensing Principles and Interpretation, W.H. Freeman and Company, New York.

Sabins, F.F., Miller, R.M. 1994. "Resource assessment—Salar Uyuni and vicinity". Proceedings of Tenth Thematic Conference on Geologic Remote Sensing. Environmental Research Institute of Michigan, Ann Arbor, MI, I92–I103.

San, B. T., Sumer, E. O., and Gurcay, B., (2004) "Comparison of Band Ratioing and Spectral Indices Methods for Detecting Alunite and Kaolinite Minerals using Aster Data in Biga Region,Turkey" *International Society for Photogrammetry and Remote Sensing, XXth Congress*, Commission 7, İstanbul.

Seymen, İ., 1982, Kaman dolayında Kırşehir masifinin jeolojisi: İstanbul Technical University Mining Faculty , Phd Thesis.

Souza Filho, C. R., and Drury, S. A., 1998, Evaluation of JERS-1 (FUYO 1) OPS and Landsat TM images for mapping of gneissic rocks in arid areas. International Journal of Remote Sensing, 19, 3569–3594.

Soha. J.M., and Schwartz, A. A., 1978, Multispectral histogram normalization contrast enhancement, in Proc. 5 th Canadian Symposium on Remote Sensing, Victoria, BC, Canada, pp. 86-93.

Şahbaz,A., Köksoy, M., 1985, Paşadağ-Aladağ (Tuzgölü Kuzeyi) yöresi Paleojen yaşlı tortul istifinin stratigrafik ve tekto nik incelenmesi, pp:1-19.

Tangestani, M. H., and Moore, F., 2001, Comparison of three principal component analysis techniques to porphyry copper alteration mapping: a case study in Meiduk area, Kerman, Iran. Canadian Journal of Remote Sensing, 27, 176–182.

Tangestani, M. H., and Moore, F., 2002, Porphyry copper alteration mapping at the Meiduk area, Iran. International Journal of Remote Sensing, 23, 4815–4826.

Taylor, M. M. (1973), Principal components color display of ERTS imagery, *Third Earth Resources Technology Satellite-1 Symposium*, 10-14, December, NASA SP-351, Vol. 1, Section B, pp. 1877-1897

Taylor, Peter J. 1977. Quantitative Methods in Geography: An Introduction to Spatial Analysis. Boston, Massachusetts: Houghton Mifflin Company.

Tommaso I.D., Rubinstein N., 2006, Hydrothermal alteration mapping using ASTER data in the Infiernillo porphyry deposit, Argentina, Ore Geology Reviews

Uğuz, F., Turhan, N., Bilgin, A. Z., Umut M., Şen M., Acarlar, M., 1999, Kulu Haymana ve Kırıkkale dolayının jeolojisi, M.T.A. Report No:10399.

URL1, USGS, 2008, http://minerals.usgs.gov/minerals

URL2, USGS, 2008, http://minerals.usgs.gov/minerals/pubs/commodity/gypsum

URL3, USGS, 2008, http://minerals.usgs.gov/minerals/pubs/commodity/gypsum/

Uygun, A., 1981. Tuz Gölü Havzası'nın bir bölümünün jeofizik yorumu. MTA Der.,85, 38-44.

Velosky, J.C., Stern, R.J., Johnson, P.R., 2003. Geological control of massive sulfide mineralization in the Neoproterozoic Wadi Bidah shear zone, southwestern Saudi Arabia, inferences from orbital remote sensing and field studies. Precambrian Research 123 (2–4), 235–247.

Wolters, J.M., Goldin, L.,Watts, D.R., Harris, N.B.W., 2005. Remote sensing of gneiss and granite in southern Tibet. Geol. Soci. America, Abstract with Program, vol. 37; 5, p. 93.

Yamaguchi, Y., and Naito, C., 2003. Spectral indices for lithologic discrimination and mapping by using the ASTER SWIR bands. *Int. J. Remote Sensing*, 24(22), pp. 4311-4323.

Yamaguchi, Y., and Takeda, I., 2003. Mineralogical mapping by ASTER in Cuprite, Nevada, USA. *Asian Journal of Geoinformatics,* 3(3), pp. 17-24.

APPENDIX A

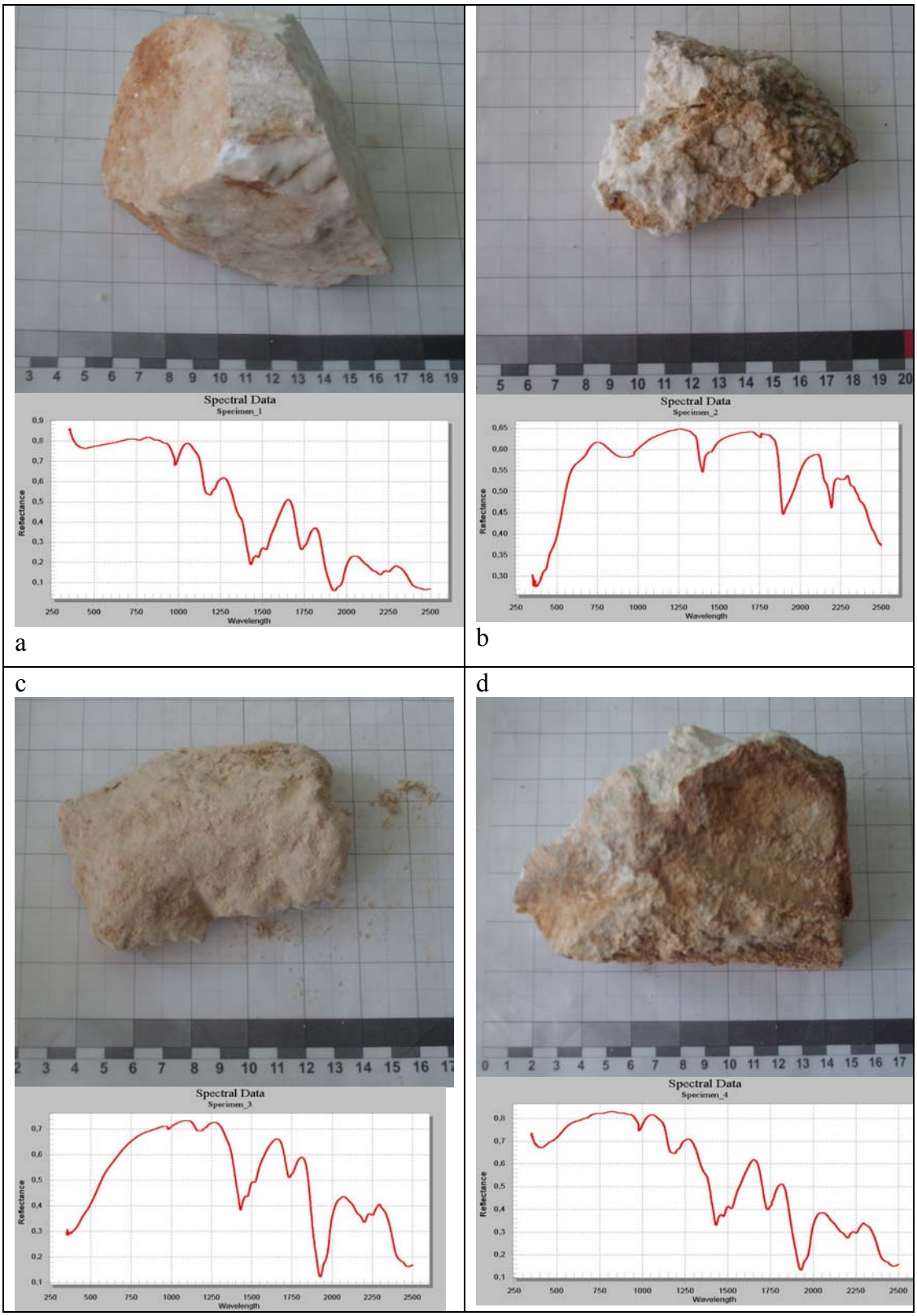

a

b

c

d

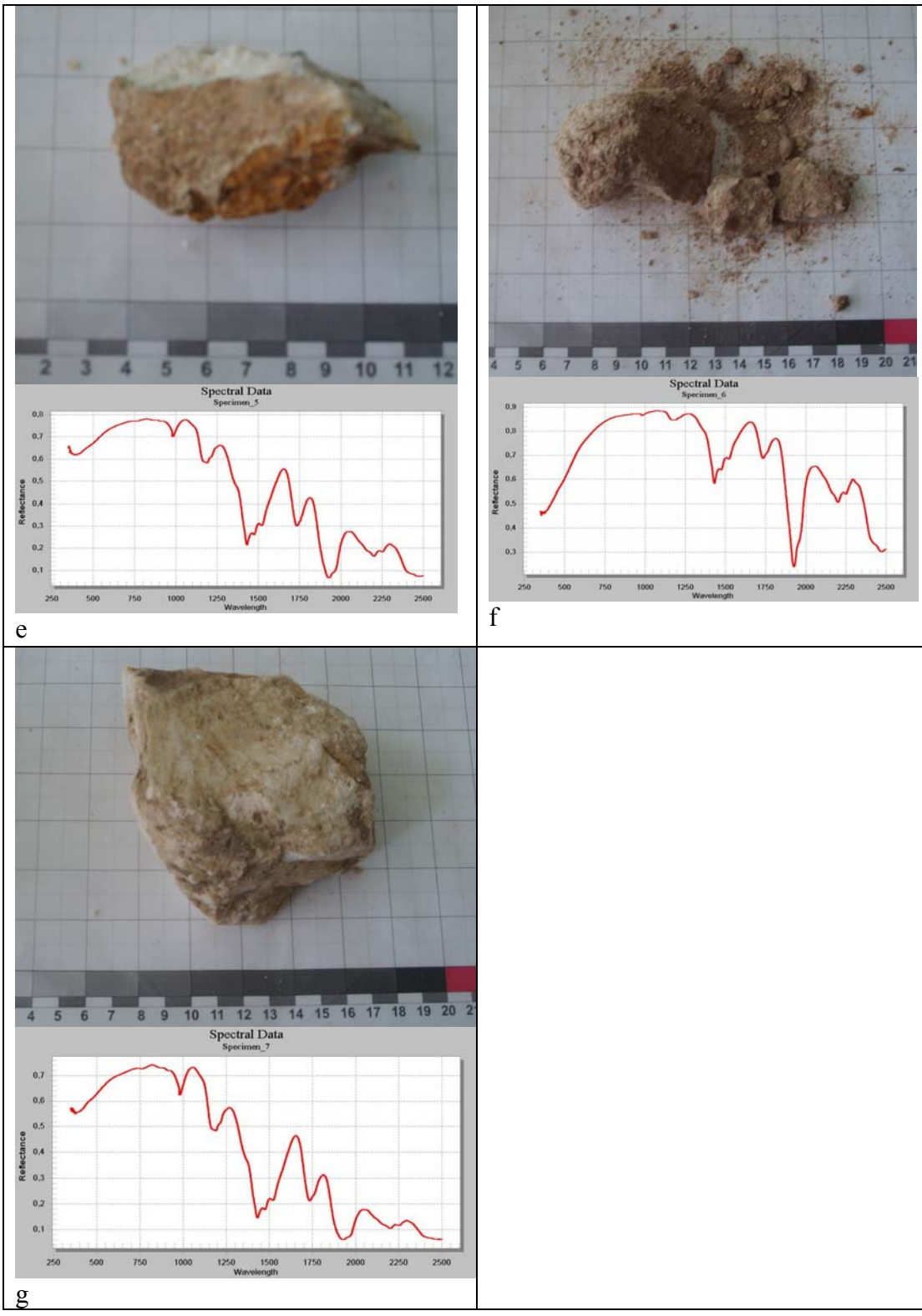

Figure A.1. The photo and spectral curves of samples taken from ground truth
a) Specimen1 b) Specimen2 c) Specimen 3 d) Specimen 4 e) Specimen 5
f) Specimen 6 g) Specimen 7

APPENDIX B

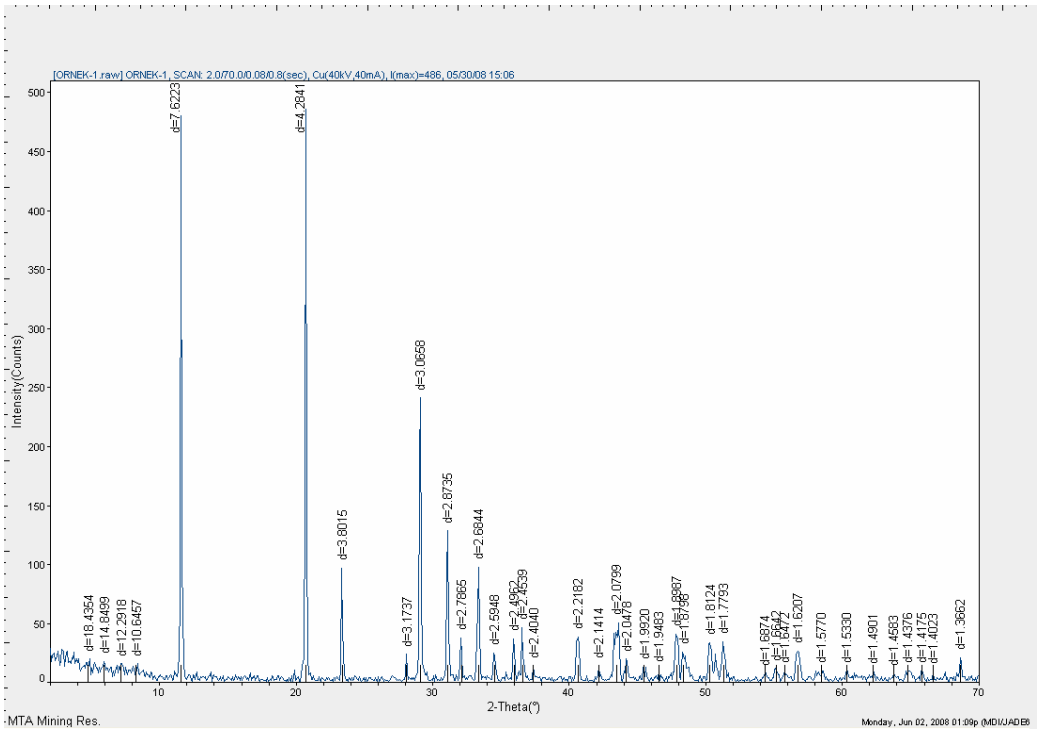

Figure B.1. X-Ray result of Specimen-1.

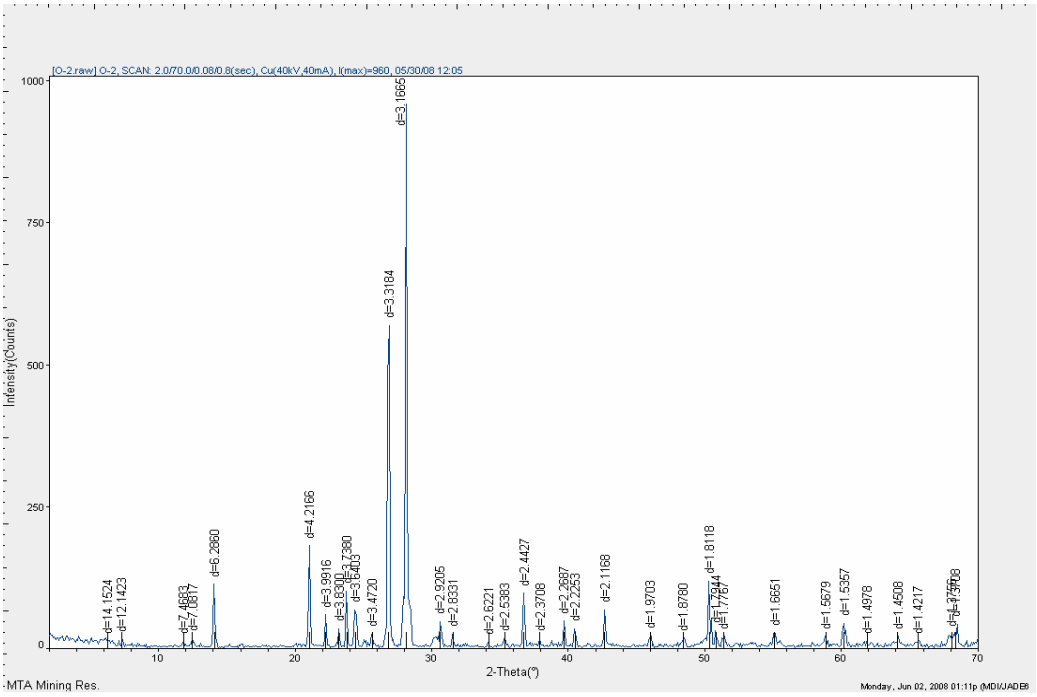

Figure B.2. X-Ray result of Specimen-2.

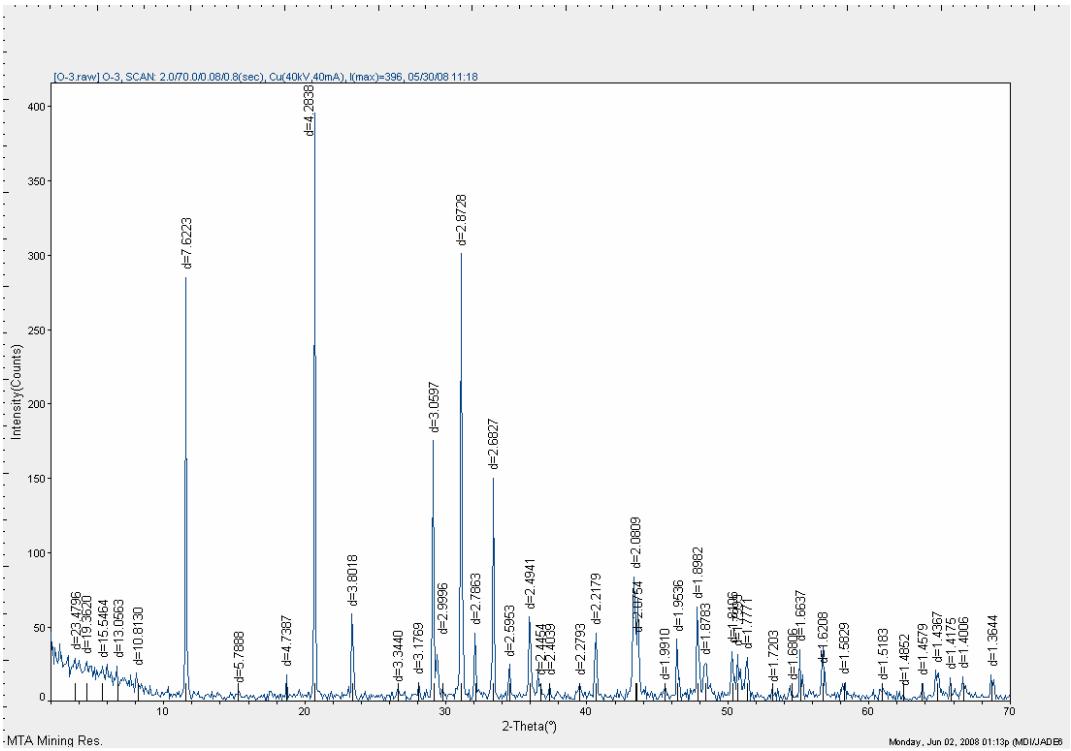

Figure B.3. X-Ray result of Specimen-3.

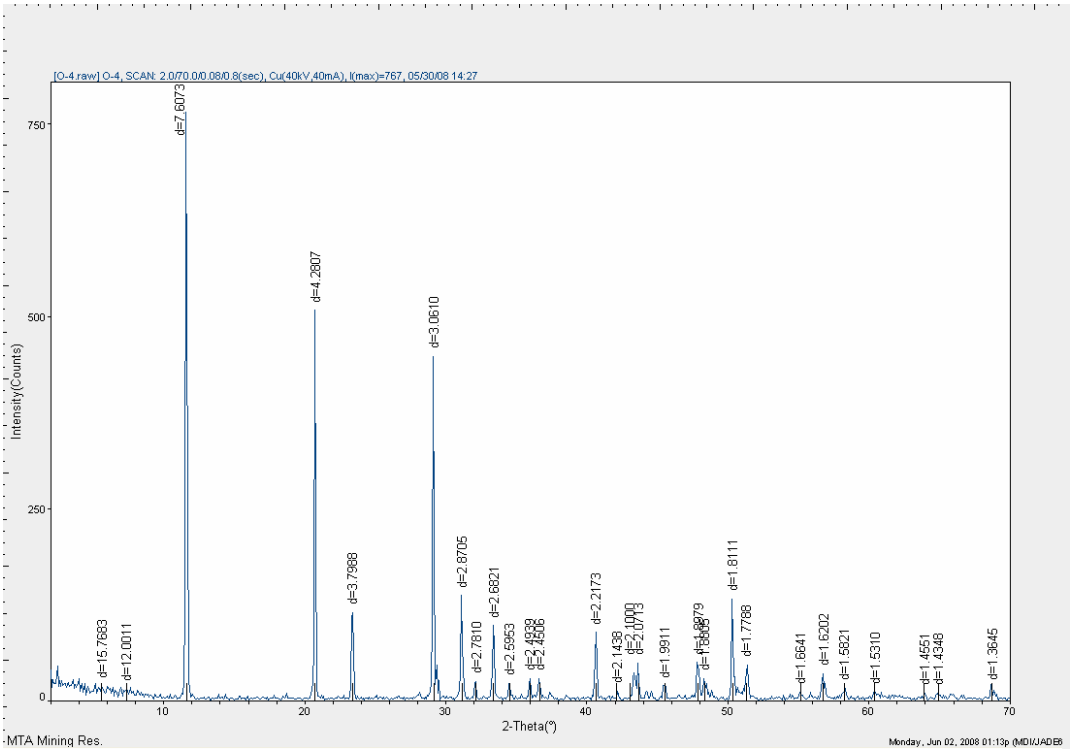

Figure B.4. X-Ray result of Specimen-4.

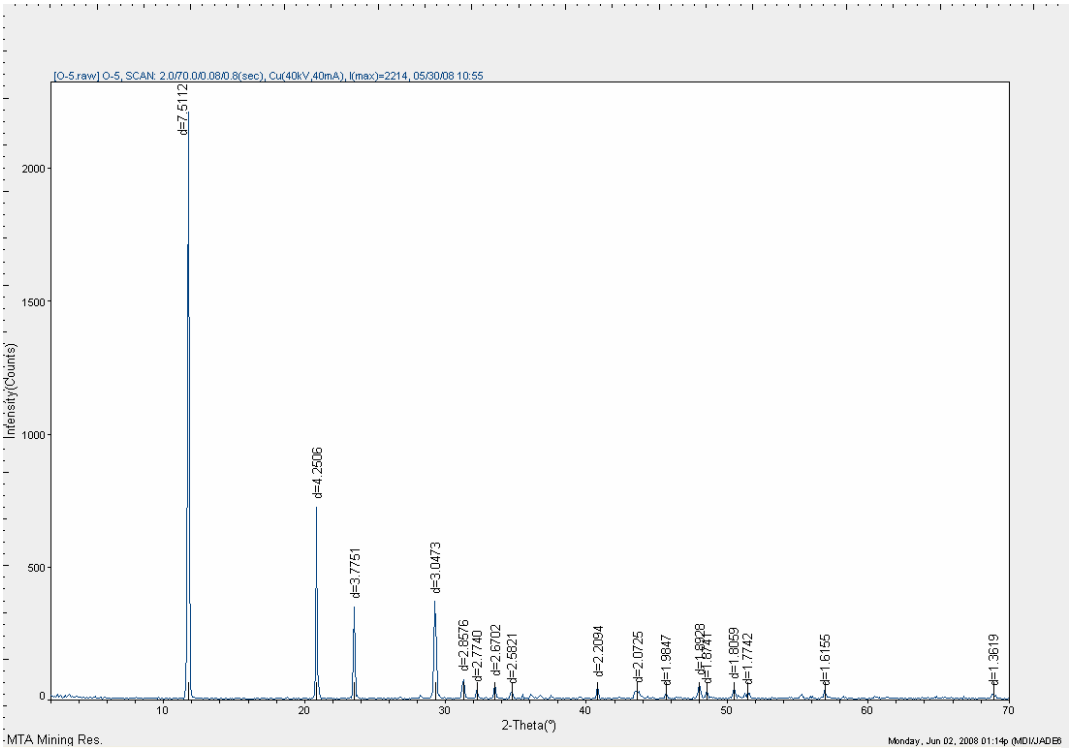

Figure B.5. X-Ray result of Specimen-5.

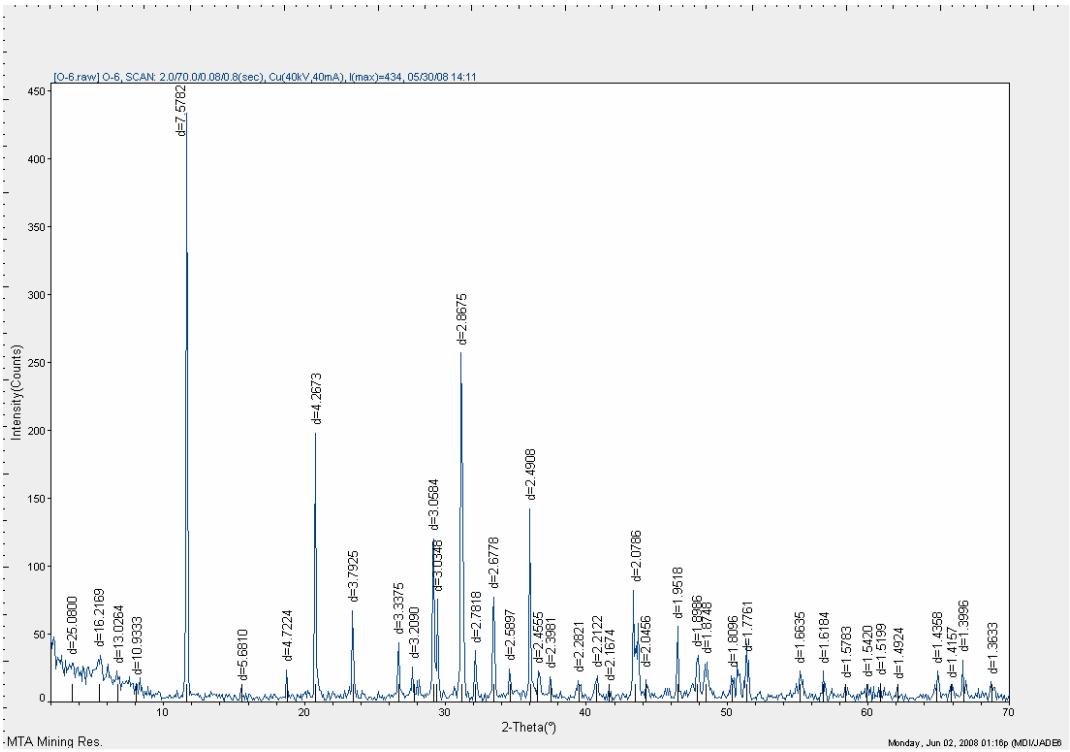

Figure B.6. X-Ray result of Specimen-6.

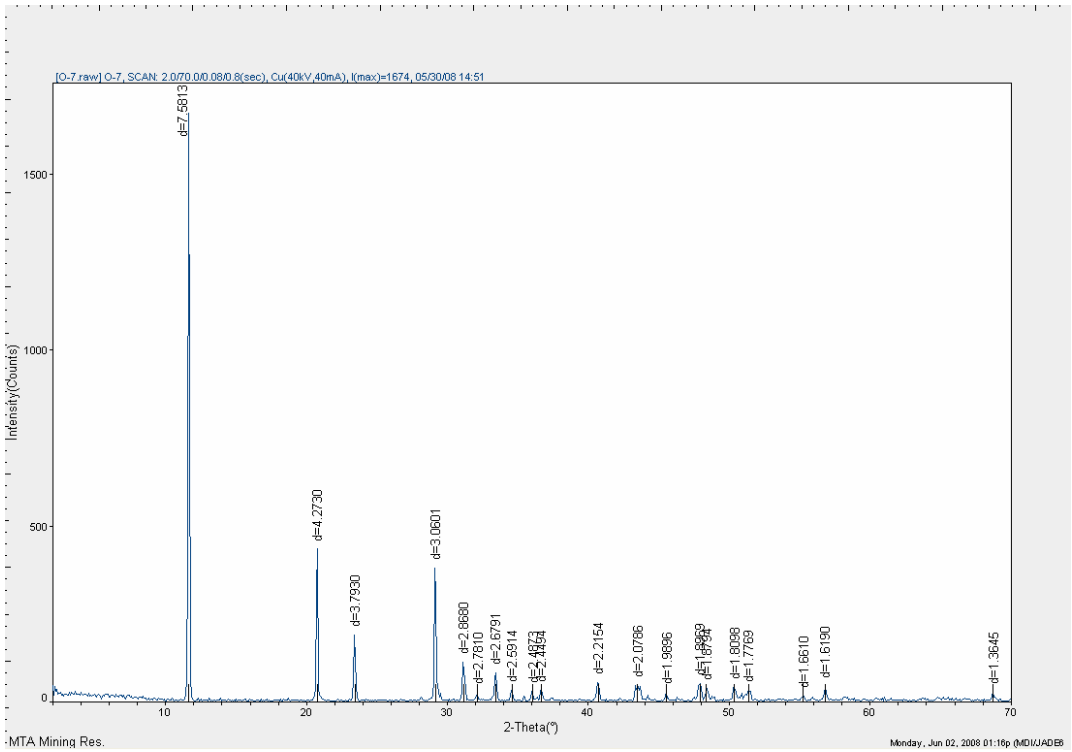

Figure B.7. X-Ray result of Specimen-7